

# Fix-lines and stability domain in the vicinity of the coupled third order resonance

G. Franchetti<sup>1</sup>, F. Schmidt<sup>2</sup>

<sup>1</sup>*GSI Darmstadt, Planckstrasse 1, 64291 Darmstadt, Germany and*

<sup>2</sup>*CERN CH-1211, Geneva 23, Switzerland*

(Dated: April 4, 2024)

The single particle stability in a circular accelerator is of concern especially for operational regimes involving beam storage of hours. In the proximity to a resonance this stability domain shrinks, and the phase space fragments into a jungle of exotic objects like for instance “fix-lines”. The concept of fix-points is easily understandable in a 2D phase space. It becomes quite challenging when the effect of resonances is considered in the 4D phase space, which leads then to the concept of fix-lines. In this paper we investigate the fix-lines in the proximity of a coupled third order resonance and find the relation of these objects with the stability of motion.

PACS numbers: 41.75.-i, 29.27.Bd

## I. INTRODUCTION

The stability of particle motion in circular accelerators has always been a topic of heated discussion in the accelerator community. In fact, the problem of localized magnet non-linearities distributed around the accelerator has invoked its own field of nonlinear dynamics studies. The most complex consequences of these non-linearities are detuning with amplitude, excitation of resonances, chaotic motion and eventually particle loss [1, 2].

The theory of resonances was developed by Hagedorn/Schoch [3–5] in the 1950’s and modified for CERN Accelerator School classes by Guignard in the 1970’s [6, 7]. This theory treats the condition under which the motion of a particle is resonant. The treatment of motion is 2D, and the theory shows that the resonant phenomena can be described by a “resonant driving term”, which is a quantity that takes into account the distribution of the multipolar errors along the ring and characterizes the resonance stop-band.

The interplay of the stability domain and resonances is a very difficult subject and there seems to be no general theory that explains it completely. However, simulations show that in the proximity to a resonance the regime with stable motion typically shrinks, and the phase space fragments into regions with very different dynamical properties: from stable motion, to unstable, and chaotic motion [1].

The difficulty of the dynamics in the vicinity of a resonance is remarkable even in regimes in which the motion do not exhibit chaoticity. Concepts as fix-points easily understandable in a 2D phase space assume quite challenging aspects when the effect of resonances is considered in the 4D phase space. For regular motion in 4D phase space, the fix-points become exotic objects that we call “fix-lines” [8]. The structures created by the 2 degree of freedom resonances have been subject of studies, which addressed the problem from the mapping approach [9, 10].

Fix-lines become particularly relevant when the non-linear dynamics is affected by space charge in bunched beams. The phenomena of periodic resonance crossing

induced by synchrotron motion and space charge, create new and more complex dynamics which is very significant for present projects like the SIS100 of the FAIR project where bunches are stored for a long term in presence of significant space charge [11], or for the LIU project at CERN, where PSB, PS and SPS are upgraded in intensity and the same topology of high intensity problem is encountered [12]. For 1D resonances the interplay of space charge with fix-points has been extensively studied, numerically and experimentally [13, 14]. On the other hand, studies on the interplay of space charge and 2D resonances has never be attempted because of the remarkable difficulty in characterizing stable resonances in 4D phase space (the fix-lines).

In this paper we investigate the fix-lines in the proximity of a coupled third order resonance and find the relation of these objects with the stability properties of motion. Hence we extend the theory as presented by Guignard [7].

The plan of the paper is the following: In Sect. II we give an overview of the 2D resonances: this phenomenological analysis categorizes the resonances and discusses the main features of 1D and 2D resonances. The concept of fix-line is introduced and examples are shown. In Sect. III the phenomenology of the third order coupled resonances is being outlined. Fix-lines and tori cut are discussed using proper cuts in two dimensional planes. Section IV describes the theory of particle motion in a constant focusing channel equipped with one sextupole, the theory is developed following a perturbative approach. Section V deals with the problem of removing the time dependence from the Hamiltonian. We find that there are infinite canonical transformations able to remove the time dependence. This finding extends the theory of Schoch, and in fact it directly leads to a theory of the fix-lines (Sect. VI). Section VII treats the issue of the stability of the motion around a fix-line, and presents exact formulas for the case of a single resonant term. The analysis of stability allows to derive the secondary tunes of the motion around the fix-lines. In Sect. VIII we discuss the stability of motion in the vicinity of the third order coupled resonance, and find with large generality

a complete characterization of the stability of motion for the case of the dynamics dominated by one single resonant term. Tests and comparison with tracking simulations are shown as well.

In Sect. IX we extend the analysis to an AG structure equipped with many thin sextupoles. Following the corresponding arguments used for the constant focusing lattice, we directly retrieve a description of the dynamics in the proximity of a third order coupled resonance in terms of the resonance driving term as obtained from the theory of Schoch (for an arbitrary distribution of perturbative sextupolar errors). The comparison with multi-particle simulations is addressed as well. Lastly, in Section X we show that our theory allows to explain the results of the tori cut presented in Sect. II. Section XI is devoted to the conclusions and Sect. XII holds the acknowledgments. In the appendix A (Sect. XIII) we discuss the perturbed solutions around the fix-lines, and in the appendix B (Sect. XIV) we elaborate in more details on mathematical aspects of the discussion in Sect. VIII.

## II. PHENOMENOLOGICAL ANALYSIS OF RESONANCE STRUCTURES IN 2 DEGREES OF FREEDOM

### A. Categories of resonances in the 4D phase space

Resonance structures in 1D of freedom have been studied in depth and will not be mentioned except for a schematic comparison with the 2D case.

In 2 degrees of freedom we have basically 3 different types of resonances. In Fig. 1 we find an example of a vertical 1D resonance addressed with “1”. In the vertical plane you do expect to see a resonance structure with distinct resonance islands, whilst in the horizontal plane the motion is non resonant. Therefore we will expect to find a number of resonances vertical islands that may be widened due to deformations in the horizontal plane. We will not follow this type of resonance any further since it is basically very similar to the classical and well-known 1D resonances.

At the heart of this paper are the coupled resonance of type “2” in Fig. 1. The theoretical understanding of such coupled resonances including detuning with amplitude will be addressed in the following chapters. Here we want to show how they affect the motion in phase space.

A peculiar type of resonance is depicted with “3” in Fig. 1. This is the 2D analogon of 1D fix-points, i.e. these fix-points are equivalent to the central fix-point at the origin of the 2D closed orbit if it is different from zero in any of the 4 coordinates. To some extent the motion in the vicinity of fix-points is better defined then close to a fix-line structure. The authors envisage a separate report just dedicated to those 2D fix-points.

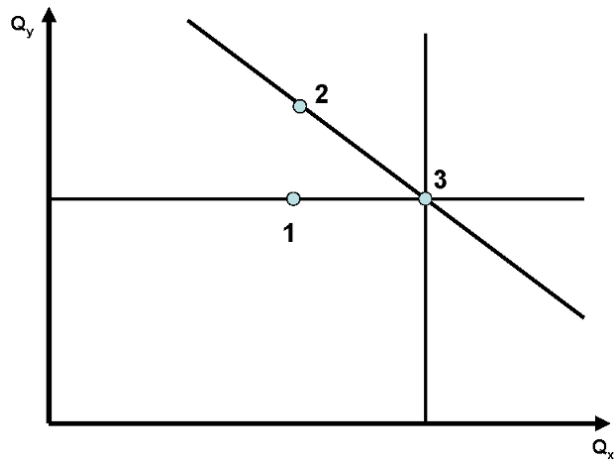


FIG. 1: Types of resonances in 4D phase space. Resonance lines are typically presented in the  $Q_x$ - $Q_y$  diagram.

### B. Schematic description of 1 and 2 degree of freedom resonances

Figure 2 shows schematically how the 2D phase space looks for a stabilized resonance, i.e. the detuning with amplitude creates island instead of unbounded motion along hyperbolic lines to infinity. It is important to mention that the phase space in the plane of the resonance for the type “1” resonance in Fig. 1 would look quite similar except that one will experience a widening of the projection of island motion that in the 1D schematic depiction is a measureless thin line around the fix-point.

This classical island structure in 1D has mostly regular motion in the inner part at small amplitude to the central closed-orbit, which is the green area in the Fig. 2. For completeness one has to mention that careful inspection of the motion in that “green” area will reveal other fine island structures. Besides the regular motion around stable 1D fix-points, depicted as the red area in Fig. 2 one finds deterministic chaotic motion in the vicinity of the unstable fix-points and the separatrix which separates the island motion from the “green” area at lower amplitude. At larger amplitude outside the island structure (for simplicity not shown in Fig. 2) one would expect regular motion up to a limit where motion becomes unbounded. This limit is called the dynamic aperture.

Notice that there is a dashed circular line that connects the fix-points which is denoted by “undisturbed” KAM torus. By that we mean the undisturbed motion in absence of the non-linearities of the system.

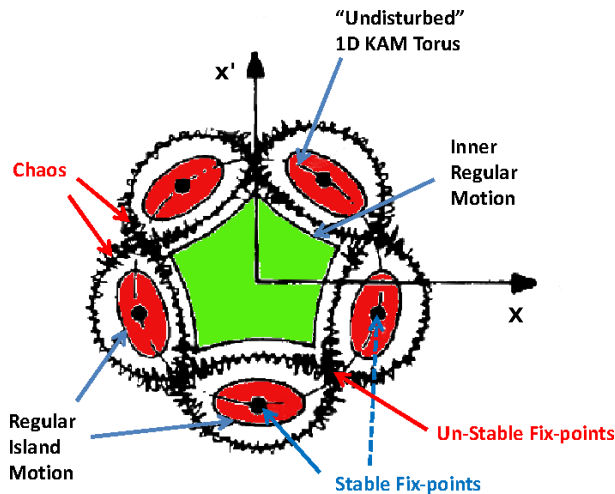


FIG. 2: Features of a 1D resonance stabilized through detuning with amplitude.

The last argument is a good link to resonances in 4D phase space, the real emphasis of this work. In 2 degrees of freedom the phase space is four dimensional. However, the motion of each individual particle is restricted to a two-dimensional manifold. In passing, we like to stress that the restriction to these two-dimensional manifolds is the very reason why there is a fundamental difference between motion in 2D and 4D phase space respectively: in the case of 1 degree of freedom each regular particle motions is on a curved line that separates phase space into an inside and outside part so that no particle can cross-over from one part to the other. However, in 2 degrees of freedom particles move on two-dimensional manifolds that cannot separate the 4D phase space into a inside and outside part since that would require a three-dimensional manifold. In consequence this means that in 4D phase space all chaotic regions are linked through-out phase space such that there is no longer a strict concept of the dynamic aperture in systems larger than 1 degree of freedom.

While particle motion in 2D phase space is pretty much self-evident one needs some preparation to find one's way in 4D phase space. To this end it is helpful to look at a 3D projection of linear and uncoupled motion in the 4D phase space. In Fig. 3 the motion in phase space of  $x, x', y$  is shown while  $y'$  is still hidden. Part a) shows  $x, x', y$  at some angle around the  $x'$  axis: it becomes evident that the motion is on a torus. When looking straight from the horizontal viewpoint ( $x, x'$  in part b) one finds a perfect ellipse without any thickness and for mixed coordinates ( $y, x'$  in part c) one finds a rectangular shape. It goes without saying that the  $(y, y')$  phase space is also an ellipse and that for all mixed coordinates one finds a rectangular shape.

It is important to realize that we are still lacking the 4<sup>th</sup> coordinate  $y'$ . A good way to describe this extra dimension is to understand that the particle moves on a double layered torus, i.e. two-dimensional manifolds in

4D. Introducing non-linearities tends to separate the layers of the torus so that very complex structures will be found in phase space. This becomes evident in Fig. 4 which shows a case with strong non-linearities switched on: large amplitudes have been chosen but the motion remains regular and refined to a two-dimensional manifold. The rotation angle of part a) is chosen to make the double layer structure strikingly visible.

Traditionally, there have been attempts to use other means E.G. a color code to allow for a full grasp of the dynamics in 4D. Set aside spectacular aesthetic pictures effectively this did little to substantially enhance our understanding of those dynamics. What really counts is that one can use cuts in phase space that take away overlapping pieces of the 2D manifold in the phase space projections.

Schematically one can have a look at how the “undisturbed” 2D KAM torus in case of linear motion is broken up into a fix-line structures as shown in Fig. 5. One finds that of this torus we are left with a set of alternating stable and unstable fix-lines: in the vicinity of the stable fix-lines the particles move on tori around the fix-line (again a 2D manifold), while the motion at the unstable fix-lines and the limiting “separatrix torus” is of chaotic nature.

The comparison of Fig. 2 and Fig. 5 shows how island structures in 2D are a generalization of those in 1D, albeit in 4D we have additional complexity. A more complete analogon to the 1D case is to be expected around 2D fix-points as shown below.

In case of a fix-line there is one condition fixed between the tunes therefore the stable 2D manifolds break up into 1D objects. In case there is a second condition fulfilled between the tunes these fix-lines are further broken up so that only fix-points, stable or unstable, remain. In Fig. 6 it is schematically shown how the particle motion evolves around stable fix-points. In fact, one expects structures that resemble the motion around the central fix-point around the closed-orbit, i.e. regular motion in small distance to the fix-point and the set-in of chaos at larger amplitudes. In the figure the lower left system the evolution of the chaotic particles is colored in green for better visibility.

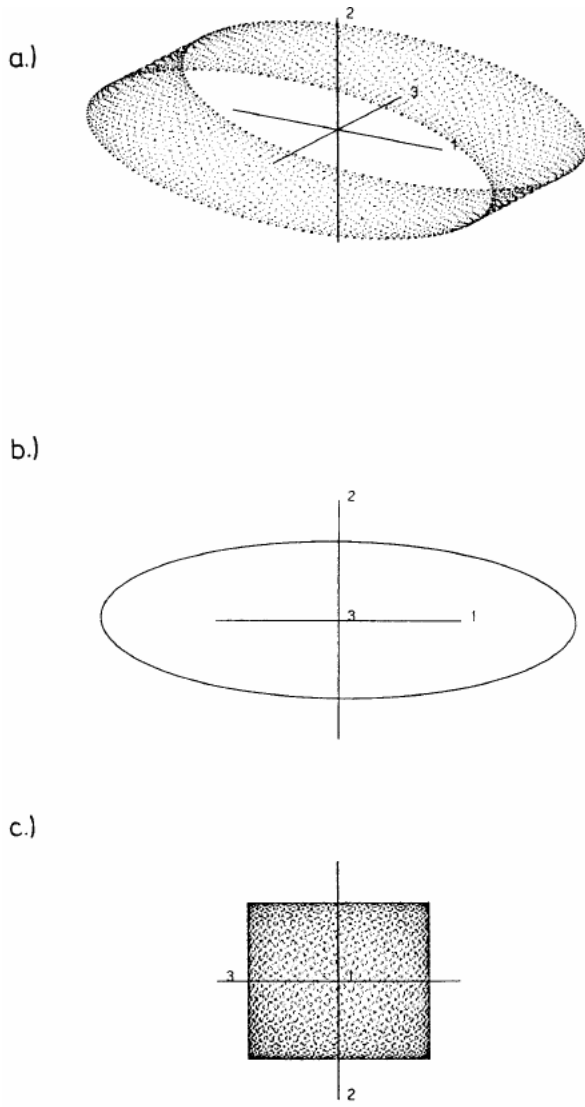


FIG. 3: Linear motion in 3D projections of the 4D phase space. The coordinate axis are denoted by 1, 2, 3 which stands for  $x, x', y$  respectively.

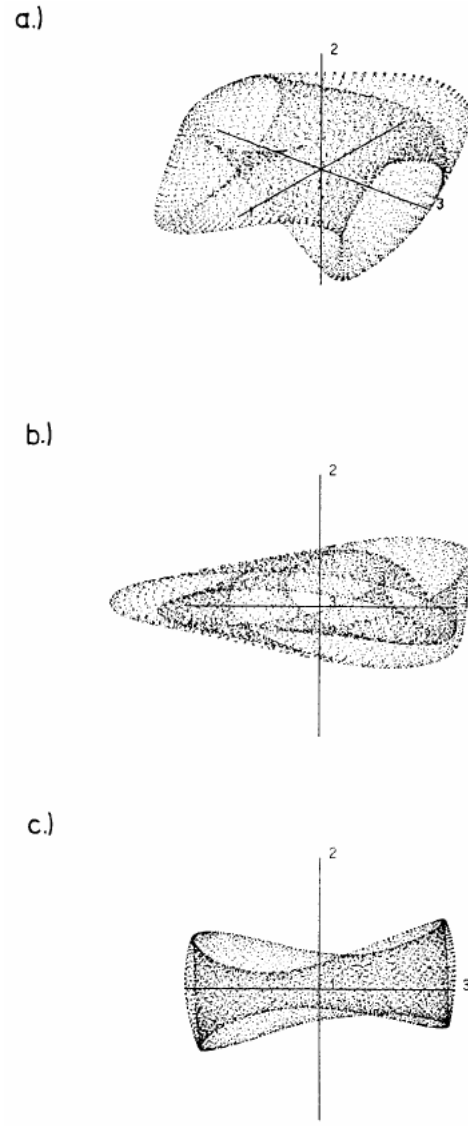


FIG. 4: Non-Linear and regular motion in 3D projections of the 4D phase space. The coordinate axis are denoted by 1, 2, 3 which stands for  $x, x', y$  respectively.



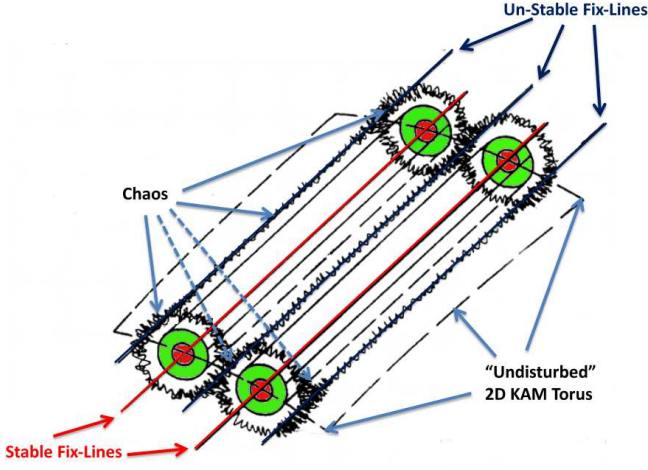


FIG. 5: Features of a 2D fix-line resonance.

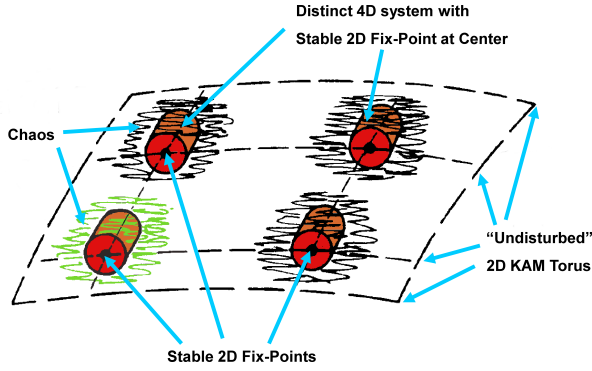


FIG. 6: Features of a 2D fix-point resonance.

### C. Simulation examples of 2D fix-line and fix-point resonances

In Fig.3 and Fig.4 we have already shown simulation examples for linear and non-linear motion. As explained above we are applying cuts in phase space such that one can inspect the two-dimensional manifold unobstructed by projections of other pieces of this manifold. Fig. 7 part a) depicts a regular and dense coverage of such a manifold.

In part b) the amplitudes have been varied in such a way that the tunes are on resonance and the motion is restricted to a torus around and with a small distance to the stable fix-lines. When the distance to the stable fix-lines is increased the motion becomes chaotic and the unstable fix-lines become visible. In Fig. 7 part c) both the stable and unstable fix-lines are indicated with red and blue arrows respectively. The two types of fix-lines are interleaved and the motion near the unstable fix-lines exhibits the typical large chaotic variations. It should be mentioned that the motion of part c) encloses that of part b).

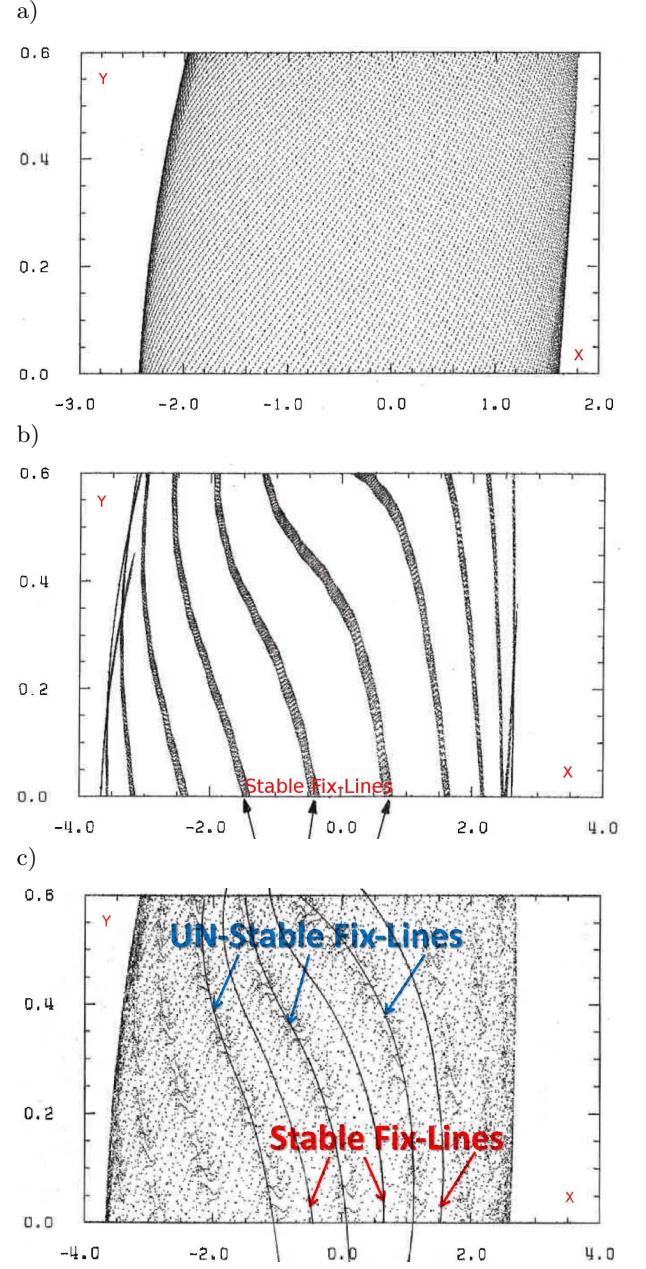


FIG. 7: 2D fix-line phase space cut-out.

Lastly, we are also presenting an example of particle motion in the vicinity of 2D fix-points. In Fig. 8 part a) close to the fix-points the motion type is regular. When the distance to the stable 2D fix-points is increased, the motion will exhibit chaotic behavior which is the case in Fig. 8 part b) where one finds fuzzy images due to the chaoticity. In part a) the motion around one of the fixed point is circled, while the motion in part b) is around the same fix-point. It is interesting to demonstrate that chaotic motion of part b) encloses the stable motion of part a). To this end these two trajectories are drawn on top of each other and turned in the three dimensional phase space projections  $x$ ,  $x$ ,  $y$  so that one can see that

both motion types evolve around the same fix-point (see Fig. 8 part c) ): one can nicely find regular motion close to the fix-point and fuzzy, i.e. chaotic motion at larger amplitude. It has to be mentioned that this holds true in all 3D projections, albeit without a visual demonstration shown here.

#### D. Locking to a 2D fix-line structure

In the analysis of motion in the vicinity of resonances it is important to consider a balance of resonance driving terms and the detuning with amplitudes. Often, too simple models do not really describe what will be found in well designed accelerators. Designers go to great pains to minimize driving terms and choose tune working points with optimal stability, i.e. large dynamic aperture.

To this end we are using an example with a sizable number of FODO structures each with sextupoles with an average non-zero value and some random component. This set-up can be seen as a reasonable good approximation for a realistic accelerator.

To study the effect of the sextupole coupling resonance  $Q_x + 2Q_y$  the bare tunes are set close to that resonance. We have tested 11 runs incremented by a fixed 4D coordinate vector.

In Fig. 9 part a) the phase advance per turn is shown over several thousand turns. Despite the apparent large variations of the phase advance one also finds the tunes of each case and a line connecting the tunes. Due to the specific detuning with amplitude the resonance line  $Q_x + 2Q_y$  (shown in the figure as well) is being approached until at step “8” when the motion is locked to the resonance. With larger amplitudes in this 2D case we are finding a phenomenon not known in 1D: for the next 3 steps the tunes are continuing to move but remaining locked to the resonance. It is important to understand that at all amplitudes in between case “8” and “11” the motions remains locked to this resonance. Each point though on the resonance line is a fix-line system in itself, as described in the previous sections: a fix-line at the center and motion around it while keeping identical horizontal and vertical tunes. In this study we have encountered rather accidentally particle “10” which fulfills almost perfectly the condition for a fix-line.

Figure 9 part b) shows a blow-up of this fix-line motion in the plane of the phases. It might be surprising at first sight that the particle is never actually on the resonance. The averaged phase advance, i.e. the tunes are indicated by the blue star in the figure. The tunes clearly never coincides with the individual phase advance values per turn (shown as red dots).

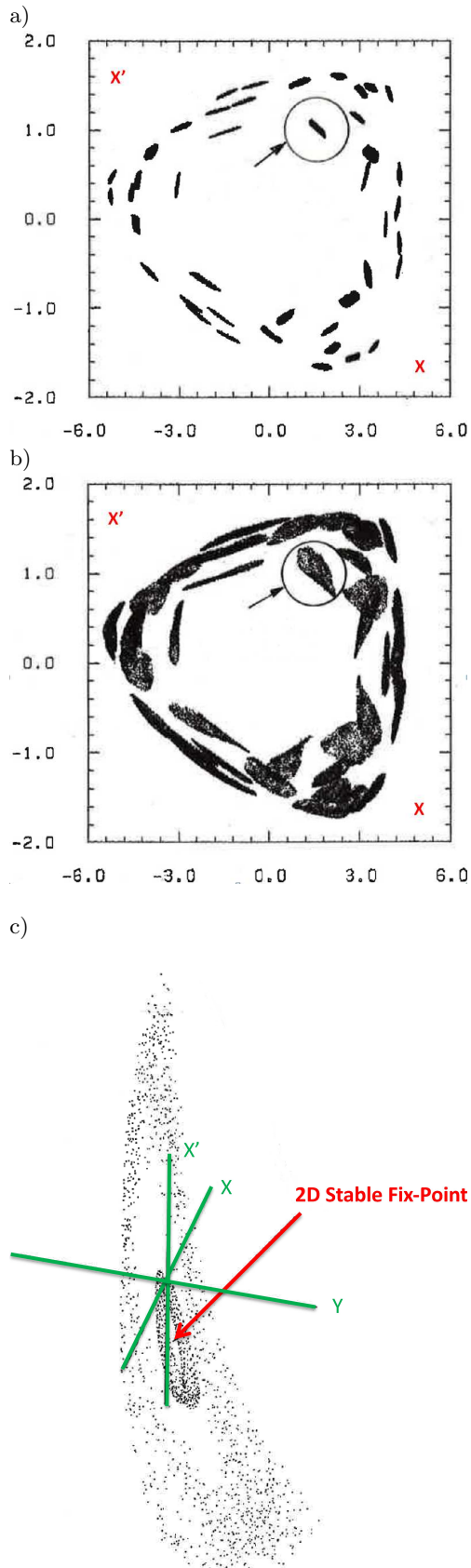


FIG. 8: 2D motion in the vicinity of a stable 2D fix-point.

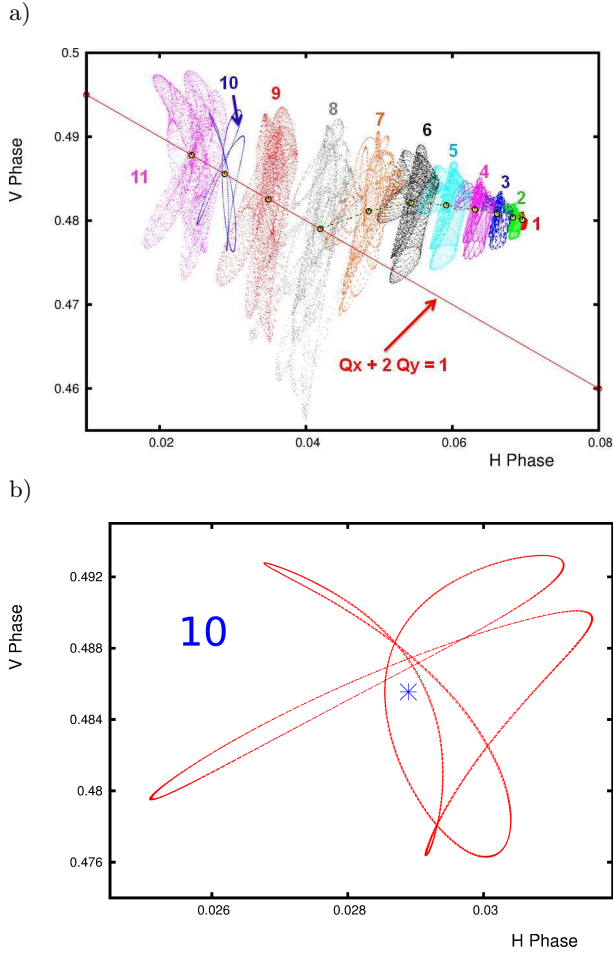


FIG. 9: Phase-advance per turn; Tunes ( $\equiv$  averaged phase advance); Orbiting around the 2D fix-line from case 8 through case 11. Part b) is a blow-up of case 10 that is an example of a fix-line in the plane of the phases. Interesting enough the phases never really respect the resonance condition instead the tunes do.

### III. LINKING THE PHENOMENOLOGICAL PHASE SPACE DEPICTION WITH THE THEORETICAL DERIVATION

The theory of fix-lines resonance structures will be derived in the following chapters. We would like to use a particular theoretical prediction to demonstrate how the particle motion of a large scale  $Q_x + 2 \times Q_y$  fix-line structure due to a single sextupole in a constant focusing lattice can be viewed in the 4D phase space.

It will be shown that in the mixed phase space plane  $y'$  versus  $x'$  we expect a figure 8 like structure (see Fig. 10) for the particle motion on the fix-line.

The particle motion on the stable fix-line and on the tori around it creates a fix-line structure that is distinct from regular motion around the closed orbit. To visualize this fix-line structure we show the stable fix-line and 3 tori around it in a restricted phase space as described in the earlier chapters. We have to do so to view only a

single passage of the fix-line structure in the  $y'$  versus  $x'$  phase space projection. To this end we restrict  $x$  and  $y$  to positive values. Figure 11 gives a first impression of this fix-line structure. However, it remains difficult to figure out graphically how the tori are stacked around the fix-line. Therefore, we apply a more vigorous cut in the phase space by restricting the particle motion to a very small angle in either the horizontal or vertical plane and depicting the resulting phase space projection in the other plane.

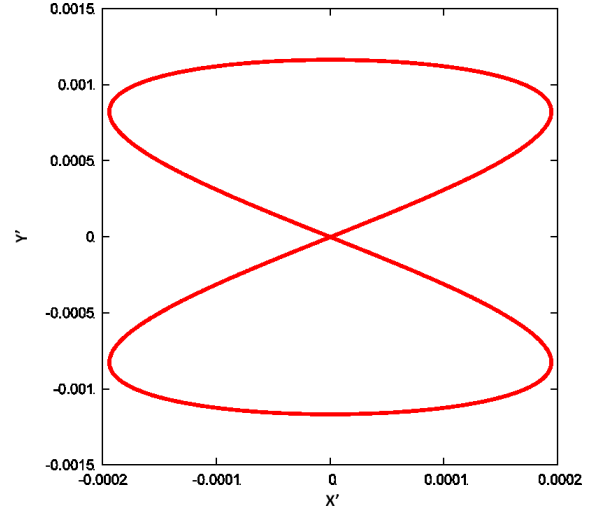


FIG. 10: The fix-line is seen in the  $y'$  versus  $x'$  plane as a figure 8 like structure.

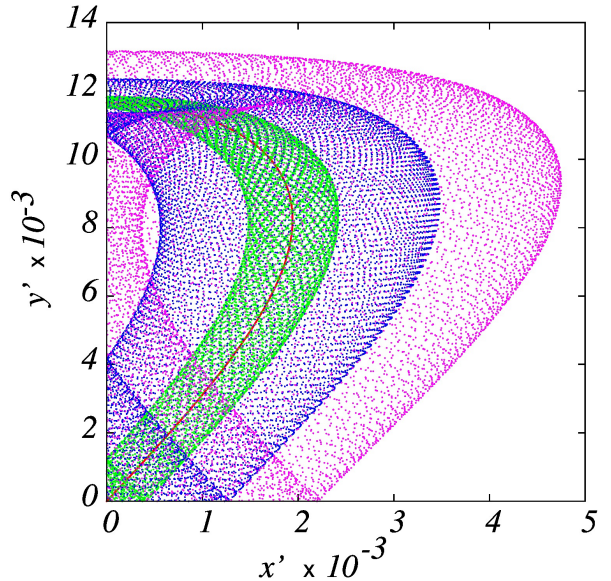


FIG. 11: Single passage of the fix-line structure in the  $y'$  versus  $x'$  phase space projection.

Figure 12 shows that in the horizontal plane the fix-line (red dots) lies indeed in the center with the particle

motion located on the three tori with increasing distance around the fix-line. The same is true in the vertical plane as seen in Fig. 13, except now we find two such structures which reflects the fact that we are investigating the  $Q_x + 2 \times Q_y$  resonance.

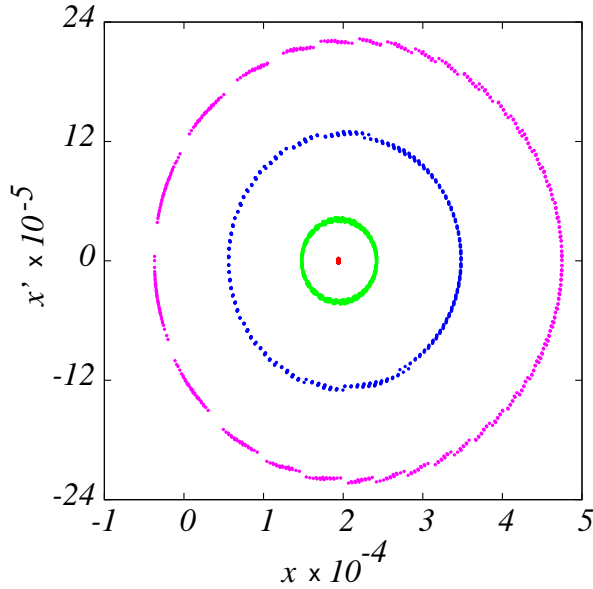


FIG. 12: Horizontal phase space projection after restricting the vertical motion to a small angle.

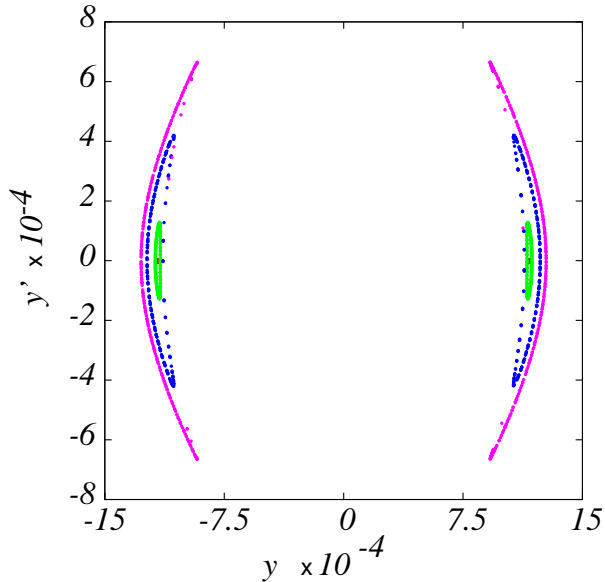


FIG. 13: Vertical phase space projection after restricting the horizontal motion to a small angle.

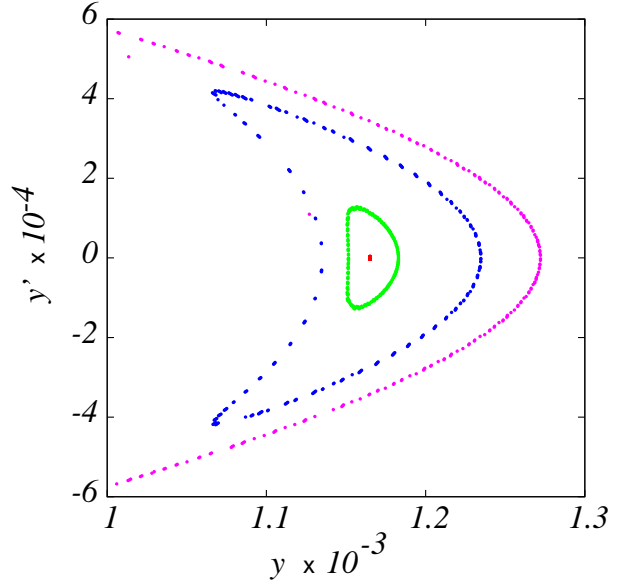


FIG. 14: Right part (see Fig. 13) of vertical phase space projection after restricting the horizontal motion to a small angle.

We have added a close-up (Fig. 14) for positive  $y$  values so that details with the tori and the fix-line at the center become more apparent.

In the following chapters we derive a theory of the particle motion in the vicinity of the third order coupling resonance. We start from a constant focusing model, which allows a simpler description of the dynamics. Starting from the description of the linear motion, we derive the motion of a particle by varying the constants (emittance  $a_x, a_y$  and phases  $\varphi_x, \varphi_y$ ). We obtain a system of differential equations in  $a_x, a_y, \varphi_x, \varphi_y$  which is “time dependent”. Then we demonstrate that there are infinite canonical transformations capable of removing the time dependence in the Hamiltonian of the system. Once the time dependence is removed, the simplest solution is obtained when the new variables are constant. This particular solution is proven to be the fix-line, and we will obtain analytically the result of Fig. 10. It turns out that the parametrization of the canonical transformation is the parametrization of the fix-lines, hence we find that there are infinite fix-lines contrary to the 1D case with one set of only 3 (unstable) fix-points. Perturbations from the solutions allow to discuss the stability of the fix-line and to derive secondary tunes, i.e. counting the oscillations around the fix-lines. Moreover, we find that sextupoles by themselves are capable to create stable fix-lines, a feature not known in the 1D case.

The particle dynamics become better described in a special combination of the “varying constants”  $a_x, a_y, \varphi_x, \varphi_y$ : we find that the motion in this special combination has another invariant that allows to discuss the stability. Consequently, we are able to describe the stability domain in the vicinity of the third order coupled resonance. As may have been expected we find that



the unstable fix-lines define the border of the stability regime. We derive the properties of the stability domain in terms of scaled quantities. The scaling factor depends on the distance from the resonance and on the driving term.

Lastly, we apply our approach to the AG machines. The conclusion remains the same, and the scaling parameters is incorporating the complexity of the AG lattice along with the distribution of sextupolar errors.

#### IV. EQUATION OF MOTION FOR LATTICE WITH CONSTANT FOCUSING

Let's start with the equations of motion describing the dynamics of a particle in a circular accelerator of radius  $R$ .

$$\begin{aligned} \frac{d^2x}{ds^2} + k_x x &= f_x(s, x, y), \\ \frac{d^2y}{ds^2} + k_y y &= f_y(s, x, y), \end{aligned} \quad (1)$$

here  $k_x, k_y$  are constants. The tunes of the machine  $Q_x, Q_y$  are defined as  $\sqrt{k_x}R = Q_x$ ,  $\sqrt{k_y}R = Q_y$ . In our discussion  $f_x, f_y$  are created by a magnetic multipole, then

$$-f_x(s) + if_y(s) = \frac{k_n(s)}{n!} (x + iy)^n. \quad (2)$$

With this notation for  $n = 1$  we get  $-f_x(s) = k_1(s)x$ ,  $f_y(s) = k_1(s)y$ , hence, a positive  $k_1$  yields a focusing force in the  $x$  plane.

Let's make the change of the variable  $s$  to the new variable  $s \rightarrow \theta$  so that  $\frac{dx}{ds} = \frac{dx}{d\theta} \frac{1}{R}$ . We use the notation  $x' = \frac{dx}{d\theta}$ . With this change of variable the equations of motion become

$$\begin{aligned} x'' + Q_x^2 x &= R^2 f_x(s(\theta), x, y), \\ y'' + Q_y^2 y &= R^2 f_y(s(\theta), x, y), \end{aligned} \quad (3)$$

and the length of the one turn is  $\Delta\theta = 2\pi$ . The integrated strength of  $k_2(\theta)$  in the  $\theta$  coordinate is linked to the integrated strength in the  $s$  coordinate via the relation

$$\int_{\theta_1}^{\theta_2} k_2(\theta) d\theta = \int_{s_1}^{s_2} k_2(s) \frac{d\theta}{ds} ds = \frac{K_2}{R} \quad (4)$$

where  $K_2$  is the integrated strength in the  $s$  coordinate.

##### A. Perturbative approach: the dynamics with one sextupole

We will consider next the accelerator with a single sextupole for exciting sextupolar resonances. The Hamiltonian of this system is  $H = H_0 + H_1$  with

$$H_0 = \frac{1}{2}x'^2 + \frac{Q_x^2}{2}x^2 + \frac{1}{2}y'^2 + \frac{Q_y^2}{2}y^2 \quad (5)$$

and

$$H_1 = R^2 k_2(\theta) \left( \frac{x^3}{6} - \frac{xy^2}{2} \right). \quad (6)$$

Therefore for a localized sextupole of integrated strength  $K_2$  located at  $\theta = 0$  in a circular machine, using Eq. 4 we write

$$k_2(\theta) = \sum_{m=-\infty}^{\infty} \frac{K_2}{R} \delta(\theta + 2\pi m). \quad (7)$$

where the sum over infinite delta functions  $\delta()$  is used for modeling the periodicity of one sextupolar error in the machine. The Hamiltonian  $H_1$  becomes then

$$H_1 = RK_2 \sum_{m=-\infty}^{\infty} \delta(\theta + 2\pi m) \left( \frac{x^3}{6} - \frac{xy^2}{2} \right). \quad (8)$$

The solution of the unperturbed system with Hamiltonian  $H_0$  is the solution of the canonical equations

$$\begin{aligned} \frac{dx}{d\theta} &= \frac{\partial H_0}{\partial x'}, & \frac{dx'}{d\theta} &= -\frac{\partial H_0}{\partial x}, \\ \frac{dy}{d\theta} &= \frac{\partial H_0}{\partial y'}, & \frac{dy'}{d\theta} &= -\frac{\partial H_0}{\partial y}, \end{aligned} \quad (9)$$

which yields the equations of motion, that are

$$x'' + Q_x^2 x = 0, \quad y'' + Q_y^2 y = 0. \quad (10)$$

The solutions are

$$\begin{aligned} x &= \sqrt{\beta_x a_x} \cos(Q_x \theta + \varphi_x), \\ y &= \sqrt{\beta_y a_y} \cos(Q_y \theta + \varphi_y), \end{aligned} \quad (11)$$

with  $\beta_x = 1/Q_x, \beta_y = 1/Q_y$ . The parameters  $a_x, a_y$  are the single particle invariant, i.e. the usual emittances expressed in the reference frame with  $\theta$  coordinate. Hence they are not the emittances in the laboratory frame.

Next we use the canonical theory of perturbation, in which we add  $H_1$  and compute the evolution in the system  $H_0 + H_1$  of the otherwise constants  $a_x, \varphi_x, a_y, \varphi_y$ . The equations of motion of  $a_x, \varphi_x, a_y, \varphi_y$  are

$$\begin{aligned} a'_x &= -2 \frac{\partial H_1}{\partial \varphi_x}, & \varphi'_x &= 2 \frac{\partial H_1}{\partial a_x}, \\ a'_y &= -2 \frac{\partial H_1}{\partial \varphi_y}, & \varphi'_y &= 2 \frac{\partial H_1}{\partial a_y}. \end{aligned} \quad (12)$$

Note that this is a canonical system with Hamiltonian  $2H_1$ . Next we substitute in  $H_1$  the Eqs. 11 re-written in the form

$$\begin{aligned} x &= \sqrt{\beta_x a_x} \frac{e^{iA_x} + e^{-iA_x}}{2} \\ y &= \sqrt{\beta_y a_y} \frac{e^{iA_y} + e^{-iA_y}}{2} \end{aligned} \quad (13)$$

with  $A_x = Q_x\theta + \varphi_x$ , and  $A_y = Q_y\theta + \varphi_y$  defined just for convenience. We also expand the periodic  $\delta$  as

$$\sum_{m=-\infty}^{\infty} \delta(\theta + 2\pi m) = \frac{1}{2\pi} \sum_{l=-\infty}^{\infty} e^{-il\theta} \quad (14)$$

and substitute it in  $H_1$ . After some algebraic calculation,  $H_1$  becomes

$$\begin{aligned} H_1 = & RK_2 \frac{1}{48\pi} (\beta_x a_x)^{3/2} \times \frac{1}{2} \times \\ & \sum_{j=0}^3 \sum_{l=-\infty}^{\infty} \binom{3}{j} \cos[((2j-3)Q_x - l)\theta + (2j-3)\varphi_x] - \\ & - RK_2 \frac{1}{16\pi} \frac{1}{2} \sqrt{\beta_x a_x \beta_y a_y} \left\{ \sum_{l=-\infty}^{\infty} \sum_{j=0}^2 \sum_{j'=0}^1 \binom{1}{j'} \binom{2}{j} \right. \\ & \left. \cos[(2j'-1)Q_x + (2j-2)Q_y - l]\theta + \right. \\ & \left. + (2j'-1)\varphi_x + (2j-2)\varphi_y \right\}. \end{aligned} \quad (15)$$

At this point we keep the slow varying terms only, that is the terms close to the resonance  $Q_x + 2Q_y = N$ . Here  $N$  is an integer used throughout this article with the same meaning: it defines the location of the resonance. Let's define

$$\Delta_r = -N + Q_x + 2Q_y, \quad (16)$$

then the slower varying terms are obtained in the second term for  $l = N, j' = 1, j = 2$ , and  $l = -N, j' = 0, j = 0$ . Hence the slower harmonics Hamiltonian  $H_{s1}$ , which mainly contributes to the dynamics is

$$H_{s1} = -RK_2 \frac{1}{16\pi} \sqrt{\beta_x a_x \beta_y a_y} \cos[\Delta_r \theta + \varphi_x + 2\varphi_y]. \quad (17)$$

We define for convenience

$$\Lambda = -RK_2 \frac{1}{16\pi} \sqrt{\beta_x \beta_y}. \quad (18)$$

If instead we consider a continuous sextupolar component with strength  $k_2(\theta) = K_2 \cos(N\theta)$ , the expression for  $\Lambda$  is

$$\Lambda = -R^2 K_2 \frac{1}{16} \sqrt{\beta_x \beta_y}. \quad (19)$$

Note that  $K_2$  in this expression is the strength of a distributed sextupole not to be confused with the integrated strength  $K_2$  in Eq. 18. We therefore find that the general form of the slowly varying Hamiltonian is

$$H_{s1} = \Lambda \sqrt{a_x a_y} \cos[\Delta_r \theta + \varphi_x + 2\varphi_y] \quad (20)$$

and that it is time dependent as

$$\frac{\partial H_{s1}}{\partial \theta} = -\Lambda \sqrt{a_x a_y} \sin[\Delta_r \theta + \varphi_x + 2\varphi_y] \Delta_r \neq 0. \quad (21)$$

## V. REMOVING THE TIME DEPENDENCY

We redefine the variables  $\varphi_x, \varphi_y$  so that they incorporate the term  $\Delta_r \theta$ . Let's define

$$\begin{aligned} \tilde{\varphi}_x &= \varphi_x + t_x \theta, \\ \tilde{\varphi}_y &= \varphi_y + t_y \theta, \end{aligned} \quad (22)$$

with  $t_x, t_y$  some constants to be defined later. Then the argument of the cosine in Eq. 20 becomes

$$\Delta_r \theta + \varphi_x + 2\varphi_y = \tilde{\varphi}_x + 2\tilde{\varphi}_y + [\Delta_r - (t_x + 2t_y)]\theta, \quad (23)$$

therefore if  $\Delta_r - (t_x + 2t_y) = 0$  the time dependence disappears. We then consider the coordinate transformation

$$\begin{aligned} \tilde{a}_x &= a_x, \\ \tilde{\varphi}_x &= \varphi_x + t_x \theta, \\ \tilde{a}_y &= a_y, \\ \tilde{\varphi}_y &= \varphi_y + t_y \theta. \end{aligned} \quad (24)$$

If we define

$$\tilde{H}_{s1}(\tilde{a}_x, \tilde{\varphi}_x, \tilde{a}_y, \tilde{\varphi}_y, \theta) = H_{s1}(\tilde{a}_x, \tilde{\varphi}_x - t_x \theta, \tilde{a}_y, \tilde{\varphi}_y - t_y \theta, \theta), \quad (25)$$

then

$$\begin{aligned} 2 \frac{\partial \tilde{H}_{s1}}{\partial \tilde{\varphi}_x} &= 2 \frac{\partial H_{s1}}{\partial \varphi_x} = -a'_x = -\tilde{a}'_x, \\ 2 \frac{\partial \tilde{H}_{s1}}{\partial \tilde{a}_x} &= 2 \frac{\partial H_{s1}}{\partial a_x} = \varphi'_x = \tilde{\varphi}'_x - t_x, \\ 2 \frac{\partial \tilde{H}_{s1}}{\partial \tilde{\varphi}_y} &= 2 \frac{\partial H_{s1}}{\partial \varphi_y} = -a'_y = -\tilde{a}'_y, \\ 2 \frac{\partial \tilde{H}_{s1}}{\partial \tilde{a}_y} &= 2 \frac{\partial H_{s1}}{\partial a_y} = \varphi'_y = \tilde{\varphi}'_y - t_y. \end{aligned} \quad (26)$$

Therefore we have constructed a function (Eq. 25) that is time independent, but if we try to derive the equations of motion from it, we find Eqs. 26. These equations are clearly not the canonical equations, that means that the function Eq. 25 is not an Hamiltonian. This happens because in

$$2 \frac{\partial \tilde{H}_{s1}}{\partial \tilde{a}_x} = \tilde{\varphi}'_x - t_x \quad (27)$$

there is the constant term  $-t_x$  that should not be there. We then define the new function

$$\begin{aligned} \tilde{H}_{s1}(\tilde{a}_x, \tilde{\varphi}_x, \tilde{a}_y, \tilde{\varphi}_y, \theta) = & H_{s1}(\tilde{a}_x, \tilde{\varphi}_x - t_x \theta, \tilde{a}_y, \tilde{\varphi}_y - t_y \theta, \theta) + \\ & + \tilde{a}_x \frac{t_x}{2} + \tilde{a}_y \frac{t_y}{2} \end{aligned} \quad (28)$$

which is also time independent. Next we check if one can get the canonical equations

$$\begin{aligned}
2\frac{\partial\tilde{H}_{s1}}{\partial\tilde{\varphi}_x} &= 2\frac{\partial H_{s1}}{\partial\varphi_x} = -\tilde{a}'_x, \\
2\frac{\partial\tilde{H}_{s1}}{\partial\tilde{a}_x} &= 2\frac{\partial H_{s1}}{\partial a_x} + t_x = \varphi'_x + t_x = \tilde{\varphi}'_x, \\
2\frac{\partial\tilde{H}_{s1}}{\partial\tilde{\varphi}_y} &= 2\frac{\partial H_{s1}}{\partial\varphi_y} = -\tilde{a}'_y, \\
2\frac{\partial\tilde{H}_{s1}}{\partial\tilde{a}_y} &= 2\frac{\partial H_{s1}}{\partial a_y} + t_y = \varphi'_y + t_y = \tilde{\varphi}'_y.
\end{aligned} \tag{29}$$

Therefore we obtain

$$\begin{aligned}
2\frac{\partial\tilde{H}_{s1}}{\partial\tilde{\varphi}_x} &= -\tilde{a}'_x \\
2\frac{\partial\tilde{H}_{s1}}{\partial\tilde{a}_x} &= \tilde{\varphi}'_x \\
2\frac{\partial\tilde{H}_{s1}}{\partial\tilde{\varphi}_y} &= -\tilde{a}'_y \\
2\frac{\partial\tilde{H}_{s1}}{\partial\tilde{a}_y} &= \tilde{\varphi}'_y
\end{aligned} \tag{30}$$

which are the canonical equations with the Hamiltonian  $2\tilde{H}_{s1}$ . By construction the Hamiltonian  $\tilde{H}_{s1}$  is time independent. In fact

$$\begin{aligned}
\tilde{H}_{s1}(\tilde{a}_x, \tilde{\varphi}_x, \tilde{a}_y, \tilde{\varphi}_y, \theta) &= \Lambda\sqrt{\tilde{a}_x\tilde{a}_y}\cos[\tilde{\varphi}_x + 2\tilde{\varphi}_y] + \\
&+ \tilde{a}_x\frac{t_x}{2} + \tilde{a}_y\frac{t_y}{2}
\end{aligned} \tag{31}$$

does not depend on  $\theta$ . Note that the procedure described here is equivalent to transform the Hamiltonian  $2H_{s1}$  (from Eq. 20) to the Hamiltonian  $2\tilde{H}_{s1}$  (from Eq. 31) through the canonical transformation Eqs. 24 constructed by using the generating function

$$F_2(\varphi_x, \varphi_y, \tilde{a}_x, \tilde{a}_y) = \varphi_x\tilde{a}_x + \varphi_y\tilde{a}_y + t_x\tilde{a}_x\theta + t_y\tilde{a}_y\theta \tag{32}$$

with  $t_x + 2t_y = \Delta_r$ .

### A. Summary

We can summarize the situation as follows. There are infinite canonical transformations of the form

$$\begin{aligned}
\varphi_x &= \tilde{\varphi}_x - t_x\theta, & a_x &= \tilde{a}_x, \\
\varphi_y &= \tilde{\varphi}_y - t_y\theta, & a_y &= \tilde{a}_y,
\end{aligned} \tag{33}$$

with  $t_x + 2t_y = \Delta_r$  that allow to describe the time evolution as solution of canonical equations of the time independent Hamiltonian

$$\begin{aligned}
\tilde{H}_{s1}(\tilde{a}_x, \tilde{\varphi}_x, \tilde{a}_y, \tilde{\varphi}_y) &= \Lambda\sqrt{\tilde{a}_x\tilde{a}_y}\cos[\tilde{\varphi}_x + 2\tilde{\varphi}_y] + \\
&+ \tilde{a}_x\frac{t_x}{2} + \tilde{a}_y\frac{t_y}{2} + \mathcal{F}(\tilde{a}_x, \tilde{a}_y).
\end{aligned} \tag{34}$$

The function  $\mathcal{F}(\tilde{a}_x, \tilde{a}_y)$  collects all the nonlinear terms arising from the theory when other multipolar components (non resonant) are included in the Hamiltonian  $H_1$ . Following the procedure previously outlined, the slowly varying terms will be found in the zero-th order harmonics, that will create an additional term in the slowly varying Hamilton  $H_{s1}$ . Space charge can be treated in the same way. The explicit form of the canonical equations in the coordinates  $\tilde{a}_x, \tilde{\varphi}_x, \tilde{a}_y, \tilde{\varphi}_y$  is

$$\begin{aligned}
-\tilde{a}'_x &= -2\Lambda\sqrt{\tilde{a}_x\tilde{a}_y}\sin[\tilde{\varphi}_x + 2\tilde{\varphi}_y] \\
\tilde{\varphi}'_x &= 2\Lambda\frac{1}{2\sqrt{\tilde{a}_x}}\tilde{a}_y\cos[\tilde{\varphi}_x + 2\tilde{\varphi}_y] + t_x + 2\mathcal{F}_x \\
-\tilde{a}'_y &= -4\Lambda\sqrt{\tilde{a}_x\tilde{a}_y}\sin[\tilde{\varphi}_x + 2\tilde{\varphi}_y] \\
\tilde{\varphi}'_y &= 2\Lambda\sqrt{\tilde{a}_x}\cos[\tilde{\varphi}_x + 2\tilde{\varphi}_y] + t_y + 2\mathcal{F}_y
\end{aligned} \tag{35}$$

where we used the short notation  $\mathcal{F}_x = \partial\mathcal{F}/\partial\tilde{a}_x$ , and  $\mathcal{F}_y = \partial\mathcal{F}/\partial\tilde{a}_y$ . From these equations we find immediately with  $2\tilde{a}'_x - \tilde{a}'_y = 0$ :

$$2\tilde{a}_x - \tilde{a}_y = C \tag{36}$$

with  $C$  a constant. As the constants  $t_x, t_y$  must satisfy the condition  $t_x + 2t_y = \Delta_r$ , the solution  $\tilde{a}_x, \tilde{\varphi}_x, \tilde{a}_y, \tilde{\varphi}_y$  depends on two free parameters, a choice could be  $t_x, C$ .

## VI. SELECTING THE CANONICAL TRANSFORMATION

In this section we search in the space  $(\tilde{a}_x, \tilde{\varphi}_x, \tilde{a}_y, \tilde{\varphi}_y)$  the solution of  $\tilde{a}'_x = 0, \tilde{\varphi}'_x = 0, \tilde{a}'_y = 0, \tilde{\varphi}'_y = 0$ . The canonical equations then read

$$\begin{aligned}
0 &= \frac{\partial\tilde{H}_{s1}}{\partial\tilde{\varphi}_x} = -\Lambda\sqrt{\tilde{a}_x\tilde{a}_y}\sin[\tilde{\varphi}_x + 2\tilde{\varphi}_y], \\
0 &= \frac{\partial\tilde{H}_{s1}}{\partial\tilde{a}_x} = \Lambda\frac{1}{2\sqrt{\tilde{a}_x}}\tilde{a}_y\cos[\tilde{\varphi}_x + 2\tilde{\varphi}_y] + \frac{t_x}{2} + \mathcal{F}_x, \\
0 &= \frac{\partial\tilde{H}_{s1}}{\partial\tilde{\varphi}_y} = -2\Lambda\sqrt{\tilde{a}_x\tilde{a}_y}\sin[\tilde{\varphi}_x + 2\tilde{\varphi}_y], \\
0 &= \frac{\partial\tilde{H}_{s1}}{\partial\tilde{a}_y} = \Lambda\sqrt{\tilde{a}_x}\cos[\tilde{\varphi}_x + 2\tilde{\varphi}_y] + \frac{t_y}{2} + \mathcal{F}_y.
\end{aligned} \tag{37}$$

The equations 37-1, 37-3 are satisfied for

$$\sin[\tilde{\varphi}_x + 2\tilde{\varphi}_y] = 0, \tag{38}$$

that is for  $\tilde{\varphi}_x + 2\tilde{\varphi}_y = \pi M$ , with  $M = 0, 1$ . The other 2 equations become

$$\begin{aligned}
0 &= \Lambda\frac{1}{2\sqrt{\tilde{a}_x}}\tilde{a}_y(-1)^M + \frac{t_x}{2} + \mathcal{F}_x, \\
0 &= \Lambda\sqrt{\tilde{a}_x}(-1)^M + \frac{t_y}{2} + \mathcal{F}_y.
\end{aligned} \tag{39}$$



From the condition  $t_x + 2t_y = \Delta_r$  we can eliminate  $t_x$  and we get the system

$$\begin{cases} 0 = \Lambda \frac{1}{2\sqrt{\tilde{a}_x}} \tilde{a}_y (-1)^M + \frac{\Delta_r}{2} - t_y + \mathcal{F}_x \\ 0 = \Lambda \sqrt{\tilde{a}_x} (-1)^M + \frac{t_y}{2} + \mathcal{F}_y. \end{cases} \quad (40)$$

This system can be solved in  $\tilde{a}_x, \tilde{a}_y$ , from which we find also  $C$  through Eq. 36. We have therefore established the correspondence

$$t_y \longrightarrow (\tilde{a}_x, \tilde{a}_y, t_x, C), \quad (41)$$

which means that all the solutions of Eqs. 39 are on a 1-dimensional curve in the plane  $(\tilde{a}_x, \tilde{a}_y)$ . This 1-dimensional curve can be expressed as a function of  $\tilde{a}_x, \tilde{a}_y$ , without any reference to  $t_x, t_y, C$ , and together with the phase relation one gets

$$\begin{cases} 0 = \Lambda (-1)^M \left[ \frac{\tilde{a}_y}{2\sqrt{\tilde{a}_x}} + 2\sqrt{\tilde{a}_x} \right] + \frac{\Delta_r}{2} + \mathcal{F}_x + 2\mathcal{F}_y \\ \tilde{\varphi}_x + 2\tilde{\varphi}_y = \pi M. \end{cases} \quad (42)$$

The significance of this equation is the following: for any pair  $(\tilde{a}_x, \tilde{a}_y)$  that satisfies Eq. 42 (top) there exists an associated canonical transformation characterized by the pair  $(t_x, t_y)$  obtained from Eqs. 39. In the new coordinates identified by  $(t_x, t_y)$  the pair  $(\tilde{a}_x, \tilde{a}_y)$  joined with  $\tilde{\varphi}_x + 2\tilde{\varphi}_y = \pi M$  solves Eq. 37, i.e. in the system of coordinates identified by  $(t_x, t_y)$ ,  $(\tilde{a}_x, \tilde{a}_y)$  are constant. Therefore all the  $(\tilde{a}_x, \tilde{a}_y)$  satisfying Eq. 42 are all possible stationary solutions of Eq. 37 (for the correspondent canonical transformations). The set of these solutions  $(\tilde{a}_x, \tilde{a}_y)$  is a 1 dimensional curve (or a collection of 1 dimensional curves for complicated  $\mathcal{F}_x, \mathcal{F}_y$  dependencies).

### A. The fix-line

Next we discuss the meaning of the solution  $\tilde{a}'_x = 0, \tilde{\varphi}'_x = 0, \tilde{a}'_y = 0, \tilde{\varphi}'_y = 0$ . As  $\tilde{\varphi}'_x = \tilde{\varphi}'_y = 0$  we get

$$\begin{aligned} \tilde{\varphi}_x &= \tilde{\varphi}_{x,0}, \\ \tilde{\varphi}_y &= \tilde{\varphi}_{y,0}, \end{aligned} \quad (43)$$

and returning back to the coordinates of the Hamiltonian  $H_{s1}$  (Eq. 20, there written without  $\mathcal{F}$ ) we find

$$\begin{aligned} \varphi_x &= \tilde{\varphi}_{x,0} - t_x \theta, \\ \varphi_y &= \tilde{\varphi}_{y,0} - t_y \theta, \end{aligned} \quad (44)$$

with  $\tilde{\varphi}_{x,0} + 2\tilde{\varphi}_{y,0} = \pi M$ , resulting for the coordinates of Eqs. 11

$$\begin{aligned} x &= \sqrt{\beta_x a_x} \cos[(Q_x - t_x)\theta + \tilde{\varphi}_{x,0}], \\ x' &= -(Q_x - t_x) \sqrt{\beta_x a_x} \sin[(Q_x - t_x)\theta + \tilde{\varphi}_{x,0}], \\ y &= \sqrt{\beta_y a_y} \cos[(Q_y - t_y)\theta + \tilde{\varphi}_{y,0}], \\ y' &= -(Q_y - t_y) \sqrt{\beta_y a_y} \sin[(Q_y - t_y)\theta + \tilde{\varphi}_{y,0}]. \end{aligned} \quad (45)$$

We will next prove that the points of this trajectory at a given longitudinal position (for example at  $\theta = 0$ ) lie on a one dimensional closed curve that we call fix-line. The proof of this follows:

By using the conditions  $\tilde{\varphi}_x + 2\tilde{\varphi}_y = \pi M$ ,  $t_x + 2t_y = \Delta_r$ , and Eq. 16, it is straightforward to find that

$$(Q_x - t_x)\theta + \tilde{\varphi}_{x,0} + 2[(Q_y - t_y)\theta + \tilde{\varphi}_{y,0}] = N\theta + \pi M. \quad (46)$$

The Poincaré surface of section is identified by the condition  $\theta = 2\pi\mathcal{N}$  with  $\mathcal{N}$  an integer correspondent to the  $\mathcal{N}$ -th turn. Next we limit the discussion to the  $x, y$  coordinates without losing generality. By using Eq. 45, we find that on the Poincaré surface of section the coordinates  $x, y$  at the turn  $\mathcal{N}$  become

$$\begin{aligned} x_{\mathcal{N}} &= \sqrt{\beta_x a_x} \cos[(Q_x - t_x)2\pi\mathcal{N} + \tilde{\varphi}_{x,0}], \\ y_{\mathcal{N}} &= \sqrt{\beta_y a_y} \cos[(Q_y - t_y)2\pi\mathcal{N} + \tilde{\varphi}_{y,0}], \end{aligned} \quad (47)$$

and using Eq. 46 we find

$$\begin{aligned} x_{\mathcal{N}} &= \sqrt{\beta_x a_x} \cos[-2(Q_y - t_y)2\pi\mathcal{N} \\ &\quad - 2\tilde{\varphi}_{y,0} + \pi M + N2\pi\mathcal{N}], \\ y_{\mathcal{N}} &= \sqrt{\beta_y a_y} \cos[(Q_y - t_y)2\pi\mathcal{N} + \tilde{\varphi}_{y,0}], \end{aligned} \quad (48)$$

with  $\tilde{\varphi}_{y,0}$  as an initial phase that sets the starting point. Therefore we reach the result that the coordinates  $x, y$  of Eq 45, on a surface of the Poincaré section, can be parameterized (ignoring multiples of  $2\pi$ ) as

$$\begin{aligned} x_t &= \sqrt{\beta_x a_x} \cos(-2t + \pi M), \\ y_t &= \sqrt{\beta_y a_y} \cos(t), \end{aligned} \quad (49)$$

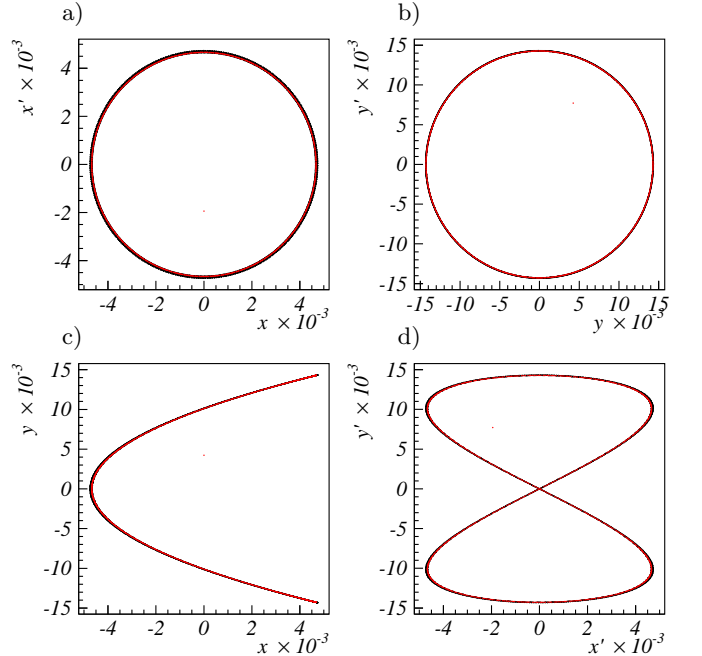


FIG. 15: The fix-line as predicted by the theory (red dots) and by simulations (black dots). Pictures a), b) circular shape shows that  $\tilde{a}_x, \tilde{a}_y$  are constant.

where  $a_x, a_y$  must satisfy Eq. 42 (top), and  $0 < t < 2\pi$  is here a variable that parameterizes the curve. Therefore the coordinates  $x, y$  of the solution in Eq. 45 are always found on the curve expressed by Eq. 49. The same argument applies to any other pairs of coordinates of Eq 45. We therefore find that at a given longitudinal position the trajectory Eq 45 lies on a closed curve. This curve is invariant in its shape, and each point in this curve is mapped after one turn again on the same curve, for this reason this curve is called fix-line, which is a generalization of the fix-point for 1D stable resonances. In Fig. 15 we compare the fix-line as predicted by the theory (red dots) with simulation results (black dots). The figure shows 4 pictures for the planes,  $x - x', y - y', x - y$ , and  $x' - y'$ . It is clearly visible that for the variables  $x, y$ , and  $x' - y'$  the shape is that one predicted from the theory. However, the planes  $x - x', y - y'$  exhibits

a circular shape showing that  $\tilde{a}_x, \tilde{a}_y$  are constant! The simulations are obtained by exciting a single harmonics, and  $Q_x = 1.324, Q_y = 1.84, \Delta_r = 4.64 \times 10^{-3}$ , and  $\Lambda = -7.444 \times 10^{-3} \text{ m}^{-1}$ .

## B. Stability

We consider here a particle slightly displaced from the stationary solution of Eqs. 37 (this solution is the fix-line) of the amount  $\delta\tilde{a}_x, \delta\tilde{a}_y, \delta\tilde{\varphi}_x, \delta\tilde{\varphi}_y$ . In order to obtain the equation of motion of the perturbation we expand equations 35 in  $\delta\tilde{a}_x, \delta\tilde{a}_y, \delta\tilde{\varphi}_x, \delta\tilde{\varphi}_y$ , and keep the first order only. The canonical equations of the perturbation take the form (properly re-arranged)

$$\begin{aligned}\delta\tilde{a}'_x &= -2\frac{\partial^2\tilde{H}_{s1}}{\partial\tilde{\varphi}_x\partial\tilde{a}_x}\delta\tilde{a}_x - 2\frac{\partial^2\tilde{H}_{s1}}{\partial\tilde{\varphi}_x\partial\tilde{a}_y}\delta\tilde{a}_y - 2\frac{\partial^2\tilde{H}_{s1}}{\partial\tilde{\varphi}_x^2}\delta\tilde{\varphi}_x - 2\frac{\partial^2\tilde{H}_{s1}}{\partial\tilde{\varphi}_x\partial\tilde{\varphi}_y}\delta\tilde{\varphi}_y, \\ \delta\tilde{a}'_y &= -2\frac{\partial^2\tilde{H}_{s1}}{\partial\tilde{\varphi}_y\partial\tilde{a}_x}\delta\tilde{a}_x - 2\frac{\partial^2\tilde{H}_{s1}}{\partial\tilde{\varphi}_y\partial\tilde{a}_y}\delta\tilde{a}_y - 2\frac{\partial^2\tilde{H}_{s1}}{\partial\tilde{\varphi}_y\partial\tilde{\varphi}_x}\delta\tilde{\varphi}_x - 2\frac{\partial^2\tilde{H}_{s1}}{\partial\tilde{\varphi}_y^2}\delta\tilde{\varphi}_y, \\ \delta\tilde{\varphi}'_x &= 2\frac{\partial^2\tilde{H}_{s1}}{\partial\tilde{a}_x^2}\delta\tilde{a}_x + 2\frac{\partial^2\tilde{H}_{s1}}{\partial\tilde{a}_x\partial\tilde{a}_y}\delta\tilde{a}_y + 2\frac{\partial^2\tilde{H}_{s1}}{\partial\tilde{a}_x\partial\tilde{\varphi}_x}\delta\tilde{\varphi}_x + 2\frac{\partial^2\tilde{H}_{s1}}{\partial\tilde{a}_x\partial\tilde{\varphi}_y}\delta\tilde{\varphi}_y, \\ \delta\tilde{\varphi}'_y &= 2\frac{\partial^2\tilde{H}_{s1}}{\partial\tilde{a}_y\partial\tilde{a}_x}\delta\tilde{a}_x + 2\frac{\partial^2\tilde{H}_{s1}}{\partial\tilde{a}_y^2}\delta\tilde{a}_y + 2\frac{\partial^2\tilde{H}_{s1}}{\partial\tilde{a}_y\partial\tilde{\varphi}_x}\delta\tilde{\varphi}_x + 2\frac{\partial^2\tilde{H}_{s1}}{\partial\tilde{a}_y\partial\tilde{\varphi}_y}\delta\tilde{\varphi}_y,\end{aligned}\tag{50}$$

where the slowly varying Hamiltonian is given by Eq. 34. Any term that has only one derivative with respect to  $\tilde{\varphi}_x, \tilde{\varphi}_y$  yields zero because that term is proportional to  $\sin[\tilde{\varphi}_x + 2\tilde{\varphi}_y]$ , which is zero on the fix-line. Therefore we get

$$\begin{aligned}\delta\tilde{a}'_x &= -2\frac{\partial^2\tilde{H}_{s1}}{\partial\tilde{\varphi}_x^2}\delta\tilde{\varphi}_x - 2\frac{\partial^2\tilde{H}_{s1}}{\partial\tilde{\varphi}_x\partial\tilde{\varphi}_y}\delta\tilde{\varphi}_y, \\ \delta\tilde{a}'_y &= -2\frac{\partial^2\tilde{H}_{s1}}{\partial\tilde{\varphi}_y\partial\tilde{\varphi}_x}\delta\tilde{\varphi}_x - 2\frac{\partial^2\tilde{H}_{s1}}{\partial\tilde{\varphi}_y^2}\delta\tilde{\varphi}_y, \\ \delta\tilde{\varphi}'_x &= 2\frac{\partial^2\tilde{H}_{s1}}{\partial\tilde{a}_x^2}\delta\tilde{a}_x + 2\frac{\partial^2\tilde{H}_{s1}}{\partial\tilde{a}_x\partial\tilde{a}_y}\delta\tilde{a}_y, \\ \delta\tilde{\varphi}'_y &= 2\frac{\partial^2\tilde{H}_{s1}}{\partial\tilde{a}_y\partial\tilde{a}_x}\delta\tilde{a}_x + 2\frac{\partial^2\tilde{H}_{s1}}{\partial\tilde{a}_y^2}\delta\tilde{a}_y.\end{aligned}\tag{51}$$

We define for convenience

$$\begin{aligned}\lambda &= 2\frac{\partial^2\tilde{H}_{s1}}{\partial\tilde{\varphi}_x^2} = 2\frac{1}{2}\frac{\partial^2\tilde{H}_{s1}}{\partial\tilde{\varphi}_x\partial\tilde{\varphi}_y} = 2\frac{1}{4}\frac{\partial^2\tilde{H}_{s1}}{\partial\tilde{\varphi}_y^2}, \\ A_{xx} &= 2\frac{\partial^2\tilde{H}_{s1}}{\partial\tilde{a}_x^2}, \quad A_{xy} = 2\frac{\partial^2\tilde{H}_{s1}}{\partial\tilde{a}_x\partial\tilde{a}_y}, \\ A_{yx} &= 2\frac{\partial^2\tilde{H}_{s1}}{\partial\tilde{a}_y\partial\tilde{a}_x}, \quad A_{yy} = 2\frac{\partial^2\tilde{H}_{s1}}{\partial\tilde{a}_y^2}.\end{aligned}\tag{52}$$

Therefore we always find that the motion of the perturbation is given by the following system of equations

$$\begin{aligned}\delta\tilde{a}'_x &= -\lambda\delta\tilde{\varphi}_x - 2\lambda\delta\tilde{\varphi}_y, \\ \delta\tilde{a}'_y &= -2\lambda\delta\tilde{\varphi}_x - 4\lambda\delta\tilde{\varphi}_y, \\ \delta\tilde{\varphi}'_x &= A_{xx}\delta\tilde{a}_x + A_{xy}\delta\tilde{a}_y, \\ \delta\tilde{\varphi}'_y &= A_{yx}\delta\tilde{a}_x + A_{yy}\delta\tilde{a}_y,\end{aligned}\tag{53}$$

which after some algebra becomes

$$\begin{aligned}\delta\tilde{a}''_x &= -\omega^2\delta\tilde{a}_x + \lambda(A_{xy} + 2A_{yy})C_p, \\ \delta\tilde{a}''_y &= -\omega^2\delta\tilde{a}_y - \lambda(A_{xx} + 2A_{yx})C_p, \\ \delta\tilde{\varphi}''_x &= -\lambda(A_{xx} + 2A_{xy})(\delta\tilde{\varphi}_x + 2\delta\tilde{\varphi}_y), \\ \delta\tilde{\varphi}''_y &= -\lambda(A_{xy} + 2A_{yy})(\delta\tilde{\varphi}_x + 2\delta\tilde{\varphi}_y),\end{aligned}\tag{54}$$

where we defined

$$\omega^2 = \lambda(A_{xx} + 2A_{yx} + 2A_{xy} + 4A_{yy}).\tag{55}$$

The coefficient  $C_p$  is a constant obtained from integrating Eqs. 53, we call it  $C_p$  with index  $p$  as we refer to the perturbation around the fix-line.

The value of  $C_p$  depends on the initial condition of the perturbation  $\delta\tilde{a}_x, \delta\tilde{a}_y, \delta\tilde{\varphi}_x, \delta\tilde{\varphi}_y$ . From Eq. 53 we find

$$2\delta\tilde{a}_x = \delta\tilde{a}_y + C_p.\tag{56}$$

We also find

$$(\delta\tilde{\varphi}_x + 2\delta\tilde{\varphi}_y)'' = -\omega^2(\delta\tilde{\varphi}_x + 2\delta\tilde{\varphi}_y). \quad (57)$$

We conclude that for

$$\omega^2 > 0 \quad (58)$$

the motion of  $\delta\tilde{a}_x, \delta\tilde{a}_y$ , and  $\delta\tilde{\varphi}_x + 2\delta\tilde{\varphi}_y$  is stable. The evolution of  $\delta\tilde{\varphi}_x, \delta\tilde{\varphi}_y$  instead is not bounded if  $C_p \neq 0$  as a term linear in  $\theta$  appears in the solution of the equation of motion. The derivation of the solution is reported in Appendix A. An interesting consequence in the case of  $C_p \neq 0$  is that there exists a neighbouring fix-line identified by  $\tilde{a}_x^c, \tilde{a}_y^c$ , and a point on it  $\tilde{a}_x^c, \tilde{a}_y^c, \tilde{\varphi}_x^c, \tilde{\varphi}_y^c$ , so that the initial perturbation assumes values  $(\delta\tilde{a}_x)_1, (\delta\tilde{a}_y)_1, (\delta\tilde{\varphi}_x)_1, (\delta\tilde{\varphi}_y)_1$ , and  $C_p' = 2(\delta\tilde{a}_x)_1 - (\delta\tilde{a}_y)_1 = 0$ . That means that the initial perturbation oscillates now around the new fix-line point. The proof of this result is shown in the Appendix A.

## VII. EQUATION OF MOTION WITH THE RESONANT TERM ONLY

We discuss the fix-lines for the simplified case of  $\mathcal{F} = 0$ , i.e. in absence of detuning induced by other nonlinearities like space charge, or strong nonlinear components due to magnets. The equation of stationary solutions reads (see Eq. 40 with  $\mathcal{F}_x = \mathcal{F}_y = 0$ )

$$\begin{cases} 0 = \Lambda \frac{1}{2\sqrt{\tilde{a}_x}} \tilde{a}_y (-1)^M + \frac{\Delta_r}{2} - t_y \\ 0 = \Lambda \sqrt{\tilde{a}_x} (-1)^M + \frac{t_y}{2}. \end{cases} \quad (59)$$

We remind here for convenience that  $\Delta_r = Q_x + 2Q_y$ . Adding the second equation multiplied by 2 to the first one  $t_y$  can be eliminated and we obtain

$$0 = \Delta_r \Lambda (-1)^M \left[ \frac{1}{2\sqrt{\tilde{a}_x}} \tilde{a}_y + 2\sqrt{\tilde{a}_x} \right] + \frac{\Delta_r^2}{2}. \quad (60)$$

Therefore if the solutions  $\tilde{a}_x, \tilde{a}_y$  exists, it also holds

$$\Delta_r \Lambda (-1)^M \leq 0, \quad (61)$$

which puts a constraints on  $t_x, t_y$  as follows

$$\begin{cases} 0 = \Delta_r \Lambda \frac{1}{2\sqrt{\tilde{a}_x}} \tilde{a}_y (-1)^M + \Delta_r \frac{t_x}{2} \\ 0 = \Delta_r \Lambda \sqrt{\tilde{a}_x} (-1)^M + \Delta_r \frac{t_y}{2} \end{cases} \rightarrow \begin{cases} \Delta_r t_x \geq 0 \\ \Delta_r t_y \geq 0 \end{cases} \quad (62)$$

As a consequence if the solution exists, then it must be

$$\Delta_r^2 \geq \Delta_r t_x \geq 0. \quad (63)$$

In that case we can parameterize  $(t_x, t_y)$  as follows

$$t_x = \tau \Delta_r, \quad t_y = \frac{\Delta_r}{2} (1 - \tau), \quad (64)$$

with  $0 \leq \tau \leq 1$  and the solutions for the fix-lines take the form

$$\begin{cases} \tilde{a}_x = \frac{\Delta_r^2}{16\Lambda^2} (1 - \tau)^2 \\ \tilde{a}_y = \frac{\Delta_r^2}{4\Lambda^2} \tau (1 - \tau) \end{cases} \quad (65)$$

At this point, as a last step, it should be checked if the solution really exists. Substituting the previous equations into Eq. 60 we find that the solution exists as long as

$$\frac{\Lambda}{|\Lambda|} \frac{\Delta_r}{|\Delta_r|} (-1)^M + 1 = 0, \quad (66)$$

which can be satisfied only if  $\Lambda \Delta_r (-1)^M < 0$ . Our analysis shows that in proximity of the coupled 3rd order resonance there exist an infinite number of fix-lines.

### A. Analysis of the stability around the fix-line

By using Eqs. 62, the stability coefficients of Eqs. 52 are

$$\begin{aligned} A_{xx} &= -2\Lambda \frac{1}{4} \tilde{a}_x^{-3/2} \tilde{a}_y (-1)^M = \frac{t_x}{2\tilde{a}_x}, \\ A_{xy} &= A_{yx} = 2\Lambda \frac{1}{2} \tilde{a}_x^{-1/2} (-1)^M = -\frac{t_x}{\tilde{a}_y}, \\ A_{yy} &= 0, \\ \lambda &= -2\Lambda \sqrt{\tilde{a}_x} \tilde{a}_y (-1)^M = \tilde{a}_y t_y, \end{aligned} \quad (67)$$

where we have used the relation Eqs. 37 on the fix-line for  $\mathcal{F} = 0$ . After some algebra we find  $\omega^2 = t_x^2 - 4t_x t_y$ , which, in terms of the parametrization of the fix-line, becomes

$$\omega^2 = \Delta_r^2 \tau (3\tau - 2). \quad (68)$$

This equation shows that with  $\tau > 2/3$ ,  $\omega^2$  is positive, hence Eqs. 54 yields stable motion, whereas for  $\tau < 2/3$ ,  $\omega^2$  is negative which means that the motion is unstable.

Therefore this analysis shows that with  $\tau > 2/3$  a fix-line is stable.

The situation is summarized in Fig. 16 top, where the collection of all fix-lines is represented. The point of merging of the stable with the unstable fix-line has  $\omega^2 = 0$  and that corresponds to  $\tau = 2/3$ .

Figure 16 bottom shows the comparison of the oscillation of an initial condition slightly off a fix-line. It is evident that the center of oscillation is not  $(0, 0)$  because  $2\delta\tilde{a}_x \neq \delta\tilde{a}_y$  (hence  $C_p \neq 0$ ). The red curve is drawn from the theoretical model by fitting the amplitude, however, the wavelength is given by  $\omega$ . The parameters of the simulations are the same as for Fig. 15, namely,  $\Delta_r = 4.64 \times 10^{-3}$ ,  $\Lambda = -7.444 \times 10^{-3} \text{ m}^{-1}$ . The fix-line is taken for  $\tau = 0.7$ , which implies  $t_x = 3.248 \times 10^{-3}$ , and  $t_y = 6.960 \times 10^{-4}$ .

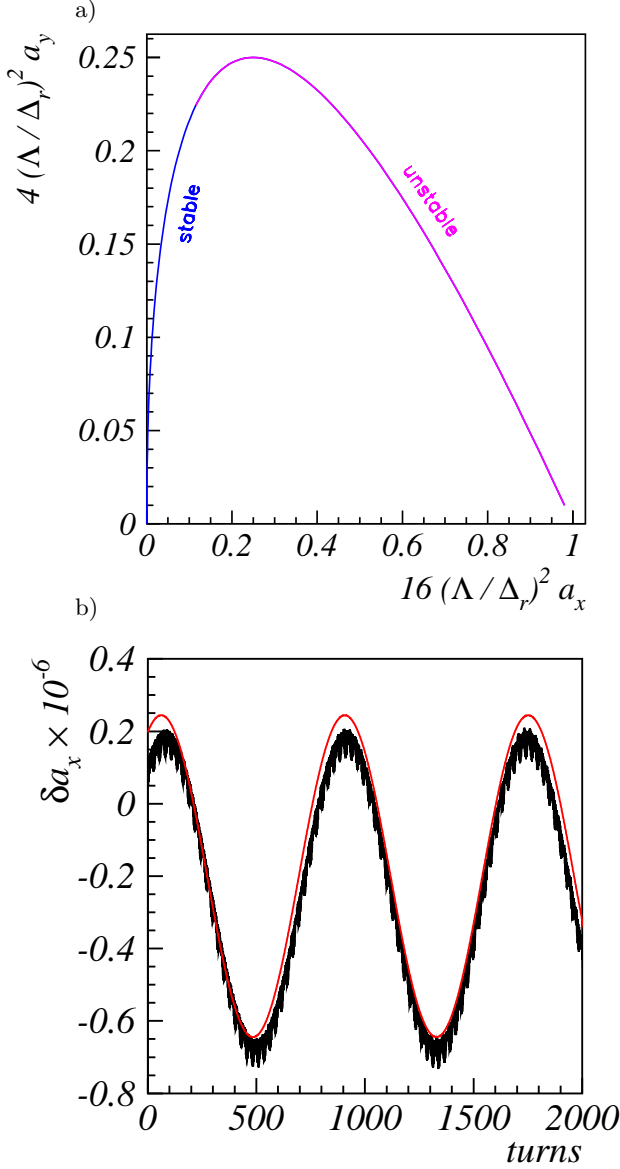


FIG. 16: On the top are shown the set of stable and unstable fix-lines. The bottom picture shows the oscillations of  $\tilde{a}_x$  around the fix-line value. In this example  $C_p \neq 0$ , hence the oscillation of the perturbation  $\delta\tilde{a}_x$ , is not centered around zero, i.e. on the unperturbed fix-line. The center of oscillation  $\delta\tilde{a}_x^c$  is located in this example at  $-0.2 \times 10^{-6}$ . The black curve is obtained from computer simulation of the accelerator model, while the red curve is obtained from the theory. The wavelength of the red curve is obtained from Eq. 68.

### VIII. STABILITY OF MOTION

We make use of the properties of the equations of motion Eqs. 35. In particular of the invariant  $2\tilde{a}_x - \tilde{a}_y = C$  (Eq. 36). By using it, we can drop one of the two equa-

tions of Eqs. 35, and summing the other two we get

$$\begin{aligned} -\tilde{a}'_x &= -2\Lambda\sqrt{\tilde{a}_x}(2\tilde{a}_x - C)\sin[\tilde{\varphi}_x + 2\tilde{\varphi}_y], \\ \tilde{\varphi}'_x + 2\tilde{\varphi}'_y &= 2\Lambda\frac{1}{2\sqrt{\tilde{a}_x}}(2\tilde{a}_x - C)\cos[\tilde{\varphi}_x + 2\tilde{\varphi}_y] + \\ &\quad + 4\Lambda\sqrt{\tilde{a}_x}\cos[\tilde{\varphi}_x + 2\tilde{\varphi}_y] + \Delta_r + 2\mathcal{F}_x + 4\mathcal{F}_y. \end{aligned} \quad (69)$$

These equations show that the natural variable for the system is  $\Omega = \tilde{\varphi}_x + 2\tilde{\varphi}_y$ , and the equations become

$$\begin{aligned} -\tilde{a}'_x &= -2\Lambda\sqrt{\tilde{a}_x}(2\tilde{a}_x - C)\sin[\Omega], \\ \Omega' &= \Lambda\left[\frac{1}{\sqrt{\tilde{a}_x}}(2\tilde{a}_x - C) + 4\sqrt{\tilde{a}_x}\right]\cos[\Omega] + \\ &\quad + \Delta_r + 2\mathcal{F}_x + 4\mathcal{F}_y. \end{aligned} \quad (70)$$

For the case in which we take only the resonant term we have  $\mathcal{F}_x = \mathcal{F}_y = 0$ , and the equations take the form

$$\begin{aligned} \tilde{a}'_x &= 2\Lambda\sqrt{\tilde{a}_x}(2\tilde{a}_x - C)\sin[\Omega], \\ \Omega' &= \Lambda\left[\frac{1}{\sqrt{\tilde{a}_x}}(2\tilde{a}_x - C) + 4\sqrt{\tilde{a}_x}\right]\cos[\Omega] + \Delta_r. \end{aligned} \quad (71)$$

Now consider the function

$$I(\tilde{a}_x, \Omega) = 2\Lambda\sqrt{\tilde{a}_x}(2\tilde{a}_x - C)\cos[\Omega] + \tilde{a}_x\Delta_r, \quad (72)$$

and note that

$$\begin{aligned} \frac{\partial I}{\partial \tilde{a}_x} &= \Lambda\left[\frac{1}{\sqrt{\tilde{a}_x}}(2\tilde{a}_x - C) + 4\sqrt{\tilde{a}_x}\right]\cos[\Omega] + \Delta_r = \Omega', \\ \frac{\partial I}{\partial \Omega} &= -2\Lambda\sqrt{\tilde{a}_x}(2\tilde{a}_x - C)\sin[\Omega] = -\tilde{a}'_x. \end{aligned} \quad (73)$$

Therefore we find

$$\frac{dI}{d\theta} = \frac{\partial I}{\partial \tilde{a}_x}\tilde{a}'_x + \frac{\partial I}{\partial \Omega}\Omega' = \Omega'\tilde{a}'_x + (-\tilde{a}'_x)\Omega' = 0. \quad (74)$$

That means that  $I(\tilde{a}_x, \Omega)$  is an invariant of motion and the trajectories of particles are set by the value of the invariant (that we call  $I_0$ ). By using  $I(\tilde{a}_x, \Omega)$  it is possible to discuss the stability of the motion of particles. In fact given the initial conditions of  $\tilde{a}_x, \tilde{a}_y, \Omega$  we find  $C$  from the relation  $2\tilde{a}_x - \tilde{a}_y = C$ , hence we find the value of the invariant  $I_0 = I(\tilde{a}_x, \Omega)$ . The trajectory of that particle is then given by the set  $\Gamma_{I_0} = \{(\tilde{a}_x, \Omega) : I(\tilde{a}_x, \Omega) = I_0\}$ . We observe that if the trajectory extends up to infinity, it means that  $\tilde{a}_x \rightarrow \infty$ , hence  $\tilde{a}_y \rightarrow \infty$ , while  $0 \leq \Omega \leq 2\pi$ . In this situation the first term of Eq. 72 diverges as  $4\Lambda\tilde{a}_x^{3/2}\cos[\Omega]$ , and this divergence is faster than the one of the second term, which diverges as  $\tilde{a}_x\Delta_r$ . That means that  $\Omega$  must change accordingly for keeping unchanged the value of the invariant, therefore for  $\tilde{a}_x \rightarrow \infty$  we find  $\Omega \rightarrow \pi/2 + n\pi$ , with  $n$  an integer.

We observe that the function  $I = I(\tilde{a}_x, \Omega)$  defines a function  $\tilde{a}_x = \tilde{a}_x(\Omega)$ , which has the following property:

if  $\Omega = 2\pi n$  ( $n$  is an integer) and  $\tilde{a}_x$  is not a fix-line, then  $\frac{d\tilde{a}_x}{d\Omega} = 0$ . In fact, as  $I$  is an invariant,  $dI/d\Omega = 0$ , but

$$\frac{dI}{d\Omega} = \frac{\partial I}{\partial \tilde{a}_x} \frac{d\tilde{a}_x}{d\Omega} + \frac{\partial I}{\partial \Omega} \quad (75)$$

that is

$$\frac{dI}{d\Omega} = \Omega' \frac{d\tilde{a}_x}{d\Omega} - \tilde{a}'_x = 0. \quad (76)$$

Therefore for  $\Omega = \pi n$  it holds  $\sin[\Omega] = 0$ , hence from Eqs. 70, we find  $\tilde{a}'_x = 0$ . On the other hand, if  $\tilde{a}_x, \Omega$  is not a fix-line then  $\Omega' \neq 0$  (because  $\tilde{\varphi}'_x = \tilde{\varphi}'_y = 0$  is the condition for finding a fix-line). Therefore if  $\Omega = 2\pi n$ , and  $\tilde{a}_x$  is not a fix-line then

$$\frac{d\tilde{a}_x}{d\Omega} = 0. \quad (77)$$

This property tells us that the implicit functions  $\tilde{a}_x = \tilde{a}_x(\Omega)$  defined by  $I = I(\tilde{a}_x, \Omega)$  are periodic in  $\Omega$  and at the periodicity they merge smoothly (that is the first order derivative in  $\Omega$  is zero at  $\Omega = 2\pi n$ ).

As the fix-lines are described by Eqs. 65 we will consider the following scaling

$$\begin{cases} \tilde{a}_x = \frac{\Delta_r^2}{16\Lambda^2} \hat{a}_x \\ \tilde{a}_y = \frac{\Delta_r^2}{16\Lambda^2} \hat{a}_y \end{cases} \quad (78)$$

The relation  $2\tilde{a}_x = \tilde{a}_y + C$  becomes

$$2\hat{a}_x = \hat{a}_y + \frac{16\Lambda^2}{\Delta_r^2} C. \quad (79)$$

It is convenient to define the parameter

$$\xi = \frac{16\Lambda^2}{\Delta_r^2} \frac{C}{2} \quad (80)$$

so that we obtain the relation  $2\hat{a}_x - \hat{a}_y = 2\xi$ . The invariant  $I$  defined in Eq. 72 rescaled in the “normalized coordinates”  $\hat{a}_x, \hat{a}_y$  reads

$$\hat{I} = \frac{I 16\Lambda^2}{\Delta_r^3} = \mu \sqrt{\hat{a}_x} (\hat{a}_x - \xi) \cos \Omega + \hat{a}_x, \quad (81)$$

with

$$\mu = \frac{\Lambda}{|\Lambda|} \frac{|\Delta_r|}{\Delta_r}. \quad (82)$$

This relation satisfies the relation  $\mu^2 = 1$ . Note that, as  $2\hat{a}_x - \hat{a}_y = 2\xi$  it follows that  $\hat{a}_x$  must simultaneously satisfy the following conditions

$$\begin{cases} \hat{a}_x \geq 0 \\ \hat{a}_x \geq \xi \end{cases} \quad (83)$$

which express simply the condition  $\hat{a}_x \geq 0, \hat{a}_y \geq 0$  intrinsic in the definition of  $\hat{a}_x, \hat{a}_y$ . In addition we observe that all the possible curves  $\hat{I}(\hat{a}_x, \Omega) = \text{const.}$  never intercept.

The trajectories can be found from  $\Omega$  as function of  $\hat{a}_x$  inverting the Eq. 81, obtaining

$$\cos[\Omega] = \mu \frac{1}{\sqrt{\hat{a}_x}} \frac{\hat{I} - \hat{a}_x}{\hat{a}_x - \xi}, \quad (84)$$

where we used the property  $\mu^2 = 1$  (from Eq. 82). To study this equation we make use of an auxiliary function defined as

$$\mathcal{Y}(\hat{a}_x) = -\mu \cos[\Omega] = -\frac{1}{\sqrt{\hat{a}_x}} \frac{\hat{I} - \hat{a}_x}{\hat{a}_x - \xi}. \quad (85)$$

This function is defined in the plane  $\hat{a}_x, \mathcal{Y}$ , which is the plane about which we will discuss next. Note that  $\xi$  is here a constant of motion defined by the initial conditions. Hence by varying  $\hat{I}$  we identify a specific level line of the invariant. If  $-1 \leq \mathcal{Y} \leq 1$  then  $\mathcal{Y} = -\mu \cos[\Omega]$  can be solved and we find  $\Omega$ ; if  $\mathcal{Y} < -1$  or  $1 < \mathcal{Y}$  then  $\mathcal{Y} = -\mu \cos[\Omega]$  cannot be solved so that these values of  $\mathcal{Y}$  are not acceptable.

#### A. Fix-lines and invariants

Next we prove the following property: consider a level line identified by  $\hat{I}$ , of the form  $\mathcal{Y} = \mathcal{Y}(\hat{a}_x, \hat{I}, \xi)$  defined by Eq. 85. If this curve is tangent to the line  $\mathcal{Y} = 1$  (in the plane  $\hat{a}_x, \mathcal{Y}$ ) then the tangent point  $(\hat{a}_x, \mathcal{Y})$  identifies a fix-line.

Proof: Firstly, we observe that Eq. 81 is simply a rewrite of the Hamiltonian, from which we can obtain the equations of motion as

$$-\hat{a}'_x = \Delta_r \frac{\partial \hat{I}}{\partial \Omega}, \quad \Omega' = \Delta_r \frac{\partial \hat{I}}{\partial \hat{a}_x}. \quad (86)$$

The function  $\mathcal{Y} = \mathcal{Y}(\hat{a}_x)$  is an implicit function of the form  $\hat{I} = \hat{I}(\hat{a}_x, \mathcal{Y}(\hat{a}_x), \xi)$  with  $\hat{I} = \text{const.}$  Therefore

$$\frac{d}{d\hat{a}_x} \hat{I}(\hat{a}_x, \mathcal{Y}(\hat{a}_x), \xi) = \frac{\partial \hat{I}}{\partial \hat{a}_x} + \frac{\partial \hat{I}}{\partial \mathcal{Y}} \frac{d\mathcal{Y}}{d\hat{a}_x} = 0. \quad (87)$$

If for  $\hat{a}_x$  the level line  $\mathcal{Y} = \mathcal{Y}(\hat{a}_x)$  is tangent to a horizontal line, then we have  $d\mathcal{Y}(\hat{a}_x)/d\hat{a}_x = 0$ . This applied in Eq. 87 implies that on the tangent point one finds

$$\frac{\partial \hat{I}}{\partial \hat{a}_x}(\hat{a}_x, \mathcal{Y}(\hat{a}_x), \xi) = 0, \quad (88)$$

which via the second part of the Eqs. 86 yields  $\Omega' = 0$  (or  $\mathcal{Y}' = 0$ ). Secondly, we use the condition that  $\mathcal{Y} = \mathcal{Y}(\hat{a}_x)$  is tangent to  $\mathcal{Y} = 1$ ; that means that  $\cos[\Omega] = -\mu$ , i.e.  $\sin[\Omega] = 0$ , which yields  $\partial \hat{I} / \partial \Omega = 0$ . Therefore via the first part of Eqs. 86 we find  $\hat{a}'_x = 0$ . If at any time  $\hat{a}'_x = \Omega' = 0$  then it follows that  $\hat{a}_x = \text{const.}, \Omega =$

const., because  $\hat{a}_x, \Omega$  are the canonical variables of the Hamiltonian Eq. 81.

The condition of  $\mathcal{V} = \mathcal{V}(\hat{a}_x)$  being tangent to  $\mathcal{V} = 1$  implies  $\cos[\Omega] = -\mu$ , which we can write as  $\cos[\Omega] = (-1)^M$ , with  $M$  an integer. By using this we find that Eq. 88 is just a reformulation of Eq. 60, which is the equation defining  $\hat{a}_x, \hat{a}_y$  of a fix-line. This equation admits always a solution, in fact the condition  $\mathcal{V} = 1$ , which reads

$$-\frac{|\Lambda|}{\Lambda} \frac{\Delta_r}{|\Delta_r|} (-1)^M = 1, \quad (89)$$

is just the condition of existence of a fix-line Eq. 66.

Therefore the point  $\hat{a}_x$  where  $\mathcal{V} = \mathcal{V}(\hat{a}_x)$  is tangent to the horizontal line  $\mathcal{V} = 1$  identifies a fix-line. As we have already seen this fix-line is parameterized by  $\tau$ , and the relation between  $\tau$  and the fix-line  $\hat{a}_x, \hat{a}_y$  (see Eq. 65) reads

$$\hat{a}_x = (1 - \tau)^2, \quad \hat{a}_y = 4\tau(1 - \tau). \quad (90)$$

For these two values of  $\hat{a}_x, \hat{a}_y$  we find that  $\tilde{\varphi}'_x = \tilde{\varphi}'_y = 0$  (Eqs. 59), and the angles  $\tilde{\varphi}_x, \tilde{\varphi}_y$  have to satisfy the condition  $\tilde{\varphi}_x + 2\tilde{\varphi}_y = M\pi$ . The relation of  $\xi$  to  $\tau$  is

$$\xi = 3\tau^2 - 4\tau + 1. \quad (91)$$

## B. Stability of motion

The stability of a trajectory is characterized by the level lines as follows:

*A particle motion defined by the initial condition  $((\hat{a}_x)_0, \mathcal{V}_0)$  is stable if  $-1 < \mathcal{V}_0 < 1$  and its level line  $(\hat{a}_x, \mathcal{V}(\hat{a}_x))$  crosses both the lines  $\mathcal{V} = 1$  and  $\mathcal{V} = -1$  or twice the same line  $\mathcal{V} = 1$  or  $\mathcal{V} = -1$ . Only in this case the motion is bounded by the periodicity of the coordinate  $\Omega$ .*

We next discuss the properties of stability as a function of  $\xi$ .

### 1. Region $1 < \xi$

Observing part a) of Fig. 17 the red line  $\hat{I} = \xi$  separates two classes of level curves, the curves below the red line go to  $-\infty$  for  $\hat{a}_x$  approaching  $\xi$ ; Appendix B discusses the geometrical properties of these level lines. It is clear that if  $1/\sqrt{\xi} < 1$ , i.e. for  $\xi > 1$ , the red curve that separates the two classes of level lines is located between  $\mathcal{V} = 1$  and  $\mathcal{V} = 0$  so that no particle can be stable. Any pair  $(\hat{a}_x, \mathcal{V})$  chosen in  $\xi < \hat{a}_x$  and  $-1 < \mathcal{V} < 1$  defines a level line that goes to  $\hat{a}_x \rightarrow \infty, \mathcal{V} \rightarrow 0$  without crossing  $\mathcal{V} = \pm 1$ .

### 2. Region $0 < \xi \leq 1$

This case is also illustrated in part a) of Fig. 17. The level line tangent to  $\mathcal{V} = 1$  determines a region dashed

in pink in which every initial  $((\hat{a}_x)_0, \mathcal{V}_0)$  evolves on a level line that is bounded. Specifically as the particle trajectory  $(\hat{a}_x, \mathcal{V})$  cannot exceed  $-1 < \mathcal{V} < 1$ , it follows that the particle bounces back and forth on the lines  $\mathcal{V} = -1$ , and  $\mathcal{V} = 1$  keeping the invariant constant. Particles on the right of the level line tangent  $\mathcal{V} = 1$  cannot be stable. It appears evident that the maximum region of stability, marked by a region of thin red lines is determined by the level line tangent to  $\mathcal{V} = 1$ . As discussed in the previous section, the point tangent to the line  $\mathcal{V} = 1$  is a fix-line. This point is indicated as  $(\hat{a}_x^*)_+$  in part a) of Fig. 17. On the same picture we also find the point  $(\hat{a}_x)_1$ , which marks the region of total stability. This means that for  $\xi < \hat{a}_x < (\hat{a}_x)_1$  particles are stable for any initial phase  $\Omega$ . For  $(\hat{a}_x)_1 < \hat{a}_x < (\hat{a}_x^*)_+$  only particles which have  $\mathcal{V}$  in the proper range (namely  $\Omega$  in the proper interval, see Fig. 22) are stable. In the laboratory frame, this means that only particles with  $\varphi_x + 2\varphi_y$  in the same range can be stable. The point  $(\hat{a}_x^*)_+$  becomes the more “external” point of stability. We note that for  $\xi = 1$  the point  $1/\sqrt{\xi}$  becomes 1, and the pink dashed area goes to zero.

### 3. Region $-1/4 < \xi \leq 0$

The properties of the level lines for  $\xi < 0$  are discussed and summarized in Fig. 29 of the Appendix B. A version of the same picture with the relevant quantities is shown in part b) of Fig. 17. In this region it holds  $1/(2\sqrt{-\xi}) > 1$ , that means that the blue curve shown in part b) of the Fig 17 will always cross the line  $\mathcal{V} = 1$  twice. The level lines on the left of (or above of) the blue curve exhibit a minimum and a maximum, while the level lines on the right of (or below of) the blue curve have only one maximum. We find that there are two curves tangent to  $\mathcal{V} = 1$ : one above the blue curve tangent in  $(\hat{a}_x^*)_-$ , and one below the blue curve tangent in  $(\hat{a}_x^*)_+$ . In the dashed blue area we find the level lines with a minimum and a maximum: we call for convenience these lines of the “second order”. The minimum of these lines has coordinate  $\hat{a}_x$  always smaller than  $(\hat{a}_x)_t$ , and the dynamics of particles in this region is to be bounded by the same curve  $\mathcal{V} = 1$ . This means that for particles in the dashed blue region their trajectory is always bounded in  $0 < \mathcal{V} < 1$ . The red dashed area characterizes instead the initial conditions where the level lines have one maximum, we call for convenience these lines of the “first order”. These first order lines always cross both lines  $\mathcal{V} = 1$ , and  $\mathcal{V} = -1$ , hence this region is stable and as discussed in the previous section the level line tangent to the line  $\mathcal{V} = 1$  identifies a fix-line. Therefore  $(\hat{a}_x^*)_+$  is on the fix-line and characterizes the outer point of stability.

The point  $(\hat{a}_x)_1$  marks the region of total stability: if  $0 < \hat{a}_x < (\hat{a}_x)_1$  particles are stable for any initial phase  $\Omega$ .

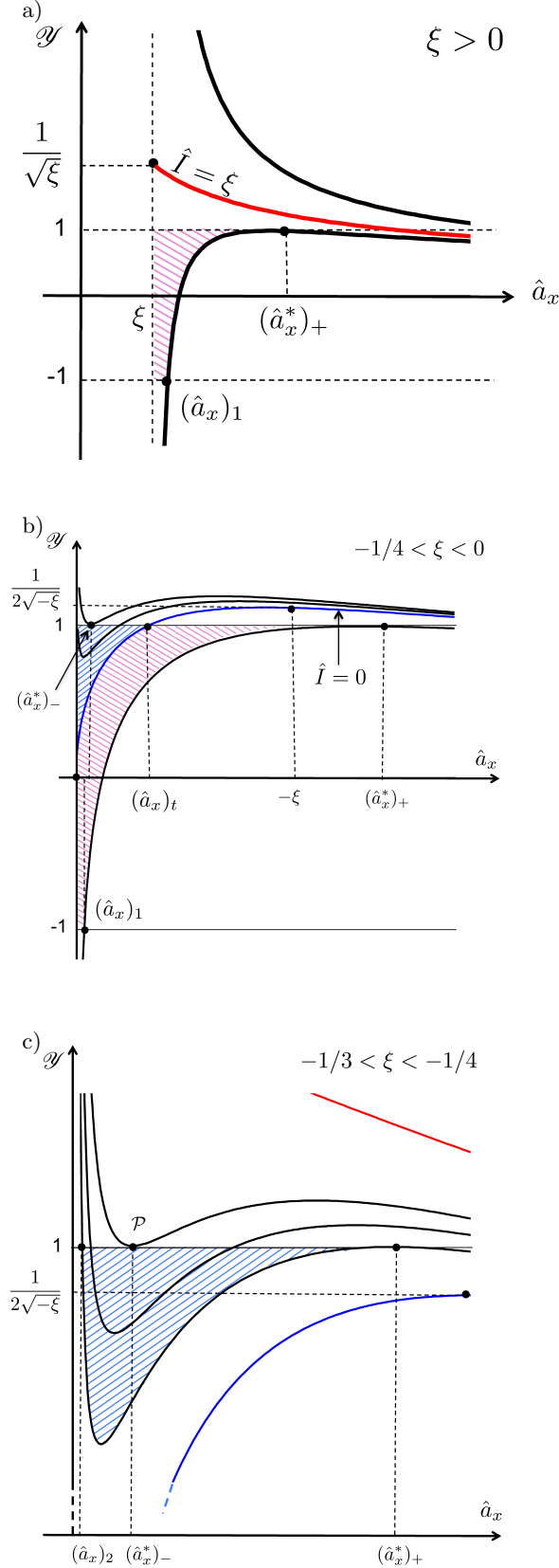


FIG. 17: Impact of the level lines on the stability of motion. The three pictures refer to the three relevant regimes. Note that in a) the curves stop at  $\hat{a}_x = \xi$  because of the condition of Eq. 83.

$$4. \quad -1/3 < \xi \leq -1/4$$

In this regime, referring to Fig. 29, we find that the maximum of the blue line is  $1/(2\sqrt{-\xi}) < 1$ , and the inflection point of the red line is  $1/(\sqrt{-3\xi}) > 1$ . As a consequence all level lines below the blue curve describe unstable dynamics. Among the level lines in the region between the red and blue line, there are two level lines tangent to the line  $\mathcal{Y} = 1$ . The situation is illustrated in part c) of Fig. 17. One level line is tangent to  $\mathcal{Y} = 1$  in  $(\hat{a}_x^*)_+$ , this curve also intercepts the line  $\mathcal{Y} = 1$  in  $(\hat{a}_x)_2$ . The second level line is tangent to  $\mathcal{Y} = 1$  in  $(\hat{a}_x^*)_-$ . Only the blue dashed area is stable as any initial condition in the system of coordinates  $(\hat{a}_x, \mathcal{Y})$  will move on a level line that crosses twice the line  $\mathcal{Y} = 1$ . Interestingly, the point  $\mathcal{P} = ((\hat{a}_x^*)_-, 1)$  is a point that does not move because it also identifies a fix-line (the level line is tangent to  $\mathcal{Y} = 1$  in  $(\hat{a}_x^*)_-$ ), but at the same time the level line tangent to  $\mathcal{P}$  has  $\mathcal{Y} > 1$ . Therefore any point in the neighborhood of  $\mathcal{P}$  with  $-1 < \mathcal{Y} < 1$  will always remain close to it, and  $\mathcal{P}$  is an equivalent of a fix point in this system of coordinates. We call this a “stationary” point.

Lastly, we also find the point  $(\hat{a}_x)_2$ , which is the extreme point of stability, for  $\hat{a}_x < (\hat{a}_x)_2$  there is no stability.

$$5. \quad \xi \leq -1/3$$

In this region the condition  $\xi \leq -1/3$  implies  $1/\sqrt{-3\xi} \leq 1$ . This means that the inflection point of the red curve in Fig. 29 is below or equal to line  $\mathcal{Y} = 1$ . Therefore if  $\xi \leq -1/3$  no point in  $\hat{a}_x > 0$ ,  $-1 < \mathcal{Y} < 1$  can be stable.

### C. Simulation examples

In order to confirm the theory as developed in this paper we directly integrated the equation of motion of the coordinates  $(\hat{a}_x, \mathcal{Y})$  and verified that the stability of particle is determined as previously discussed. The vicinity of the resonance is explored here on parameters that will be used later in multi-particle simulations. We use the following parameters  $\Lambda = -7.44 \times 10^{-3} \text{ m}^{-1}$ , and  $\Delta_r = 4.64 \times 10^{-3}$ , from which we find the scaling factor of Eq. 78 equal to  $\Delta_r^2/(16\Lambda^2) = 0.024 \text{ m}^2$ , and the  $\mu = -1$ .

In Fig. 18 we show an example of level lines for  $\xi = 0.32$ , where each curve corresponds to a different  $\hat{I}$ . The green curve is the level curve of the fix-line defined by  $\tau = 0.2$ , the corresponding invariant in the laboratory frame is  $C = 0.0155 \text{ m}^2$ . The set of orange dots in the picture shows the set of initial conditions that are stable. It is evident that the green curve bounds the set of stable initial conditions as discussed in the previous section.

Part a) of Fig. 19 shows simulations in the regime  $-1/4 < \xi < 0$ . The parameters of the plot are  $\tau =$



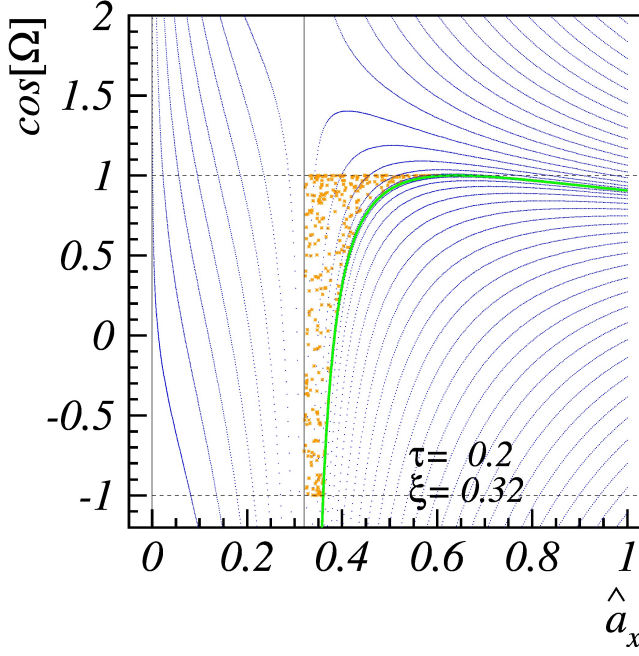


FIG. 18: Level lines of the invariant. The green curve touches both the lines  $\mathcal{V} = \pm 1$  and bound the stability region marked by the orange dots, which are the set of stable initial condition obtained from simulations.

0.4,  $\xi = -0.12$ . Among the level lines, two are of relevance and colored with green and red. The green curve is a level curve of the first order. This curve touches  $\cos[\Omega] = 1$  in one point (fix-line), and the set of orange dots on the left of the green curve in  $-1 \leq \mathcal{V} \leq 1$  are all the stable initial conditions. In the picture there is also a red line, which is of the second order, and this curve also touches  $\cos[\Omega] = 1$  in one point.

In part b) of Fig. 19 the parameters of the level line associated to the fix-line are  $\tau = 0.81$ ,  $\xi = -0.268$ , therefore the level lines have pattern typical of the region  $-1/3 < \xi < -1/4$ . The green curve is a level line of the second order and it bounds the stable initial conditions (orange dots) with the line  $\cos[\Omega] = 1$ . For sake of clarity we show in the part c) of Fig. 19 the same scenario in the  $\hat{a}_x, \Omega$  plane. The role of the fix-line is very evident. It also becomes clear that there is a “stationary” fix point where the red level line touches the line  $\Omega = 0$ , and a single red dot is in the center of an “island”.

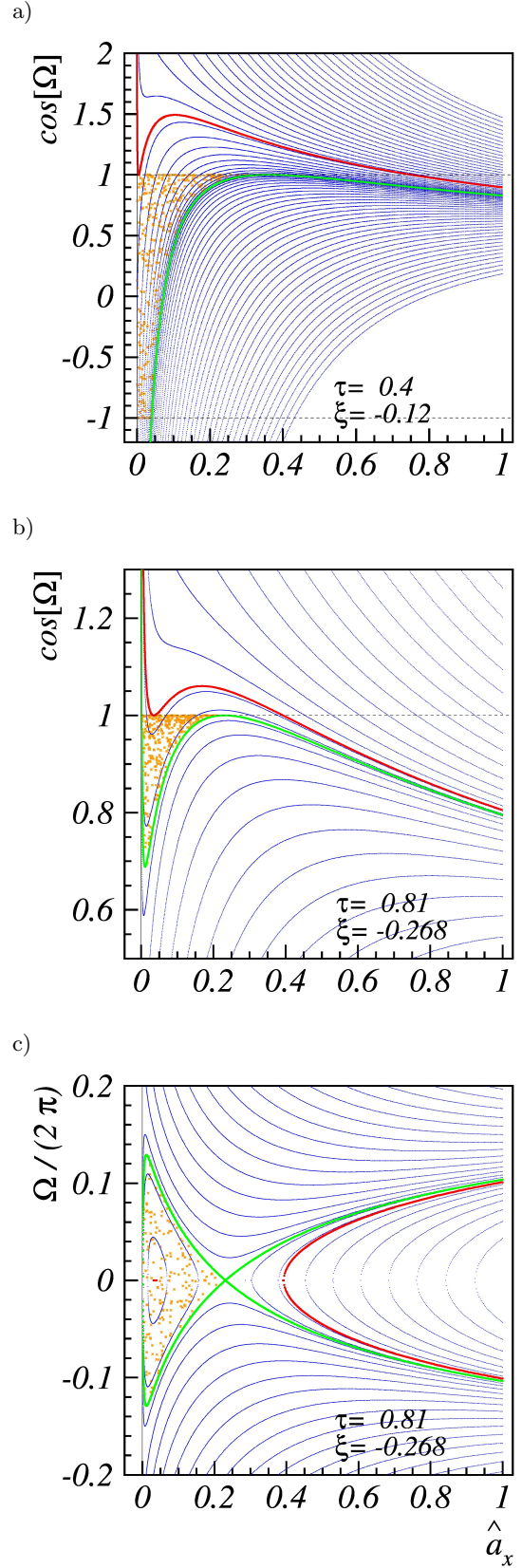


FIG. 19: a)  $\tau = 0.4$ ,  $\xi = -0.12$ . Level curves of the invariant. The two curves correspondent to the fix-lines are in red and green. Note that the level line of the unstable fix-line (green) is bounding the stable particles; b)  $\tau = 0.81$ ,  $\xi = -0.268$ . Level curves correspondent to the fix-lines, they are curves of the second order (see text). The orange dots are in the region of stable trajectories; c) the same situation as in part b) but now in the  $\hat{a}_x, \Omega$  coordinates.

## D. Summary

Because of the resonance the motion of a particle is also affected by the time dependence of the variables  $\hat{a}_x, \hat{a}_y, \tilde{\varphi}_x, \tilde{\varphi}_y$ . At any time the variables  $\hat{a}_x, \hat{a}_y$  are forced to lie on the straight line  $2\hat{a}_x - \hat{a}_y = 2\xi$ , hence the motion of a particle is bounded, if  $\hat{a}_x$  remains bounded. The stability properties are retrieved as follows: given the initial condition  $\hat{a}_x, \hat{a}_y, \tilde{\varphi}_x, \tilde{\varphi}_y$ , we find  $\xi$  and  $\Omega$ , from which  $\mathcal{V}$  is computed. The pair  $(\hat{a}_x, \mathcal{V})$  with  $\xi$  allows to identify to which region the motion belongs to and correspondingly to which type of stability (discussed in Sec. VIII B Figs. 17).

In order to classify the stability properties we will make use of two definitions of stability based on the discussion made in Sec. VIII B: We call **stability of type 1** the stability of a particle, when its motion is associated to a level line of the first order. Similarly we define a **stability of type 2** when the stability is associated to a level line of the second order.

The findings on the stability in the proximity of the third order coupled resonance  $Q_x + 2Q_y = N$  are summarized in Fig. 21. In these pictures the fix-lines define the border of the domain of stability (pink line unstable fix-lines, and blue line stable fix-lines). As each fix-line is characterized by  $0 \leq \tau \leq 1$ ,  $\tau$  parameterizes the border of stability in  $\hat{a}_x, \hat{a}_y$  coordinates as well. The relation of  $\tau$  with  $\xi$  is shown in Fig. 20.

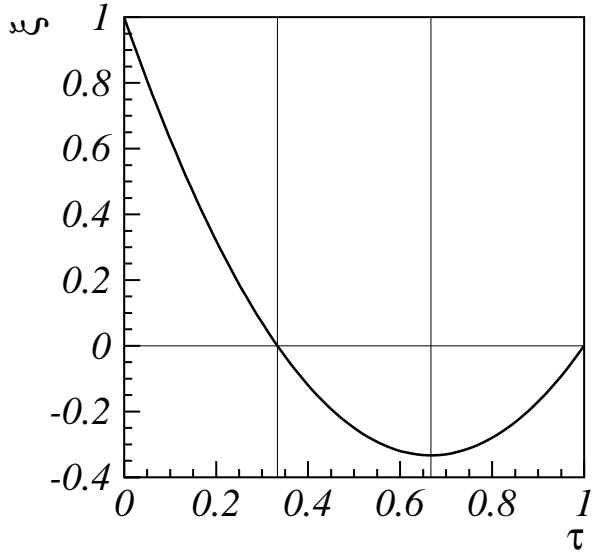


FIG. 20:  $\xi$  as function of  $\tau$ . The curve shows a symmetry at  $\tau = 2/3$ , because for  $\tau > 1/3$  the line  $2\hat{a}_x - \hat{a}_y = C$  crosses the fix-line parabolic-like curve twice.

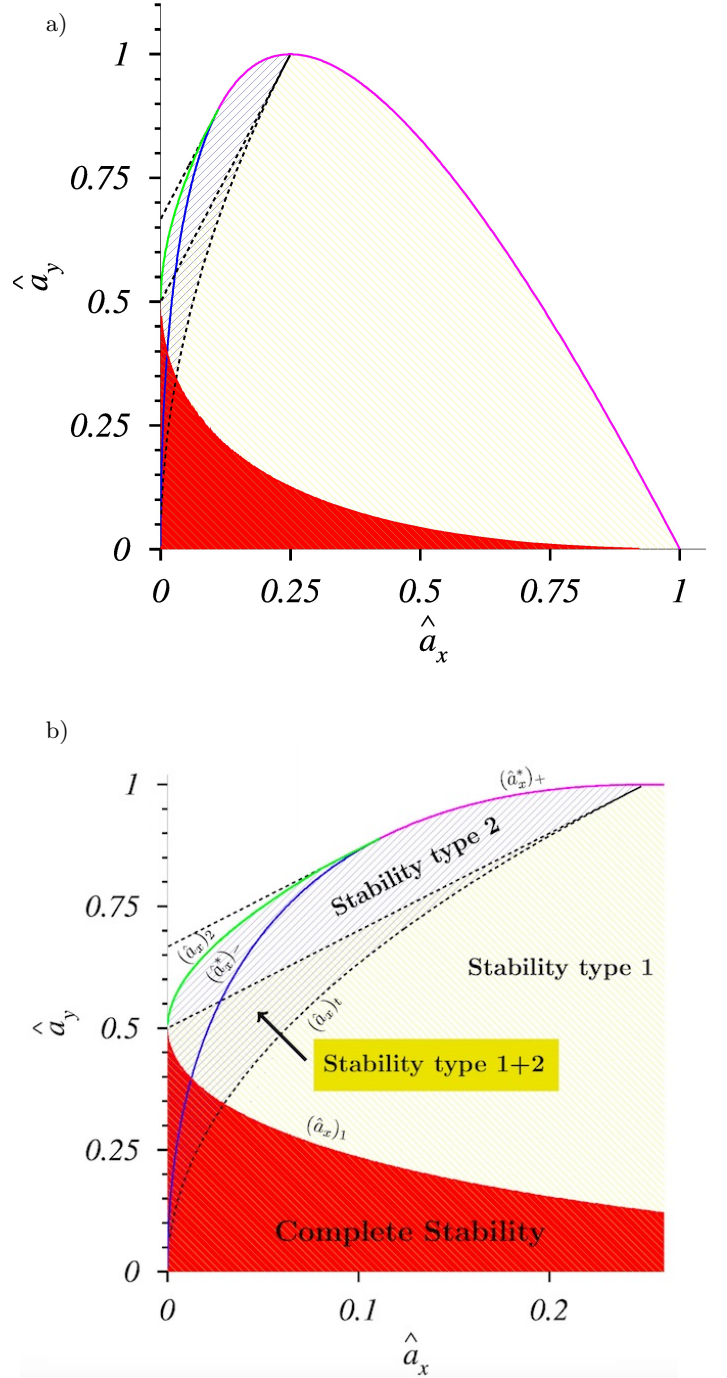


FIG. 21: Summary of all the parameters that characterize the stability domain. On the bottom is a zoom for the sake of clarity. The border dividing the red dashed area from the yellow dashed area is the collection of the  $(\hat{a}_x)_1$  defined in Fig. 18 part a) and b). The green line is the collection of the  $(\hat{a}_x)_2$ , i.e. is the part of initial condition that are stable beyond the fix-line. The blue line is the collection of the stable fix-line  $(\hat{a}_x^*)_-$ , the pink line is the collection of the unstable fix-lines  $(\hat{a}_x^*)_+$ . The points  $(\hat{a}_x)_t$  are defined in part b) of Fig. 17.

The stability properties are summarized in Fig. 21 in terms of curves collecting the points  $(\hat{a}_x)_2, (\hat{a}_x^*)_-, (\hat{a}_x^*)_+, (\hat{a}_x)_1, (\hat{a}_x)_t$  defined in Fig. 17. The bottom picture of Fig. 21 provides a zoom with the summary of all the symbols. We can therefore make the following general classification of the regions of stability:

**Complete stability** The red wide area in Fig. 21 is the region of complete stability, i.e. particles with  $\hat{a}_x \hat{a}_y$  inside this area are stable for any  $\tilde{\varphi}_x, \tilde{\varphi}_y$ . The upper edge of the red area is the set of the points  $(\hat{a}_x)_1$  identified in part a), b) of Fig. 17;

**Partial stability type 1** The yellow dashed area is a region of partial stability that extend in the region  $-1/4 \leq \xi \leq 1$ . The allowed angles  $\Omega$  are given by

$$|\Omega - \pi(1 + \mu)/2 + 2\pi N'| \leq \Delta\Omega \quad (92)$$

with  $N'$  an integer. The angle  $\Delta\Omega$  is represented in Fig. 22 for the case of  $\xi > 0$ , and is obtained directly from Eq. 84 as

$$\Delta\Omega(\hat{a}_x, \hat{a}_y) = \arccos \left[ \frac{1}{\mu} \frac{\hat{I}_{fl} - \hat{a}_x}{\sqrt{\hat{a}_x}(\hat{a}_x - \xi)} \right], \quad (93)$$

with  $\hat{I}_{fl}$  the invariant correspondent to the fix-line defined by  $\xi$  (or  $\tau$ ). We here consider  $0 \leq \Delta\Omega \leq \pi$ .

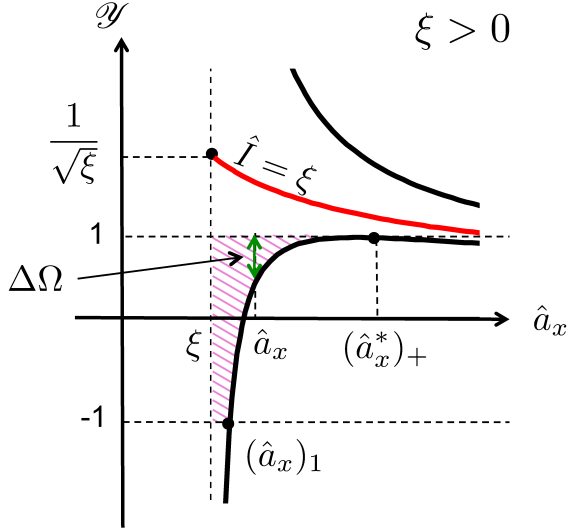


FIG. 22: Definition of  $\Delta\Omega$  for the case  $\xi > 0$ . A similar definition applies for other value of  $\xi$  seen in the different parts of Fig. 17.

**Partial stability type 2** This region is found for  $-1/3 < \xi < -1/4$ , and is shown by the blue dashed area in Fig. 21, the stability is type 2, and  $\Omega$  is bounded to oscillate around  $\Omega = 0$  or  $\Omega = 2\pi$ . The green line is the collection of the points  $(\hat{a}_x)_2$  identified in part c) of Fig. 17 and is the edge of the stability domain. This curve is not a collection of

fix-lines, which indeed correspond to the blue curve (the stationary points). The stability angles  $\Delta\Omega$  are given by Eq. 93.

**Partial stability type 1+2** In Fig. 21 this region is the overlapping of the region of partial stability type 2 (blue dashed area) with the region of partial stability of type 1 (yellow dashed area). This area is characterized by a stability shown in part b) of Fig. 17 for  $(\hat{a}_x)_1 < \hat{a}_x < (\hat{a}_x)_t$ . In Fig. 21 the bend curve  $(\hat{a}_x)_t$  is the collection of the points  $(\hat{a}_x)_t$  defined in part b) of Fig. 17. In this region of Fig. 21, according to the initial condition a particle may have an evolution of  $\Omega$  that is bounded to 0 or  $2\pi$  (stability type 2, blue dashed area of part b) of Fig. 17), or an unbounded evolution of  $\Omega$  that spans periodically all  $[0, 2\pi]$  values (stability type 1, red dashed area of part b) of Fig. 17). Also in this case the angles that are stable are given by Eq. 93.

With this theoretical considerations in mind we compare the stability domain as predicted by our theory with multi-particle simulations. In the part a) of the Fig. 23 we show the stability domain as obtained from theory, in an  $\hat{a}_x, \hat{a}_y$  chart. The color code provides the information on the allowed angle  $\Delta\Omega$ . The picture retrieves the discussed properties and shows that the allowed range of angles becomes smaller when approaching the unstable fix-lines. The picture also shows the partial stable region beyond the stable fix-lines (blue line from theory). In the red area the motion is stable (complete stability).

Part b) of the Fig. 23 shows the same result obtained by tracking. In order to test the theory we considered for this simulation a constant focusing lattice where a single harmonics was created. The strength of the driving term is  $\Lambda = -7.44 \times 10^{-3} \text{ m}^{-1}$ , and  $\Delta_r = 4.64 \times 10^{-3}$ . The stability domain was sampled with  $100 \times 100 \times 51 \times 51$  initial conditions, and the stability was assessed over 1000 turns. The pink and blue curves in the picture are the collection of fix-lines as from the theory. These results are in good agreement with the theoretical predictions.

Part c) of the Fig. 23 shows the stability domain obtained when a single sextupolar kick is used on a constant focusing lattice. In this case we are not in the ideal condition of the theory, stated in Sect. IV, and some deviation is to be expected, resulting in an enlarging of the stability domain closes to the  $a_x$  axis. For this simulation the parameters are  $\Delta_r = 4.64 \times 10^{-3}$ , and  $K_2 = 2.52 \times 10^{-5} \text{ m}^{-2}$  that makes  $\Lambda = -2.36 \times 10^{-5} \text{ m}^{-1}$ .

Note that in spite of the fact that the strength of the sextupole is very small, part c) of Fig. 23 respects the scaling expected from the theory (apart from the deviation along  $\hat{a}_x$ ).

For more realistic cases in which a lattice with alternating magnet is used, or an arbitrary distribution of sextupolar errors is employed, this scaling will be similar. This subject will be discussed in the following chapters.

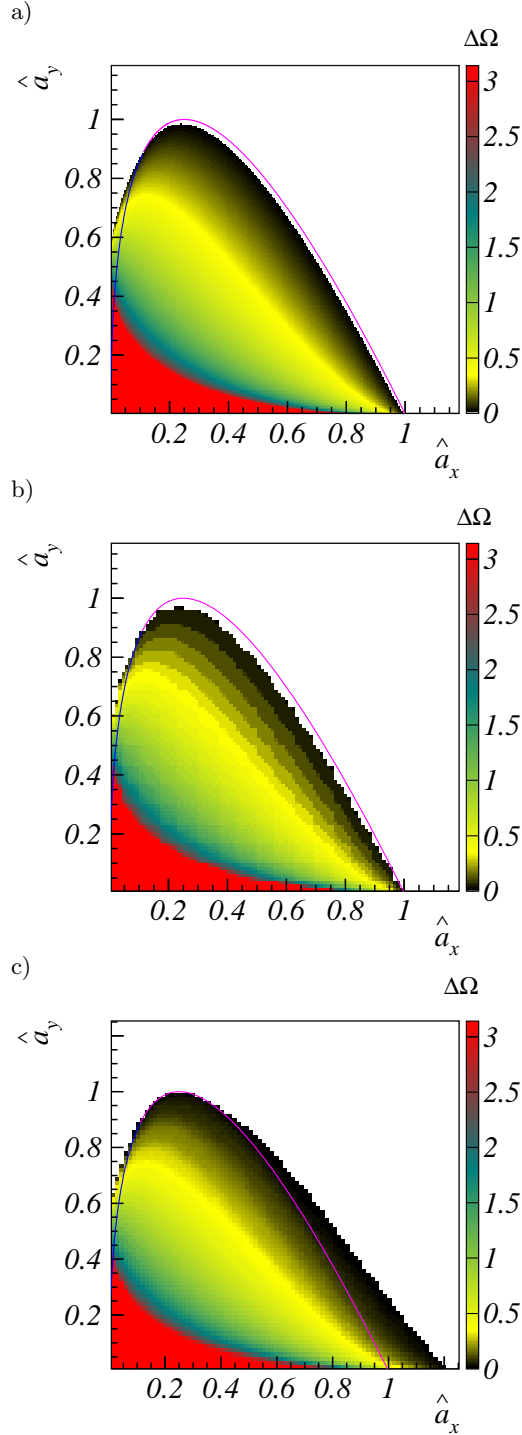


FIG. 23: Complete stability domain for a constant focusing circular accelerator. Part a) the stability domain as obtained by the analytic theory; Part b) the same result obtained by a particle tracking, with a computer code, of 100x100x51x51 initial conditions, and particles are tracked for 1000 turns. Part c) shows the stability domain obtained for one sextupolar kick (to be explained in the following chapter). The result shows an enlarging of the stability domain closes to the  $\tilde{a}_x$  axis.

## IX. ANALYSIS IN AN AG CIRCULAR ACCELERATOR

Previously we have made the analysis for the constant focusing case for a resonance excited by a single sextupole term, we will repeat here the analysis in the case of an alternating gradient (AG) structure. We discuss the effect of a distribution of errors and use the strategy previously discussed to formulate a theory of particle motion and fix-lines stability. We study the onset of stable motion in the proximity of a third order coupled resonance.

### A. AG structure set-up

We consider the equations of motion in an AG structure. The equations of motion take the form

$$\begin{aligned} \frac{d^2x}{ds^2} + k_x(s)x &= f_x(s, x, y), \\ \frac{d^2y}{ds^2} + k_y(s)y &= f_y(s, x, y). \end{aligned} \quad (94)$$

Here the  $k_x(s), k_y(s)$  are the “time dependent” focusing/defocusing quadrupole strength. The solutions of these equations for  $f_x = f_y = 0$  are

$$\begin{aligned} x(s) &= \sqrt{\beta_x a_x} \cos(\phi_x(s) + \varphi_x), \\ y(s) &= \sqrt{\beta_y a_y} \cos(\phi_y(s) + \varphi_y), \end{aligned} \quad (95)$$

where  $\beta_x, \beta_y$  are the well known beta function and  $\phi_x(s) = \int_0^s \beta_x(s)^{-1} ds$ ,  $\phi_y(s) = \int_0^s \beta_y(s)^{-1} ds$ . The Hamiltonian of the system has the form

$$H_0 = \frac{(x')^2}{2} + k_x(s) \frac{x^2}{2} + \frac{(y')^2}{2} + k_y(s) \frac{y^2}{2}, \quad (96)$$

where  $x' = dx/ds, y' = dy/ds$ , and the canonical equations are

$$\begin{aligned} \frac{dx}{ds} &= \frac{\partial H_0}{\partial x'}, & \frac{dx'}{ds} &= -\frac{\partial H_0}{\partial x}, \\ \frac{dy}{ds} &= \frac{\partial H_0}{\partial y'}, & \frac{dy'}{ds} &= -\frac{\partial H_0}{\partial y}. \end{aligned} \quad (97)$$

### B. Equations of the constants

Despite the fact that the unperturbed motion is time dependent, the equations of the otherwise constants  $a_x, \varphi_x, a_y, \varphi_y$  for the perturbed system with Hamiltonian  $H = H_0 + H_1$  are as before

$$\begin{aligned} \frac{da_x}{ds} &= -2 \frac{\partial H_1}{\partial \varphi_x}, & \frac{d\varphi_x}{ds} &= 2 \frac{\partial H_1}{\partial a_x}, \\ \frac{da_y}{ds} &= -2 \frac{\partial H_1}{\partial \varphi_y}, & \frac{d\varphi_y}{ds} &= 2 \frac{\partial H_1}{\partial a_y}, \end{aligned} \quad (98)$$



where we set the perturbing Hamiltonian  $H_1$  due to distributed sextupoles as

$$H_1 = k_2(s) \left( \frac{x^3}{6} - \frac{xy^2}{2} \right). \quad (99)$$

Let's consider a distribution of sextupolar errors localized at specific positions  $s_j$ . The function  $k_2(s)$  in this case reads

$$k_2(s) = \sum_{j,m} K_{2j} \delta(s - s_j + mL), \quad (100)$$

where  $L$  is the periodicity of the system, hence the length of the accelerator, and  $K_{2j}$  is the integrated strength of the sextupolar error located at the position  $s_j$ . The unperturbed solution reads

$$\begin{aligned} x &= \sqrt{\beta_x a_x} \frac{e^{iA_x} + e^{-iA_x}}{2} \\ y &= \sqrt{\beta_y a_y} \frac{e^{iA_y} + e^{-iA_y}}{2} \end{aligned} \quad (101)$$

with  $A_x = \phi_x(s) + \varphi_x$ ,  $A_y = \phi_y(s) + \varphi_y$ . We substitute  $(x, y)$  into the Hamiltonian  $H_1$  and obtain

$$\begin{aligned} H_1 &= \sum_{j,m} K_{2j} \delta(s - s_j + mL) \frac{1}{48} (\beta_x a_x)^{3/2} (e^{iA_x} + e^{-iA_x})^3 - \\ &- \sum_{j,m} K_{2j} \delta(s - s_j + mL) \frac{1}{16} \sqrt{\beta_x a_x} \beta_y a_y \times \\ &(e^{iA_x} + e^{-iA_x})(e^{iA_y} + e^{-iA_y})^2. \end{aligned} \quad (102)$$

Note that the function  $\phi_x(s)$  has the property

$$\phi_x(mL) = 2\pi Q_x m, \quad (103)$$

with  $m$  an integer ( $\phi_x$  is defined for the linear case). Therefore we can define the function

$$\mathcal{D}_x(s) = \phi_x(s) - 2\pi Q_x \frac{s}{L}, \quad (104)$$

which is a periodic function with  $\mathcal{D}_x(mL) = 0$ . In a similar way we define  $\mathcal{D}_y(s)$ . Therefore

$$\begin{aligned} A_x &= \mathcal{D}_x(s) + 2\pi Q_x \frac{s}{L} + \varphi_x, \\ A_y &= \mathcal{D}_y(s) + 2\pi Q_y \frac{s}{L} + \varphi_y. \end{aligned} \quad (105)$$

We therefore find that the Hamiltonian Eq. 102 is composed of the periodic functions  $\mathcal{D}_x(s)$ ,  $\mathcal{D}_y(s)$ ,  $\beta_x(s)$ ,  $\beta_y(s)$ , which have the periodicity of the accelerator  $L$ , and also by non-periodic functions like the term  $2\pi Q_x s/L$  (etc.). On the other hand the delta function in Eq. 102 is different from zero only at the longitudinal positions  $s_j - mL$ , and at these positions the periodic functions  $\mathcal{D}_x(s)$ ,  $\mathcal{D}_y(s)$ ,  $\beta_x(s)$ ,  $\beta_y(s)$  assume the value  $\mathcal{D}_x(s_j)$ ,  $\mathcal{D}_y(s_j)$ ,  $\beta_x(s_j)$ ,  $\beta_y(s_j)$  independently on  $m$ . We can therefore replace in all the periodic functions of Eq. 102 the coordinate  $s$  by  $s_j$ .

To this purpose we call

$$\begin{aligned} A_{xj} &= \mathcal{D}_x(s_j) + 2\pi Q_x \frac{s}{L} + \varphi_x, \\ A_{yj} &= \mathcal{D}_y(s_j) + 2\pi Q_y \frac{s}{L} + \varphi_y, \end{aligned} \quad (106)$$

and  $\beta_{xj} = \beta_x(s_j)$ ,  $\beta_{yj} = \beta_y(s_j)$ . Hence

$$\begin{aligned} H_1 &= \sum_{j,m} K_{2j} \delta(s - s_j + mL) \frac{1}{48} (\beta_{xj} a_x)^{3/2} (e^{iA_{xj}} + e^{-iA_{xj}})^3 - \\ &- \sum_{j,m} K_{2j} \delta(s - s_j + mL) \frac{1}{16} \sqrt{\beta_{xj} a_x} \beta_{yj} \times \\ &a_y (e^{iA_{xj}} + e^{-iA_{xj}})(e^{iA_{yj}} + e^{-iA_{yj}})^2. \end{aligned} \quad (107)$$

We substitute the delta expansion and  $A_{xj}$ ,  $A_{yj}$  obtaining

$$\begin{aligned} H_1 &= \frac{1}{48L} a_x^{3/2} \sum_j \sum_t \sum_{q=0}^3 K_{2j} \beta_{xj}^{3/2} \binom{3}{q} \times \\ &\exp\{i2\pi \frac{s - s_j}{L} t + i(\mathcal{D}_x(s_j) + 2\pi Q_x \frac{s}{L} + \varphi_x)[2q - 3]\} - \\ &- \frac{1}{16L} \sqrt{a_x a_y} \sum_j \sum_t \sum_{q=0}^1 \sum_{p=0}^2 K_{2j} \sqrt{\beta_{xj}} \beta_{yj} \binom{1}{q} \binom{2}{p} \times \\ &\times \exp\{i[2\pi \frac{-s_j}{L} t + \mathcal{D}_x(s_j)(2q - 1) + \mathcal{D}_y(s_j)(2p - 2)]\} \times \\ &\times \exp\{i2\pi[Q_x(2q - 1) + Q_y(2p - 2) + t] \frac{s}{L}\} \times \\ &\times \exp\{i[\varphi_x(2q - 1) + \varphi_y(2p - 2)]\}. \end{aligned} \quad (108)$$

As the tunes  $Q_x, Q_y$  are close the resonance, meaning  $\Delta_r = Q_x + 2Q_y - N$  is small, it follows that between all oscillating terms in Eq. 108, only two have a very slow frequency of oscillation, while all the other can be considered as fast oscillating. We neglect the fast oscillating terms and keep just the slowly oscillating ones, that is we select  $q, p, t$  in  $Q_x(2q - 1) + Q_y(2p - 2) + t$  such as to obtain slow frequencies. This happens for  $q = 1, p = 2, t = -N$ , and  $q = 0, p = 0, t = N$ . Consequently the slowly varying Hamiltonian reads

$$\begin{aligned} H_{s1} &= -\frac{1}{8L} \sqrt{a_x a_y} \sum_j K_{2j} \sqrt{\beta_{xj}} \beta_{yj} \\ &\cos[2\pi \frac{s_j}{L} N + \mathcal{D}_x(s_j) + 2\mathcal{D}_y(s_j) + 2\pi \Delta_r \frac{s}{L} + \varphi_x + 2\varphi_y], \end{aligned} \quad (109)$$

we re-write  $H_{s1}$  in the following form

$$\begin{aligned} H_{s1} &= \sqrt{a_x a_y} \{ \Lambda_c \cos \left[ \varphi_x + 2\varphi_y + 2\pi \Delta_r \frac{s}{L} \right] - \\ &- \Lambda_s \sin \left[ \varphi_x + 2\varphi_y + 2\pi \Delta_r \frac{s}{L} \right] \} \end{aligned} \quad (110)$$

with

$$\begin{aligned}\Lambda_c &= - \sum_j \frac{1}{8L} K_{2j} \sqrt{\beta_{xj} \beta_{yj}} \times \\ &\quad \times \cos \left[ 2\pi \frac{s_j}{L} N + \mathcal{D}_x(s_j) + 2\mathcal{D}_y(s_j) \right], \\ \Lambda_s &= - \sum_j \frac{1}{8L} K_{2j} \sqrt{\beta_{xj} \beta_{yj}} \times \\ &\quad \times \sin \left[ 2\pi \frac{s_j}{L} N + \mathcal{D}_x(s_j) + 2\mathcal{D}_y(s_j) \right].\end{aligned}\quad (111)$$

The coefficients  $\Lambda_c, \Lambda_s$  depend only on the distribution of the sextupolar errors, on the optics, and on the selected resonance (in this case  $Q_x + 2Q_y = N$ ). Next we remove the time dependence in the argument of the trigonometric function in Eqs. 110 with the transformation

$$\begin{aligned}a_x &= \tilde{a}_x \\ a_y &= \tilde{a}_y \\ \varphi_x &= \tilde{\varphi}_x - t_x 2\pi \Delta_r \frac{s}{L} \\ \varphi_y &= \tilde{\varphi}_y - t_y 2\pi \Delta_r \frac{s}{L}\end{aligned}\quad (112)$$

where we require that

$$t_x + 2t_y = 1. \quad (113)$$

The new Hamiltonian reads

$$\begin{aligned}\tilde{H}_{s1} &= \sqrt{\tilde{a}_x \tilde{a}_y} \{ \Lambda_c \cos [\tilde{\varphi}_x + 2\tilde{\varphi}_y] - \Lambda_s \sin [\tilde{\varphi}_x + 2\tilde{\varphi}_y] \} + \\ &\quad + (\tilde{a}_x t_x + \tilde{a}_y t_y) 2\pi \frac{\Delta_r}{2L}.\end{aligned}\quad (114)$$

The last term is equivalent to the similar term in the Hamiltonian for the constant focusing Eq. 31. It arises from the requirement of making the Hamiltonian time independent. At this point it is convenient to define the angle  $\alpha$  as

$$\cos \alpha = \frac{\Lambda_c}{\Lambda}, \quad \sin \alpha = \frac{\Lambda_s}{\Lambda}, \quad (115)$$

with  $\Lambda = \sqrt{\Lambda_s^2 + \Lambda_c^2} > 0$ . Therefore the final form of the slowly varying Hamiltonian in an AG lattice becomes

$$\tilde{H}_{s1} = \Lambda \sqrt{\tilde{a}_x \tilde{a}_y} \cos(\tilde{\varphi}_x + 2\tilde{\varphi}_y + \alpha) + (\tilde{a}_x t_x + \tilde{a}_y t_y) \frac{2\pi \Delta_r}{2L}. \quad (116)$$

The canonical equations are

$$\begin{aligned}-\tilde{a}'_x &= 2 \frac{\partial \tilde{H}_{s1}}{\partial \tilde{\varphi}_x} = 2 \sqrt{\tilde{a}_x \tilde{a}_y} \Lambda \sin(\tilde{\varphi}_x + 2\tilde{\varphi}_y + \alpha) \\ \tilde{\varphi}'_x &= 2 \frac{\partial \tilde{H}_{s1}}{\partial \tilde{a}_x} = 2 \frac{1}{2\sqrt{\tilde{a}_x}} \tilde{a}_y \Lambda \cos(\tilde{\varphi}_x + 2\tilde{\varphi}_y + \alpha) + t_x \frac{2\pi \Delta_r}{L} \\ -\tilde{a}'_y &= 2 \frac{\partial \tilde{H}_{s1}}{\partial \tilde{\varphi}_y} = 4 \sqrt{\tilde{a}_x \tilde{a}_y} \Lambda \sin(\tilde{\varphi}_x + 2\tilde{\varphi}_y + \alpha) \\ \tilde{\varphi}'_y &= 2 \frac{\partial \tilde{H}_{s1}}{\partial \tilde{a}_y} = 2 \sqrt{\tilde{a}_x} \Lambda \cos(\tilde{\varphi}_x + 2\tilde{\varphi}_y + \alpha) + t_y \frac{2\pi \Delta_r}{L}\end{aligned}\quad (117)$$

multiplying the first equation by 2 and subtracting the third one we find that

$$2\tilde{a}_x - \tilde{a}_y = C \quad (118)$$

where  $C$  is a constant. The previous expression is then an invariant of motion.

### C. Special solutions

Via Eq. 117 the equations of the fix-line are

$$\begin{aligned}-\tilde{a}'_x = 0 &= \Lambda 2 \sqrt{\tilde{a}_x \tilde{a}_y} \sin(\tilde{\varphi}_x + 2\tilde{\varphi}_y + \alpha) \\ \tilde{\varphi}'_x = 0 &= \Lambda 2 \frac{1}{2\sqrt{\tilde{a}_x}} \tilde{a}_y \cos(\tilde{\varphi}_x + 2\tilde{\varphi}_y + \alpha) + t_x \frac{2\pi \Delta_r}{L} \\ -\tilde{a}'_y = 0 &= \Lambda 4 \sqrt{\tilde{a}_x \tilde{a}_y} \sin(\tilde{\varphi}_x + 2\tilde{\varphi}_y + \alpha) \\ \tilde{\varphi}'_y = 0 &= \Lambda 2 \sqrt{\tilde{a}_x} \cos(\tilde{\varphi}_x + 2\tilde{\varphi}_y + \alpha) + t_y \frac{2\pi \Delta_r}{L}\end{aligned}\quad (119)$$

The condition  $\tilde{a}'_x = \tilde{a}'_y = 0$  is obtained from the condition

$$\sin(\tilde{\varphi}_x + 2\tilde{\varphi}_y + \alpha) = 0 \quad (120)$$

which yields

$$\tilde{\varphi}_x + 2\tilde{\varphi}_y + \alpha = \pi M \quad (121)$$

with  $M$  an integer. That means that the other two equations become

$$\begin{cases} 0 = \Lambda 2 \frac{1}{2\sqrt{\tilde{a}_x}} \tilde{a}_y (-1)^M + t_x \frac{2\pi \Delta_r}{L} \\ 0 = \Lambda 2 \sqrt{\tilde{a}_x} (-1)^M + t_y \frac{2\pi \Delta_r}{L} \end{cases} \quad (122)$$

Multiplying the second by 2 and summing them up and recalling Eq. 113 we find that the equation for the fix-line reads

$$0 = \Lambda \left( \frac{1}{\sqrt{\tilde{a}_x}} \tilde{a}_y + 4\sqrt{\tilde{a}_x} \right) (-1)^M + \frac{2\pi \Delta_r}{L} \quad (123)$$

and the condition for its existence is that

$$\Lambda \Delta_r (-1)^M < 0. \quad (124)$$

Therefore from the equations for the fix-line we write

$$\begin{aligned}0 &= \Lambda \frac{1}{\sqrt{\tilde{a}_x}} \tilde{a}_y (-1)^M \Delta_r + \frac{2\pi \Delta_r^2}{L} t_x \\ 0 &= \Lambda 2 \sqrt{\tilde{a}_x} (-1)^M \Delta_r + \frac{2\pi \Delta_r^2}{L} t_y\end{aligned}\quad (125)$$

from which we conclude that  $t_x \geq 0$  and  $t_y \geq 0$ . That means that  $t_x \geq 0$  and  $1 - t_x \geq 0$ , so that we get  $1 \geq t_x \geq 0$ . We then parameterize  $t_x, t_y$  as follows

$$\begin{aligned}t_x &= \tau, \\ t_y &= \frac{1}{2}(1 - \tau),\end{aligned}\quad (126)$$

with  $0 \leq \tau \leq 1$ . We write the solution for the fix-line as a function of  $\tau$ , and get

$$\begin{aligned}\tilde{a}_y &= \frac{(2\pi\Delta_r)^2}{4\Lambda^2 L^2} \tau(1-\tau), \\ \tilde{a}_x &= \frac{(2\pi\Delta_r)^2}{16\Lambda^2 L^2} (1-\tau)^2.\end{aligned}\quad (127)$$

We find the same solution as for the case of the constant focusing except that the scaling depends on  $\Lambda/L$ , with  $\Lambda$  being the driving term of the resonance as already computed by Hagedorn/Schoch [3-5], Guignard [6, 7].

#### D. Fix-line

The analytic form of the fix-line can now be found. From  $\tilde{\varphi}'_x = \tilde{\varphi}'_y = 0$  we get

$$\tilde{\varphi}_x = \tilde{\varphi}_{x,0}, \quad \tilde{\varphi}_y = \tilde{\varphi}_{y,0}, \quad (128)$$

and returning back to the coordinates of the Hamiltonian  $H_{s1}$  we find

$$\begin{aligned}\varphi_x &= \tilde{\varphi}_{x,0} - t_x 2\pi\Delta_r \frac{s}{L}, \\ \varphi_y &= \tilde{\varphi}_{y,0} - t_y 2\pi\Delta_r \frac{s}{L},\end{aligned}\quad (129)$$

with  $\sin(\tilde{\varphi}_{x,0} + 2\tilde{\varphi}_{y,0} + \alpha) = 0$ . The solution has therefore the form

$$\begin{aligned}x &= \sqrt{\beta_x a_x} \cos \left[ \phi_x(s) - t_x 2\pi\Delta_r \frac{s}{L} + \tilde{\varphi}_{x,0} \right] \\ x' &= -\frac{\alpha_x}{\sqrt{\beta_x}} \sqrt{a_x} \cos \left[ \phi_x(s) - t_x 2\pi\Delta_r \frac{s}{L} + \tilde{\varphi}_{x,0} \right] - \\ &\quad - \sqrt{\beta_x a_x} \sin \left[ \phi_x(s) - t_x 2\pi\Delta_r \frac{s}{L} + \tilde{\varphi}_{x,0} \right] \left( \frac{1}{\beta_x} - t_x 2\pi\Delta_r \frac{1}{L} \right) \\ y &= \sqrt{\beta_y a_y} \cos \left[ \phi_y(s) - t_y 2\pi\Delta_r \frac{s}{L} + \tilde{\varphi}_{y,0} \right] \\ y' &= -\frac{\alpha_y}{\sqrt{\beta_y}} \sqrt{a_y} \cos \left[ \phi_y(s) - t_y 2\pi\Delta_r \frac{s}{L} + \tilde{\varphi}_{y,0} \right] - \\ &\quad - \sqrt{\beta_y a_y} \sin \left[ \phi_y(s) - t_y 2\pi\Delta_r \frac{s}{L} + \tilde{\varphi}_{y,0} \right] \left( \frac{1}{\beta_y} - t_y 2\pi\Delta_r \frac{1}{L} \right).\end{aligned}\quad (130)$$

This is the equation of the fix-line, which is a closed line in the 4D phase space.

The Poincaré surface of section is identified by the condition  $s = L\mathcal{N}$  with  $\mathcal{N}$  an integer correspondent to the  $\mathcal{N}$ -th turn. From the solution of the fix-line equation we have  $\sin(\tilde{\varphi}_{x,0} + 2\tilde{\varphi}_{y,0} + \alpha) = 0$  and we find

$$\tilde{\varphi}_{x,0} + 2\tilde{\varphi}_{y,0} + \alpha = \pi M, \quad (131)$$

with  $M$  an integer properly taken to guarantee the existence of the solution. It is straightforward to show that

$$\begin{aligned}(Q_x - t_x \Delta_r) 2\pi\mathcal{N} + \tilde{\varphi}_{x,0} + \\ 2(Q_y - t_y \Delta_r) 2\pi\mathcal{N} + 2\tilde{\varphi}_{y,0} = \\ 2\pi N\mathcal{N} + \pi M - \alpha.\end{aligned}\quad (132)$$

Therefore, by using Eq. 132, we find that on the Poincaré surface of section we have

$$\begin{aligned}x &= \sqrt{\beta_x a_x} \cos [-2(Q_y - t_y \Delta_r) 2\pi\mathcal{N} - 2\tilde{\varphi}_{y,0} - \alpha + \pi M], \\ y &= \sqrt{\beta_y a_y} \cos [(Q_y - t_y \Delta_r) 2\pi\mathcal{N} + \tilde{\varphi}_{y,0}],\end{aligned}\quad (133)$$

with  $\tilde{\varphi}_{y,0}$  an initial phase that sets the starting point. Lastly, we find the result that the fix-line can be parameterized as

$$\begin{aligned}x_t &= \sqrt{\beta_x a_x} \cos [-2(Q_y - t_y \Delta_r)t - \alpha + \pi M], \\ y_t &= \sqrt{\beta_y a_y} \cos [(Q_y - t_y \Delta_r)t].\end{aligned}\quad (134)$$

The presence of the angle  $\alpha$  is the only difference with respect to the case of the constant focusing lattice. However, by changing the longitudinal position of the Poincaré surface of section,  $\alpha$  can be made equal to zero.

#### E. Stability

The discussion of the stability of the fix-line is the same as for the case of the constant focusing system. The conclusion holds as before: for  $\tau > 2/3$  the fix-line is stable, and for  $2/3 < \tau < 1$  the fix-line is unstable.

#### F. Stability of Motion

Next we study the onset of unstable motion. From the canonical equation Eqs. 117, we keep the first equation; due to  $2\tilde{a}_x - \tilde{a}_y = C$  the third equation is redundant. The second and fourth equations can be summed up to yield

$$\begin{cases} -\tilde{a}'_x = 2\sqrt{\tilde{a}_x \tilde{a}_y} \Lambda \sin(\Omega + \alpha) \\ \Omega' = \left[ 2\frac{1}{2\sqrt{\tilde{a}_x}} \tilde{a}_y + 4\sqrt{\tilde{a}_x} \right] \Lambda \cos(\Omega + \alpha) + \frac{2\pi\Delta_r}{L} \end{cases}\quad (135)$$

with  $\Omega = \tilde{\varphi}_x + 2\tilde{\varphi}_y$ . Therefore we re-write the set of equations as

$$\begin{cases} -\tilde{a}'_x = 2\sqrt{\tilde{a}_x}(2\tilde{a}_x - C)\Lambda \sin(\Omega + \alpha) \\ \Omega' = \left[ \frac{1}{\sqrt{\tilde{a}_x}}(2\tilde{a}_x - C) + 4\sqrt{\tilde{a}_x} \right] \Lambda \cos(\Omega + \alpha) + \frac{2\pi\Delta_r}{L} \end{cases}\quad (136)$$

The function

$$I(\tilde{a}_x, \Omega) = 2\Lambda\sqrt{\tilde{a}_x}(2\tilde{a}_x - C) \cos(\Omega + \alpha) + \tilde{a}_x \frac{2\pi\Delta_r}{L} \quad (137)$$

is the invariant of the system as obtained for the constant focusing discussion, except for the presence of the angle  $\alpha$  in the cosine function, but this is just a shift of the stability diagram. Hence, the conclusions obtained for the case of the constant focusing structure hold in the AG structure as well.



### G. Comparison with simulations

In Fig. 25 we compare the reconstruction of the stability domain with part a) of Fig. 25 that is derived from the theory and numerical simulations. As a practical example part b) of Fig. 25 shows instead the same result for the SIS18 reference lattice equipped with a single sextupolar kick. As for the case of the constant focusing we find an enlarging of the stability near the  $a_x$  axis. Part c) of Fig. 25 shows the stability domain for the SIS18 where 12 sextupolar errors are randomly excited. The sextupoles are all placed at the beginning of each super-period. Interestingly the results are still close to those predicted by the theory. A small shrinking of the stability is found anywhere close to the axis  $a_x$ . The discrepancy can be attributed to the effect of high order harmonics not included in the theory.

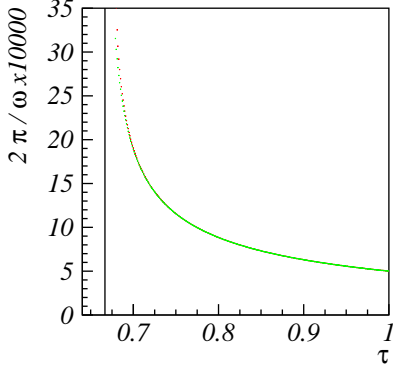


FIG. 24: Comparison of the wavelength from analytic theory (blue dots) and retrieved from simulations (horizontal color black and vertical color red). This result is obtained for a FODO cell with one sextupolar kick. The agreement is excellent with a discrepancy that increases in the proximity of  $\tau = 2/3$ .

We have verified this ansatz by simulations in a FODO structure where we artificially made a single harmonics stronger by placing a sequence of sextupoles with alternating sign of strength. The results are shown in part d) of Fig. 25: the stability domain very well retrieves the theoretical one of part a) of Fig. 25.

Lastly, we tested the prediction of the secondary tunes for a particle slightly off a fix-line. These results are shown in Fig. 24. The simulation is made in a FODO cell equipped with a single sextupole. The secondary frequency is measured by comparing the side bands to the nominal tunes. The theoretical prediction is obtained from Eq. 68 where  $\Delta_r$  is replaced by  $2\pi\Delta_r/L$  (green dots). From the simulations we retrieved the wavelength in  $x, y$  (red dots). The picture shows an excellent agreement except for slight deviations of the side bands where the curves diverges and high order terms become relevant (near  $\tau \simeq 2/3$ ).

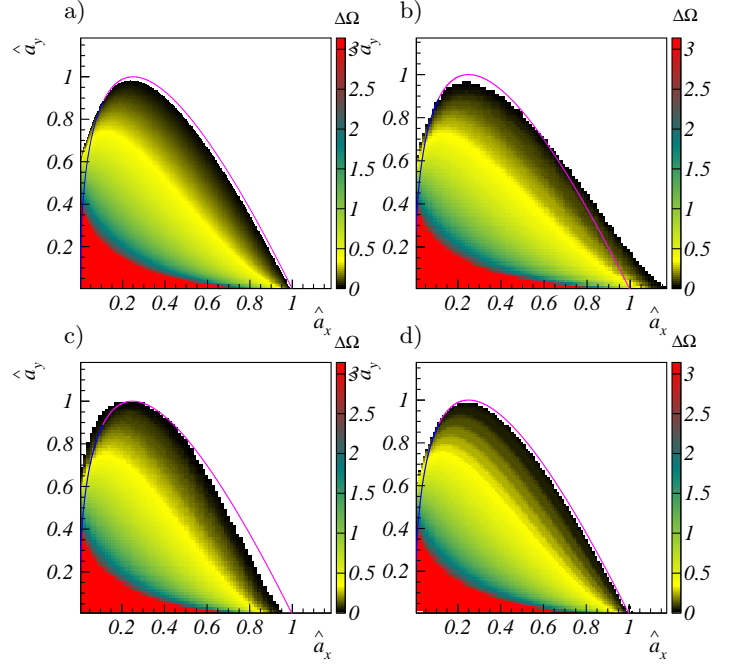


FIG. 25: Complete stability domain for an AG circular accelerator. Part a) the stability domain as obtained by the analytic theory for the SIS18 lattice with a distribution of sextupolar errors. Part b) shows the stability domain of SIS18 obtained for one sextupolar kick. The result shows a slight enlarging of the stability domain close to the  $a_x$  axis. Part c) the same result obtained by tracking of  $100 \times 100 \times 51 \times 51$  initial conditions, and tracked for 1000 turns. Part d) is an example of a FODO cell with a distribution of sextupoles such as to excite only one harmonic. We find a good confirmation of the theory at the edge of the stability domain.

### X. TORI CUT

In this section we discuss the Poincaré surface of section of the tori surrounding the fix-line. We have already obtained those orbits from the numerical simulations in Figs. 12, 13, 14. We show here that these orbits will be retrieved from the invariants. In those figures the orbits in  $x - x'$  are obtained by tracking one single particle for many turns, and plotting  $x, x'$  at each turn when the condition  $y'/y < \epsilon$  and  $y > 0$  are satisfied; here  $\epsilon$  is a positive small number. The orbits in  $y - y'$  are obtained by making a selection of the particle when  $x'/x < \epsilon$  and  $x > 0$ .

Without losing generality we make the discussion for the case of the constant focusing structure as presented in Sect. IV, V, VI, VII, VIII. Our starting point is to consider a tori, identified by the invariants  $I = I(\tilde{a}_x, \Omega)$ , and  $2\tilde{a}_x - \tilde{a}_y = C$ , filled with particles. That means that a particle in the tori have  $\tilde{a}_x, \tilde{a}_y, \Omega$  satisfying the two invariants, with phases  $\tilde{\varphi}_x, \tilde{\varphi}_y$  satisfying  $\tilde{\varphi}_x + 2\tilde{\varphi}_y = \Omega$  (the  $\Omega$  variable is defined in Eq. 70). The situation is equivalent to what is done in the simulations when tracking one particle repeatedly for many turns, in the

condition that the particle explores all the tori.

The spatial coordinates of the particles populating the tori are given by

$$\frac{x}{\sqrt{\beta_x}} = \sqrt{a_x} \cos(\psi_x), \quad \frac{y}{\sqrt{\beta_y}} = \sqrt{a_y} \cos(\psi_y) \quad (138)$$

where we define for convenience

$$\psi_x = Q_x \theta + \varphi_x, \quad \psi_y = Q_y \theta + \varphi_y, \quad (139)$$

where the quantities  $a_x, a_y, \varphi_x, \varphi_y$  vary in time. For this case (constant focusing) the beta functions are  $\beta_x = 1/Q_x, \beta_y = 1/Q_y$ . As discussed before, a specific set of initial particle coordinates is identified by the initial condition  $a_{x0}, a_{y0}, \varphi_{x0}, \varphi_{y0}$ , and this condition is used for integrating the equation of motions of  $a'_x, a'_y, \varphi'_x, \varphi'_y$  (these are the Eqs. 35 with  $\mathcal{F}_x = \mathcal{F}_y = 0$ ). The momentum coordinates are obtained by differentiation

$$\begin{aligned} \left( \frac{x}{\sqrt{\beta_x}} \right)' &= \frac{a'_x}{2\sqrt{a_x}} \cos(\psi_x) - \sqrt{a_x} \sin(\psi_x) (Q_x + \varphi'_x), \\ \left( \frac{y}{\sqrt{\beta_y}} \right)' &= \frac{a'_y}{2\sqrt{a_y}} \cos(\psi_y) - \sqrt{a_y} \sin(\psi_y) (Q_y + \varphi'_y). \end{aligned} \quad (140)$$

The variables  $a'_x, a'_y, \varphi'_x, \varphi'_y$  can be expressed in terms of  $\tilde{a}'_x, \tilde{a}'_y, \tilde{\varphi}'_x, \tilde{\varphi}'_y$ , by using the transformations

$$\begin{aligned} a_x &= \tilde{a}_x, & a_y &= \tilde{a}_y, \\ \varphi_x &= \tilde{\varphi}_x - t_x \theta, & \varphi_y &= \tilde{\varphi}_y - t_y \theta. \end{aligned} \quad (141)$$

and in these variables we know what is  $\tilde{a}'_x, \tilde{a}'_y, \tilde{\varphi}'_x, \tilde{\varphi}'_y$  from the equation 35 (with  $\mathcal{F}_x = \mathcal{F}_y = 0$ ). By substituting the equations of motion Eqs. 35 in Eqs. 140, and after some algebraic calculations we obtain

$$\begin{aligned} \left( \frac{x}{\sqrt{\beta_x}} \right)' &= \Lambda \tilde{a}_y \sin(-\psi_x + \Omega) - \sqrt{\tilde{a}_x} \sin(\psi_x) Q_x, \\ \left( \frac{y}{\sqrt{\beta_y}} \right)' &= 2\Lambda \sqrt{\tilde{a}_x \tilde{a}_y} \sin(-\psi_y + \Omega) - \sqrt{\tilde{a}_y} \sin(\psi_y) Q_y. \end{aligned} \quad (142)$$

At this point we define the “normalized” coordinates (suggested by Eq. 78)

$$\begin{aligned} \chi &= \frac{x}{\sqrt{\beta_x}} \left| \frac{4\Lambda}{\Delta_r} \right| \\ \chi_p &= \left( \frac{d}{d\theta} \frac{x}{\sqrt{\beta_x}} \right) \beta_x \left| \frac{4\Lambda}{\Delta_r} \right| = x' \sqrt{\beta_x} \left| \frac{4\Lambda}{\Delta_r} \right| \end{aligned} \quad (143)$$

$$\begin{aligned} y &= \frac{y}{\sqrt{\beta_y}} \left| \frac{4\Lambda}{\Delta_r} \right| \\ y_p &= \left( \frac{d}{d\theta} \frac{y}{\sqrt{\beta_y}} \right) \beta_y \left| \frac{4\Lambda}{\Delta_r} \right| = y' \sqrt{\beta_y} \left| \frac{4\Lambda}{\Delta_r} \right| \end{aligned} \quad (144)$$

Therefore the particle in the “normalized” coordinates reads

$$\begin{aligned} \chi &= \sqrt{\hat{a}_x} \cos(\psi_x) \\ \chi_p &= \frac{\beta_x}{4} \mu \Delta_r \hat{a}_y \sin(-\psi_x + \Omega) - \sqrt{\hat{a}_x} \sin(\psi_x) \\ y &= \sqrt{\hat{a}_y} \cos(\psi_y) \\ y_p &= \frac{\beta_y}{2} \mu \Delta_r \sqrt{\hat{a}_x \hat{a}_y} \sin(-\psi_y + \Omega) - \sqrt{\hat{a}_y} \sin(\psi_y) \end{aligned} \quad (145)$$

where the coordinates  $\hat{a}_x, \hat{a}_y$  are those defined in Eq. 78.

Using the definition  $\tilde{\varphi}_x + 2\tilde{\varphi}_y = \Omega$ , we find that  $\psi_x, \psi_y$  are bounded by the relation  $\psi_x + 2\psi_y = N\theta + \Omega$ . As the Tori is being filled, we make sure which particles satisfy some special condition at say  $\theta = 0$  (we do not need to consider many turns, because the tori is completely populated with particles, and after each turn the tori remain populated in the same way). Hence the tori cut at  $\theta = 0$  yields

$$\psi_x + 2\psi_y = \Omega. \quad (146)$$

In order to obtain the orbits in  $x - x'$ , i.e. in  $\chi - \chi_p$ , we require that we select only the particles with  $y_p = 0$ . For small  $\Delta_r$ , this happens for all particles in the Tori, which have  $\psi_y = \pi m$ , with  $m$  an integer. That means that we choose particles with a phase in the  $x$  plane as

$$\psi_x = -2\pi m + \Omega. \quad (147)$$

By substituting Eq. 147 into the Eq. 145 (formula for  $\chi_p$ ) we find that the coordinates of the orbits obtained by cutting the tori imposing  $y_p = 0$  are given by the map

$$\begin{cases} \chi = \sqrt{\hat{a}_x} \cos(\Omega) \\ \chi_p = -\sqrt{\hat{a}_x} \sin(\Omega) \end{cases} \quad (148)$$

where  $\hat{a}_x, \Omega$  must satisfy the invariants that defines the tori. As we started with the filled tori, any pair  $\hat{a}_x, \Omega$  satisfying  $\hat{I} = \hat{I}(\hat{a}_x, \Omega), 2\hat{a}_x - \hat{a}_y = 2\xi$  will identify a particle initially populating the tori, and can be used in Eq. 148. The condition  $y > 0$ , i.e.  $y > 0$ , implies  $m = 2n$  with  $n$  an integer. However, this condition does not change Eq. 148.

We proceed in a similar way for the cut in  $\chi_p = 0$ , we select the particles that satisfies  $\psi_x = \pi m$ , with  $m$  an integer, in addition the condition that  $x > 0$ , i.e.,  $\chi > 0$ , implies  $m = 2n$ , with  $n$  an integer. As discussed before we consider the tori at  $\theta = 0$ . Therefore once we fix  $\Omega$ , there are the following phases possible

$$\psi_y = \frac{\Omega}{2} - \pi n. \quad (149)$$

Substituting it in Eq. 145 (last two equations) we find the following map

$$\begin{cases} y = (-1)^n \sqrt{\hat{a}_y} \cos\left(\frac{\Omega}{2}\right) \\ y_p = -(-1)^n \sqrt{\hat{a}_y} \sin\left(\frac{\Omega}{2}\right) \end{cases} \quad (150)$$

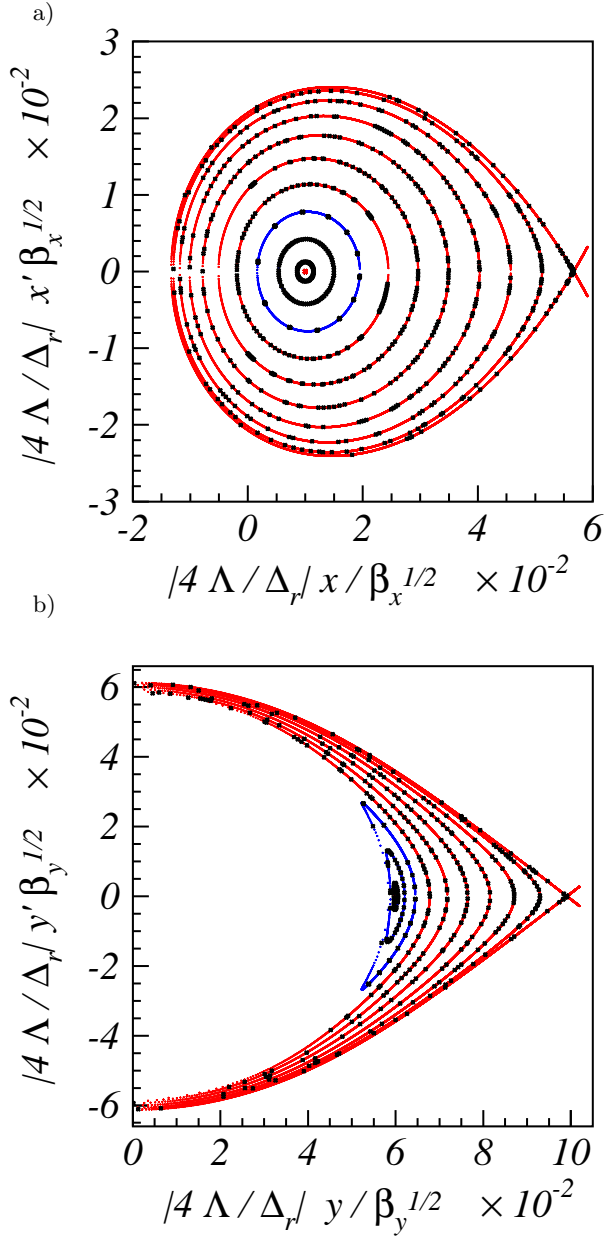


FIG. 26: Tori cut for parameters  $\Delta_r, \Delta$  such that  $\mu = -1$ . The solid curves are the orbits obtained from the analytic theory, while the dots are the coordinates of one particle tracked and plot when it satisfies the tori cut condition. The red curves are the orbits of particles in the red dashed region of part b) of Fig. 17 (stability type 1); The blue orbits are for particles with initial condition in the blue dashed region of part b) of Fig. 17 (stability type 2); Note in the center of the circular blue orbits one red dot: this is the “stationary point” discussed in Sec. VIII B 4.

As before  $\hat{a}_x, \Omega$  must satisfy the invariants that define the tori, i.e.  $\hat{I} = \hat{I}(\hat{a}_x, \Omega)$ ,  $2\hat{a}_x - \hat{a}_y = 2\xi$ . We recall that the fix-lines are defined by the level lines of  $\hat{I} = \hat{I}(\hat{a}_x, \Omega)$  that are tangent to the line  $\mathcal{Y} = 1$ , with  $\mathcal{Y} = -\mu \cos \Omega$ , being  $\mu = \pm 1$ , the sign depends on the combination of the signs of  $\Delta, \Delta_r$ . That simply means that  $\Omega$  of the fix-line is given by  $\Omega = \Omega_{fl} = \frac{\pi}{2}(1+\mu)$ . Substituting this value into Eq. 150 we find that the fix-line are located at  $y = 0, y_p =$

$-(-1)^n \sqrt{\hat{a}_y}$  for  $\mu = 1$ , and at  $y = (-1)^n \sqrt{\hat{a}_y}, y_p = 0$  for  $\mu = -1$  under the tori cut conditions. Figure 26 shows a comparison of the orbits in  $x - x'$  and  $y - y'$  with the particle tracking. For this simulation it holds  $\mu = -1$ . The color of the curves is associated to the stability properties of the level lines as discussed in Fig. 17.

## XI. CONCLUSION

We have derived the theory of the fix-lines and the stability domain close to a third order coupled resonance.

We find that the number of fix-lines is infinite, and that they are of stable or unstable type. The set of fix-lines form a continuous curve of parabolic shape in the plane of the single particle emittances  $\tilde{a}_x, \tilde{a}_y$ . The theory suggests a natural parametrization of the fix-lines based on the canonical transformation that makes the system time independent.

Our theory predicts the behavior of perturbation close to a fix-line and we find the property that the perturbation oscillates along a line with  $2\delta\tilde{a}_x = \delta\tilde{a}_y$ . Our analysis shows that these objects define the border of stability when a single harmonics is excited. The structure of the canonical equation of the constants suggests a natural symmetry set by the resonance condition. We find that for the variables  $\tilde{a}_x, \Omega$  the dynamics imposes an invariant, and using this invariant we discuss the complete set of topological properties of the level lines. It turns out that the level line associated to the fix-line creates a barrier to particles, hence they set the edge of the stability domain.

The extension of the theory to the alternating gradient circular structure has been worked out essentially retrieving the driving term of Hagedorn/Schoch [3–5] Guignard [6, 7], setting then the relation between the fix-lines and the onset of unbounded motion. The distributions of errors creates mainly an angle  $\alpha$  that enters into the theory, but it does not otherwise change the conclusion found for the constant focusing case.

This work will be the foundation for the study of the resonance crossing induced by space charge conjoint with a coupled resonance line.

## XII. ACKNOWLEDGMENT

“The research leading to these results has received funding from the European Commission under the FP7 Research Infrastructures project EuCARD-2, grant agreement no.312453”

### XIII. APPENDIX A: THE PERTURBED MOTION AROUND A FIX-LINE

The starting point are the equations of the perturbed system, Eq. 53, that we report here for convenience

$$\begin{aligned}\delta\tilde{a}'_x &= -\lambda\delta\tilde{\varphi}_x - 2\lambda\delta\tilde{\varphi}_y, \\ \delta\tilde{a}'_y &= -2\lambda\delta\tilde{\varphi}_x - 4\lambda\delta\tilde{\varphi}_y, \\ \delta\tilde{\varphi}'_x &= A_{xx}\delta\tilde{a}_x + A_{xy}\delta\tilde{a}_y, \\ \delta\tilde{\varphi}'_y &= A_{yx}\delta\tilde{a}_x + A_{yy}\delta\tilde{a}_y,\end{aligned}\quad (151)$$

after some algebra they become

$$\begin{aligned}\delta\tilde{a}''_x &= -\omega^2\delta\tilde{a}_x + \lambda(A_{xy} + 2A_{yy})C_p, \\ \delta\tilde{a}''_y &= -\omega^2\delta\tilde{a}_y - \lambda(A_{xx} + 2A_{yx})C_p, \\ \delta\tilde{\varphi}''_x &= -\lambda(A_{xx} + 2A_{xy})(\delta\tilde{\varphi}_x + 2\delta\tilde{\varphi}_y), \\ \delta\tilde{\varphi}''_y &= -\lambda(A_{yx} + 2A_{yy})(\delta\tilde{\varphi}_x + 2\delta\tilde{\varphi}_y),\end{aligned}\quad (152)$$

where we defined

$$\omega^2 = \lambda(A_{xx} + 2A_{yx} + 2A_{xy} + 4A_{yy}). \quad (153)$$

The coefficient  $C_p$  is a constant obtained from integrating Eqs. 151

$$2\delta\tilde{a}_x = \delta\tilde{a}_y + C_p. \quad (154)$$

From equation Eq. 152 we also find

$$(\delta\tilde{\varphi}_x + 2\delta\tilde{\varphi}_y)'' = -\omega^2(\delta\tilde{\varphi}_x + 2\delta\tilde{\varphi}_y). \quad (155)$$

The general conclusion is that for

$$\omega^2 > 0 \quad (156)$$

the quantity  $\delta\tilde{\varphi}_x + 2\delta\tilde{\varphi}_y$  is stable and oscillate around zero as well as  $\delta\tilde{a}_x$ , and  $\delta\tilde{a}_y$ . We now consider the case  $\omega^2 > 0$ . Integrating Eq. 155 we find

$$\delta\tilde{\varphi}_x + 2\delta\tilde{\varphi}_y = A \cos(\omega\theta + \xi) \quad (157)$$

with  $A, \xi$  some constant. Using this result in Eq. 152 we find

$$\begin{aligned}\delta\tilde{\varphi}''_x &= -\lambda(A_{xx} + 2A_{xy})A \cos(\omega\theta + \xi), \\ \delta\tilde{\varphi}''_y &= -\lambda(A_{yx} + 2A_{yy})A \cos(\omega\theta + \xi).\end{aligned}\quad (158)$$

The integration of these equations yields

$$\begin{aligned}\delta\tilde{\varphi}_x &= \lambda(A_{xx} + 2A_{xy})\frac{A}{\omega^2} \cos(\omega\theta + \xi) + C_x\theta + D_x, \\ \delta\tilde{\varphi}_y &= \lambda(A_{yx} + 2A_{yy})\frac{A}{\omega^2} \cos(\omega\theta + \xi) + C_y\theta + D_y,\end{aligned}\quad (159)$$

with  $C_x, C_y, D_x, D_y$  the integration constants to be determined later. The first two equations of Eq 152 can be integrated as well, we find

$$\begin{aligned}\delta\tilde{a}_x &= B_x \sin(\omega\theta + \tau_x) + \frac{\lambda}{\omega^2}(A_{xy} + 2A_{yy})C_p, \\ \delta\tilde{a}_y &= B_y \sin(\omega\theta + \tau_y) - \frac{\lambda}{\omega^2}(A_{xx} + 2A_{yx})C_p,\end{aligned}\quad (160)$$

with integration constants  $B_x, B_y, \tau_x, \tau_y$ . The equations 159, and 160 are obtained from Eq. 152, but these solutions must be consistent with Eq. 151. We next find the constraint imposed by this condition.

We use the first two equations of Eq. 151

$$\begin{aligned}\delta\tilde{a}'_x &= -\lambda\delta\tilde{\varphi}_x - 2\lambda\delta\tilde{\varphi}_y, \\ \delta\tilde{a}'_y &= -2\lambda\delta\tilde{\varphi}_x - 4\lambda\delta\tilde{\varphi}_y,\end{aligned}\quad (161)$$

and substitute Eq. 160 and Eq. 157. We find

$$\begin{aligned}B_x\omega \cos(\omega\theta + \tau_x) &= -\lambda A \cos(\omega\theta + \xi) \\ B_y\omega \cos(\omega\theta + \tau_y) &= -2\lambda A \cos(\omega\theta + \xi)\end{aligned}\quad (162)$$

therefore it must be  $\tau_x = \tau_y = \xi$ ,  $B_x = -\lambda A/\omega$ , and  $B_y = -2\lambda A/\omega$ . The solution becomes

$$\begin{aligned}\delta\tilde{a}_x &= -\frac{\lambda A}{\omega} \sin(\omega\theta + \xi) + \frac{\lambda}{\omega^2}(A_{xy} + 2A_{yy})C_p, \\ \delta\tilde{a}_y &= -\frac{2\lambda A}{\omega} \sin(\omega\theta + \xi) - \frac{\lambda}{\omega^2}(A_{xx} + 2A_{yx})C_p, \\ \delta\tilde{\varphi}_x &= \lambda(A_{xx} + 2A_{xy})\frac{A}{\omega^2} \cos(\omega\theta + \xi) + C_x\theta + D_x, \\ \delta\tilde{\varphi}_y &= \lambda(A_{yx} + 2A_{yy})\frac{A}{\omega^2} \cos(\omega\theta + \xi) + C_y\theta + D_y,\end{aligned}\quad (163)$$

Now we use the last two equations of Eqs. 151

$$\begin{aligned}\delta\tilde{\varphi}'_x &= A_{xx}\delta\tilde{a}_x + A_{xy}\delta\tilde{a}_y, \\ \delta\tilde{\varphi}'_y &= A_{yx}\delta\tilde{a}_x + A_{yy}\delta\tilde{a}_y,\end{aligned}\quad (164)$$

and substituting the Eqs. 163 we find

$$\begin{aligned}C_x &= 2\frac{\lambda}{\omega^2}C_p(A_{xx}A_{yy} - A_{xy}A_{yx}), \\ C_y &= -\frac{\lambda}{\omega^2}C_p(A_{yy}A_{xx} - A_{yx}A_{xy}).\end{aligned}\quad (165)$$

Therefore the solutions take the form

$$\begin{aligned}\delta\tilde{a}_x &= -\frac{\lambda A}{\omega} \sin(\omega\theta + \xi) + \frac{\lambda}{\omega^2}(A_{xy} + 2A_{yy})C_p, \\ \delta\tilde{a}_y &= -\frac{2\lambda A}{\omega} \sin(\omega\theta + \xi) - \frac{\lambda}{\omega^2}(A_{xx} + 2A_{yx})C_p, \\ \delta\tilde{\varphi}_x &= \lambda(A_{xx} + 2A_{xy})\frac{A}{\omega^2} \cos(\omega\theta + \xi) \\ &\quad + 2\frac{\lambda}{\omega^2}C_p(A_{xx}A_{yy} - A_{xy}A_{yx})\theta + D_x, \\ \delta\tilde{\varphi}_y &= \lambda(A_{yx} + 2A_{yy})\frac{A}{\omega^2} \cos(\omega\theta + \xi) \\ &\quad - \frac{\lambda}{\omega^2}C_p(A_{xx}A_{yy} - A_{xy}A_{yx})\theta + D_y.\end{aligned}\quad (166)$$

As

$$\delta\tilde{\varphi}_x + 2\delta\tilde{\varphi}_y = A \cos(\omega\theta + \xi) \quad (167)$$

substituting we find

$$D_x + 2D_y = 0 \quad (168)$$

Therefore the general evolution of a perturbation around a fix-line point takes the form

$$\begin{aligned}
\delta\tilde{a}_x &= -\frac{\lambda A}{\omega} \sin(\omega\theta + \xi) + \frac{\lambda}{\omega^2} (A_{xy} + 2A_{yy})C_p, \\
\delta\tilde{a}_y &= -\frac{2\lambda A}{\omega} \sin(\omega\theta + \xi) - \frac{\lambda}{\omega^2} (A_{xx} + 2A_{yx})C_p, \\
\delta\tilde{\varphi}_x &= \lambda(A_{xx} + 2A_{xy})\frac{A}{\omega^2} \cos(\omega\theta + \xi) \\
&\quad + 2\frac{\lambda}{\omega^2} C_p (A_{xx}A_{yy} - A_{xy}A_{yx})\theta - 2D_y, \\
\delta\tilde{\varphi}_y &= \lambda(A_{yx} + 2A_{yy})\frac{A}{\omega^2} \cos(\omega\theta + \xi) \\
&\quad - \frac{\lambda}{\omega^2} C_p (A_{xx}A_{yy} - A_{xy}A_{yx})\theta + D_y.
\end{aligned} \tag{169}$$

The free parameters  $A, \xi, C_p, D_y$  are found from Eq. 169 at  $\theta = 0$  using the initial conditions

$$\begin{aligned}
(\delta\tilde{a}_x)_0 &= -\frac{\lambda A}{\omega} \sin(\xi) + \frac{\lambda}{\omega^2} (A_{xy} + 2A_{yy})C_p, \\
(\delta\tilde{a}_y)_0 &= -\frac{2\lambda A}{\omega} \sin(\xi) - \frac{\lambda}{\omega^2} (A_{xx} + 2A_{yx})C_p, \\
(\delta\tilde{\varphi}_x)_0 &= \lambda(A_{xx} + 2A_{xy})\frac{A}{\omega^2} \cos(\xi) - 2D_y, \\
(\delta\tilde{\varphi}_y)_0 &= \lambda(A_{yx} + 2A_{yy})\frac{A}{\omega^2} \cos(\xi) + D_y.
\end{aligned} \tag{170}$$

### A. Discussion

Suppose we consider a fix-line defined by  $\tilde{a}_x, \tilde{a}_y$ . This means that a particle on this fix-line has constant  $\tilde{a}_x, \tilde{a}_y$ , while its phases  $\tilde{\varphi}_x, \tilde{\varphi}_y$  are also constant, and satisfy the condition  $\tilde{\varphi}_x + 2\tilde{\varphi}_y = \pi M$ . Taking any other pair of  $\tilde{\varphi}_x, \tilde{\varphi}_y$  that satisfy  $\tilde{\varphi}_x + 2\tilde{\varphi}_y = \pi M$  simply means to take another point on the fix-line, but again  $\tilde{\varphi}_x, \tilde{\varphi}_y$  remain constant. Therefore any phases  $\tilde{\varphi}_x, \tilde{\varphi}_y$  satisfying  $\tilde{\varphi}_x + 2\tilde{\varphi}_y = \pi M$  are equally good.

By saying that  $\tilde{a}_x, \tilde{a}_y$  identify a fix-line we intend the identification of the fix-line without any reference to the phases of a particle on it.

Consider now at  $\theta = 0$  a point of coordinates  $\tilde{a}_x, \tilde{a}_y, \tilde{\varphi}_x, \tilde{\varphi}_y$  lying on the fix-line identified by  $\tilde{a}_x, \tilde{a}_y$ . Consider now a perturbation  $\delta\tilde{a}_x, \delta\tilde{a}_y, \delta\tilde{\varphi}_x, \delta\tilde{\varphi}_y$  from that point, and consider the particle with coordinates

$$\tilde{a}_x + \delta\tilde{a}_x, \tilde{a}_y + \delta\tilde{a}_y, \tilde{\varphi}_x + \delta\tilde{\varphi}_x, \tilde{\varphi}_y + \delta\tilde{\varphi}_y. \tag{171}$$

The evolution of the coordinates of the particle is given by  $\tilde{a}_x = \text{const}, \tilde{a}_y = \text{const}, \tilde{\varphi}_x = \text{const}, \tilde{\varphi}_y = \text{const}$ , and by the evolution of the perturbation  $\delta\tilde{a}_x, \delta\tilde{a}_y, \delta\tilde{\varphi}_x, \delta\tilde{\varphi}_y$ , which is given by the equations Eq. 169. We note that if  $C_p = 2(\delta\tilde{a}_x)_0 - (\delta\tilde{a}_y)_0 \neq 0$ , the oscillation of the perturbation  $\delta\tilde{a}_x, \delta\tilde{a}_y$  is not around  $\tilde{a}_x, \tilde{a}_y$ , while the perturbations  $\delta\tilde{\varphi}_x, \delta\tilde{\varphi}_y$  are unbounded. The perturbative analysis seems to collapse. On the other hand the quantity  $\delta\tilde{\varphi}_x + 2\delta\tilde{\varphi}_y$  (Eq. 167) remains bounded around zero!

Lets now consider the point with coordinates

$$\begin{aligned}
\tilde{a}_x^c &= \tilde{a}_x + \delta\tilde{a}_x^c = \tilde{a}_x + \frac{\lambda}{\omega^2} (A_{xy} + 2A_{yy})C_p, \\
\tilde{a}_y^c &= \tilde{a}_y + \delta\tilde{a}_y^c = \tilde{a}_y - \frac{\lambda}{\omega^2} (A_{xx} + 2A_{yx})C_p, \\
\tilde{\varphi}_x^c &= \tilde{\varphi}_x + \delta\tilde{\varphi}_x^c = \tilde{\varphi}_x - 2\alpha, \\
\tilde{\varphi}_y^c &= \tilde{\varphi}_y + \delta\tilde{\varphi}_y^c = \tilde{\varphi}_y + \alpha,
\end{aligned} \tag{172}$$

where we defined for convenience  $\delta\tilde{a}_x^c, \delta\tilde{a}_y^c, \delta\tilde{\varphi}_x^c, \delta\tilde{\varphi}_y^c$ . The parameter  $\alpha$  is an arbitrary parameter that defines the point. We observe that the coordinates  $\tilde{a}_x + \delta\tilde{a}_x, \tilde{a}_y + \delta\tilde{a}_y$  oscillate around  $\tilde{a}_x^c, \tilde{a}_y^c$ .

By construction the coordinates,  $\tilde{a}_x^c, \tilde{a}_y^c, \tilde{\varphi}_x^c, \tilde{\varphi}_y^c$  do not change in time. We will prove that they identify a fix-line point of a new fix-line identified by  $\tilde{a}_x^c, \tilde{a}_y^c$ .

We start by writing the equation of the fix-line in the general form

$$\frac{\partial \tilde{H}_{s1}}{\partial \tilde{a}_x} + 2\frac{\partial \tilde{H}_{s1}}{\partial \tilde{a}_y} = 0, \tag{173}$$

this equation is Eq. 42 (top) expressed in terms of the slowly varying Hamiltonian  $\tilde{H}_{s1}$ . We now check if  $\tilde{a}_x^c, \tilde{a}_y^c$  satisfies the previous equation (Eq. 173). We find

$$\begin{aligned}
\frac{\partial \tilde{H}_{s1}}{\partial \tilde{a}_x}(\tilde{a}_x^c, \tilde{a}_y^c) + 2\frac{\partial \tilde{H}_{s1}}{\partial \tilde{a}_y}(\tilde{a}_x^c, \tilde{a}_y^c) &= \frac{\partial \tilde{H}_{s1}}{\partial \tilde{a}_x}(\tilde{a}_x, \tilde{a}_y) + \frac{\partial^2 \tilde{H}_{s1}}{\partial \tilde{a}_x^2}(\tilde{a}_x, \tilde{a}_y)\delta\tilde{a}_x^c + \frac{\partial^2 \tilde{H}_{s1}}{\partial \tilde{a}_x \partial \tilde{a}_y}(\tilde{a}_x, \tilde{a}_y)\delta\tilde{a}_y^c + \\
&\quad + 2\frac{\partial \tilde{H}_{s1}}{\partial \tilde{a}_y}(\tilde{a}_x, \tilde{a}_y) + 2\frac{\partial^2 \tilde{H}_{s1}}{\partial \tilde{a}_y \partial \tilde{a}_x}(\tilde{a}_x, \tilde{a}_y)\delta\tilde{a}_x^c + 2\frac{\partial^2 \tilde{H}_{s1}}{\partial \tilde{a}_y^2}(\tilde{a}_x, \tilde{a}_y)\delta\tilde{a}_y^c.
\end{aligned} \tag{174}$$

Taking into account that  $\tilde{a}_x, \tilde{a}_y$  is a fix-line, then

$$\begin{aligned} \frac{\partial \tilde{H}_{s1}}{\partial \tilde{a}_x}(\tilde{a}_x^c, \tilde{a}_y^c) + 2 \frac{\partial \tilde{H}_{s1}}{\partial \tilde{a}_y}(\tilde{a}_x^c, \tilde{a}_y^c) &= \frac{\partial^2 \tilde{H}_{s1}}{\partial \tilde{a}_x^2}(\tilde{a}_x, \tilde{a}_y) \delta \tilde{a}_x^c + \frac{\partial^2 \tilde{H}_{s1}}{\partial \tilde{a}_x \partial \tilde{a}_y}(\tilde{a}_x, \tilde{a}_y) \delta \tilde{a}_y^c + \\ &+ 2 \frac{\partial^2 \tilde{H}_{s1}}{\partial \tilde{a}_y \partial \tilde{a}_x}(\tilde{a}_x, \tilde{a}_y) \delta \tilde{a}_x^c + 2 \frac{\partial^2 \tilde{H}_{s1}}{\partial \tilde{a}_y^2}(\tilde{a}_x, \tilde{a}_y) \delta \tilde{a}_y^c. \end{aligned} \quad (175)$$

Using the definitions for  $A_{xx}, A_{xy}, A_{yx}, A_{yy}$  the previous equation becomes

$$\begin{aligned} \frac{\partial \tilde{H}_{s1}}{\partial \tilde{a}_x}(\tilde{a}_x^c, \tilde{a}_y^c) + 2 \frac{\partial \tilde{H}_{s1}}{\partial \tilde{a}_y}(\tilde{a}_x^c, \tilde{a}_y^c) &= \\ \frac{1}{2} [(A_{xx} + 2A_{yx}) \delta \tilde{a}_x^c + (A_{xy} + 2A_{yy}) \delta \tilde{a}_y^c]. \end{aligned} \quad (176)$$

Now we substitute  $\delta \tilde{a}_x^c, \delta \tilde{a}_y^c$  from Eq. 172, and we find

$$\begin{aligned} \frac{\partial \tilde{H}_{s1}}{\partial \tilde{a}_x}(\tilde{a}_x^c, \tilde{a}_y^c) + 2 \frac{\partial \tilde{H}_{s1}}{\partial \tilde{a}_y}(\tilde{a}_x^c, \tilde{a}_y^c) &= \\ \frac{1}{2} \frac{\lambda}{\omega^2} C_p [(A_{xx} + 2A_{yx})(A_{xy} + 2A_{yy}) & \\ - (A_{xy} + 2A_{yy})(A_{xx} + 2A_{yx})] &= 0. \end{aligned} \quad (177)$$

We conclude that  $\tilde{a}_x^c, \tilde{a}_y^c$  satisfy the equation for the fix-line, and therefore it identifies a fix-line. The phases  $\tilde{\varphi}_x^c, \tilde{\varphi}_y^c$  also satisfy the condition of a fix-line, in fact we find

$$\tilde{\varphi}_x^c + 2\tilde{\varphi}_y^c = \tilde{\varphi}_x - 2\alpha + 2\tilde{\varphi}_y + 2\alpha = \tilde{\varphi}_x + 2\tilde{\varphi}_y = \pi M. \quad (178)$$

Therefore  $\tilde{a}_x^c, \tilde{a}_y^c, \tilde{\varphi}_x^c, \tilde{\varphi}_y^c$  is a point on another fix-line identified by  $\tilde{a}_x^c, \tilde{a}_y^c$ .

The initial perturbation with respect to this new point belonging to another fix-line reads

$$\begin{aligned} (\delta \tilde{a}_x)_1 &= \tilde{a}_x + (\delta \tilde{a}_x)_0 - \tilde{a}_x^c = (\delta \tilde{a}_x)_0 - \frac{\lambda}{\omega^2} (A_{xy} + 2A_{yy}) C_p, \\ (\delta \tilde{a}_y)_1 &= \tilde{a}_y + (\delta \tilde{a}_y)_0 - \tilde{a}_y^c = (\delta \tilde{a}_y)_0 + \frac{\lambda}{\omega^2} (A_{xx} + 2A_{yx}) C_p, \\ (\delta \tilde{\varphi}_x)_1 &= \tilde{\varphi}_x + (\delta \tilde{\varphi}_x)_0 - \tilde{\varphi}_x^c = (\delta \tilde{\varphi}_x)_0 + 2\alpha, \\ (\delta \tilde{\varphi}_y)_1 &= \tilde{\varphi}_y + (\delta \tilde{\varphi}_y)_0 - \tilde{\varphi}_y^c = (\delta \tilde{\varphi}_y)_0 - \alpha. \end{aligned} \quad (179)$$

We use the index 1 to denote the initial condition of the original perturbation now re-written with respect to the new fix-line. Therefore

$$C'_p = 2(\delta \tilde{a}_x)_1 - (\delta \tilde{a}_y)_1 = 0 \quad (180)$$

This means that the initial perturbation with respect to the point belonging to the new fix-line has the correspondent  $C'_p$  equal to zero, and the evolution of the initial

perturbation with respect to the new point reads

$$\begin{aligned} \delta \tilde{a}_x &= -\frac{\lambda' A'}{\omega'} \sin(\omega' \theta + \xi'), \\ \delta \tilde{a}_y &= -\frac{2\lambda' A'}{\omega'} \sin(\omega' \theta + \xi'), \\ \delta \tilde{\varphi}_x &= \lambda' (A'_{xx} + 2A'_{xy}) \frac{A'}{\omega'^2} \cos(\omega' \theta + \xi') - 2D'_y, \\ \delta \tilde{\varphi}_y &= \lambda' (A'_{xy} + 2A'_{yy}) \frac{A'}{\omega'^2} \cos(\omega' \theta + \xi') + D'_y, \end{aligned} \quad (181)$$

where now  $A'_{xx}, A'_{xy}, A'_{yx}, A'_{yy}, \lambda', \omega'$  are evaluated at  $\tilde{a}_x^c, \tilde{a}_y^c$ , and the constants  $A', \xi', D'_y$  are computed from the initial condition  $(\delta \tilde{a}_x)_1, (\delta \tilde{a}_y)_1, (\delta \tilde{\varphi}_x)_1, (\delta \tilde{\varphi}_y)_1$ . We find

$$\begin{aligned} (\delta \tilde{a}_x)_1 &= -\frac{\lambda' A'}{\omega'} \sin(\xi'), \\ (\delta \tilde{a}_y)_1 &= -\frac{2\lambda' A'}{\omega'} \sin(\xi'), \\ (\delta \tilde{\varphi}_x)_1 &= \lambda' (A'_{xx} + 2A'_{xy}) \frac{A'}{\omega'^2} \cos(\xi') - 2D'_y, \\ (\delta \tilde{\varphi}_y)_1 &= \lambda' (A'_{xy} + 2A'_{yy}) \frac{A'}{\omega'^2} \cos(\xi') + D'_y. \end{aligned} \quad (182)$$

Now we use the definition of  $(\delta \tilde{a}_x)_1, (\delta \tilde{a}_y)_1, (\delta \tilde{\varphi}_x)_1, (\delta \tilde{\varphi}_y)_1$  and get

$$\begin{aligned} (\delta \tilde{a}_x)_1 &= -\frac{\lambda A}{\omega} \sin(\xi), \\ (\delta \tilde{a}_y)_1 &= -\frac{2\lambda A}{\omega} \sin(\xi), \\ (\delta \tilde{\varphi}_x)_1 &= \lambda (A_{xx} + 2A_{xy}) \frac{A}{\omega^2} \cos(\xi) - 2D_y + 2\alpha, \\ (\delta \tilde{\varphi}_y)_1 &= \lambda (A_{xy} + 2A_{yy}) \frac{A}{\omega^2} \cos(\xi) + D_y - \alpha. \end{aligned} \quad (183)$$

Substituting Eq. 183 into Eq. 182 we find that

$$\begin{aligned} -\frac{\lambda A}{\omega} \sin(\xi) &= -\frac{\lambda' A'}{\omega'} \sin(\xi'), \\ \lambda (A_{xx} + 2A_{xy}) \frac{A}{\omega^2} \cos(\xi) - 2D_y + 2\alpha &= \\ = \lambda' (A'_{xx} + 2A'_{xy}) \frac{A'}{\omega'^2} \cos(\xi') - 2D'_y, \\ \lambda (A_{xy} + 2A_{yy}) \frac{A}{\omega^2} \cos(\xi) + D_y - \alpha &= \\ = \lambda' (A'_{xy} + 2A'_{yy}) \frac{A'}{\omega'^2} \cos(\xi') + D'_y. \end{aligned} \quad (184)$$



The parameters on the L.H.S. are determined by the perturbation with respect to the original fix-line point. The parameters on the R.H.S  $A', \xi', D'_y$  are the new parameters that identify the original perturbation with respect to the new fix-line point. Multiplying the last by 2 and summing with the second equation we find

$$A \cos(\xi) = A' \cos(\xi'), \quad (185)$$

which combined with the first of Eq. 184 yields

$$\begin{cases} A' \cos(\xi') = A \cos(\xi) \\ A' \sin(\xi') = \frac{\lambda \omega'}{\lambda' \omega} A \sin(\xi). \end{cases} \quad (186)$$

From this system we obtain  $A', \xi'$ .

Now we use the free parameter  $\alpha$  to require that  $D'_y = 0$ . We take the second equation of Eq. 184 and we find

$$\alpha = \lambda(A_{xy} + 2A_{yy}) \frac{A}{\omega^2} \cos(\xi) + D_y - \lambda'(A'_{xy} + 2A'_{yy}) \frac{A'}{\omega'^2} \cos(\xi') \quad (187)$$

substituting this value into the first equation of Eq. 184 we find

$$-2D'_y = A \cos(\xi) - A' \cos(\xi') = 0. \quad (188)$$

Therefore the parameter  $\alpha$  defined in Eq. 187 yields  $D'_y = 0$  in both second and third equations of Eq. 184.

We conclude that the original perturbation around the new fix-line point identified by  $\alpha$  with the value in Eq. 187 evolves according to

$$\begin{aligned} \delta \tilde{a}_x &= -\frac{\lambda' A'}{\omega'} \sin(\omega' \theta + \xi'), \\ \delta \tilde{a}_y &= -\frac{2\lambda' A'}{\omega'} \sin(\omega' \theta + \xi'), \\ \delta \tilde{\varphi}_x &= \lambda'(A'_{xx} + 2A'_{xy}) \frac{A'}{\omega'^2} \cos(\omega' \theta + \xi'), \\ \delta \tilde{\varphi}_y &= \lambda'(A'_{yx} + 2A'_{yy}) \frac{A'}{\omega'^2} \cos(\omega' \theta + \xi'). \end{aligned} \quad (189)$$

That is, the initial perturbation is oscillating around the point  $\tilde{a}_x^c, \tilde{a}_y^c, \tilde{\varphi}_x^c, \tilde{\varphi}_y^c$  of the new fix-line identified by  $\tilde{a}_x^c, \tilde{a}_y^c$ . In fact, in Eq. 169 we simply replace all constant with the primed ones and set  $C_p = 0$ . This results let's us proceed with the most simple case, i.e. with  $C_p = 0$ .

#### XIV. APPENDIX B: PROPERTIES OF THE LEVEL LINES

We address here the properties of the level lines as defined by Eq. 85. We distinguish the following cases.

##### A. $\xi > 0$

The level lines have the following properties:

- 1) The range of  $\hat{a}_x$  is  $\xi < \hat{a}_x < \infty$ , because  $\hat{a}_y \geq 0$ , and at  $\hat{a}_x = \xi$  the function  $\mathcal{Y}$  is not defined.
- 2) For  $\hat{a}_x \rightarrow +\infty$  we always find  $\mathcal{Y}(\hat{a}_x) \rightarrow 0$ .
- 3) Given  $\epsilon$  a positive, very small number, we find that for  $\hat{a}_x = \xi + \epsilon$  the following approximation holds

$$\mathcal{Y}(\xi + \epsilon) = -\frac{\hat{I} - \xi}{\sqrt{\xi} \epsilon}. \quad (190)$$

Therefore the asymptotic behaviour of the curve  $\mathcal{Y}$  for  $\hat{a}_x \rightarrow \xi^+$  changes according whether  $\hat{I} \gtrless \xi$ . We find

$$\hat{a}_x \rightarrow \xi^+ \implies \begin{cases} \mathcal{Y} \rightarrow -\infty & \text{for } \hat{I} > \xi \\ \mathcal{Y} \rightarrow +\infty & \text{for } \hat{I} < \xi \end{cases} \quad (191)$$

If  $\hat{I} = \xi$  then  $\mathcal{Y}$  takes the special form

$$\mathcal{Y}(\hat{a}_x) = \frac{1}{\sqrt{\hat{a}_x}}, \quad (192)$$

and for  $\hat{a}_x \rightarrow \xi^+$  we find  $\mathcal{Y} \rightarrow \mathcal{Y} = \frac{1}{\sqrt{\xi}}$ . Therefore the level line for  $\hat{I} = \xi$  separates the level lines into two classes of curves: one class where the curves diverge to  $+\infty$  when  $\hat{a}_x \rightarrow \xi^+$ , while in the other class the curves diverges to  $-\infty$  when  $\hat{a}_x \rightarrow \xi^+$ . This level line is shown by the red line in Fig. 27. Other two curves for  $\hat{I} < \xi$  and  $\hat{I} > \xi$  show the divergence property of  $\mathcal{Y}$ .

- 4) If  $\hat{a}_x = \hat{I}$  and  $\hat{I} \neq \xi$  we always find  $\mathcal{Y} = 0$ . Therefore for  $\hat{I} > \xi$  the level curve identified by  $\hat{I}$  will always cross  $\mathcal{Y} = 0$ .
- 5) The curves identified by the invariant  $\hat{I}$  can have: 1) no maximum and no minimum; 2) one maximum; 3) both maximum and minimum.

The solution of  $\mathcal{Y}'(\hat{a}_x^*) = 0$  for a level line defined by  $\hat{I}$  satisfies the relation

$$\hat{I} = \frac{(\hat{a}_x^*)^2 + \hat{a}_x^* \xi}{3\hat{a}_x^* - \xi} \quad (193)$$

and the value of  $\mathcal{Y}(\hat{a}_x^*)$  is given by

$$\mathcal{Y}(\hat{a}_x^*) = \frac{2\sqrt{\hat{a}_x^*}}{3\hat{a}_x^* - \xi}. \quad (194)$$

- 6) We observe that

$$\mathcal{Y}(\xi + \epsilon) \mathcal{Y}(\hat{a}_x^*) = \begin{cases} < 0 & \text{for } \hat{I} > \xi \\ > 0 & \text{for } \hat{I} < \xi \end{cases} \quad (195)$$

That means that for  $\hat{I} > \xi$  the point  $\mathcal{Y}(\hat{a}_x^*)$  is always on the opposite plane of where  $\mathcal{Y}$  diverges. This situation is shown in Fig. 27. The level line below the red curve has a maximum in  $(\hat{a}_x^*)_+$ , of value  $\mathcal{Y}((\hat{a}_x^*)_+)$ . The point  $(\hat{a}_x^*)_+, \mathcal{Y}((\hat{a}_x^*)_+)$ , is located in the half plane  $\mathcal{Y} > 0$ . In the other half the curve diverges for  $\hat{a}_x \rightarrow \xi^+$ .

- 7) The points of maximum or minimum are obtained by the equation  $\mathcal{Y}'(\hat{a}_x) = 0$ , which reads

$$\hat{a}_x^2 + (\xi - 3\hat{I})\hat{a}_x + \hat{I}\xi = 0, \quad (196)$$

and the values of the invariant for which the level curves can have a maximum or minimum are

$$\xi \geq 9\hat{I} \quad \text{or} \quad \xi \leq \hat{I}. \quad (197)$$

- 8) If  $\hat{I}$  is in the ranges of Eqs. 197 the two solutions of Eq. 196 are

$$(\hat{a}_x^*)_{\pm} = \frac{-\xi + 3\hat{I} \pm \sqrt{(\xi - 3\hat{I})^2 - 4\hat{I}\xi}}{2}. \quad (198)$$

We next have to control which of these solutions is consistent with the point 1). That defines the criteria if the solution is acceptable or not, (i.e. the criteria Eq. 83). We accept only the solution satisfying  $\xi < \hat{a}_x < \infty$ . According to the values of  $\hat{I}$ , and  $\xi$  the solution of Eq. 198 have the following properties

$$\hat{I} \leq \frac{\xi}{9} \implies \begin{cases} (\hat{a}_x^*)_+ < \xi & \text{not acceptable} \\ (\hat{a}_x^*)_- < 0 & \text{not acceptable} \end{cases} \quad (199)$$

$$\hat{I} \geq \xi \implies \begin{cases} (\hat{a}_x^*)_+ > \xi & \text{acceptable} \\ (\hat{a}_x^*)_+ = \xi & \text{not acceptable} \\ (\hat{a}_x^*)_- \leq \xi & \text{not acceptable} \end{cases} \quad (200)$$

We conclude that the level lines in the region  $\hat{I} > \xi$  have a maximum at  $(\hat{a}_x^*)_+$  and a minimum at  $\hat{a}_x \rightarrow \infty$ . For  $\hat{I} \leq \xi$  the level curves have no maximum. The general properties of the level lines for  $\xi > 0$  are summarized in the Fig. 27. The red curve separates all the level lines into two classes: one class of lines without any maximum, and a second class of lines with a maximum.

### B. $\xi = 0$

The level lines have the following properties:

- 1) The range of  $\hat{a}_x$  is  $0 < \hat{a}_x$ , because on  $\hat{a}_x = 0$  the function  $\mathcal{Y}$  is not defined.
- 2) For  $\hat{a}_x \rightarrow +\infty$  we consistently find  $\mathcal{Y}(\hat{a}_x) \rightarrow 0$ .
- 3) Let's study  $\mathcal{Y}$  in proximity of  $\hat{a}_x = 0$ . We take  $\epsilon$  an arbitrarily small, positive number. For  $\hat{a}_x = \epsilon$  we find

$$\mathcal{Y}(\epsilon) = -\frac{\hat{I}}{\epsilon^{3/2}}. \quad (201)$$

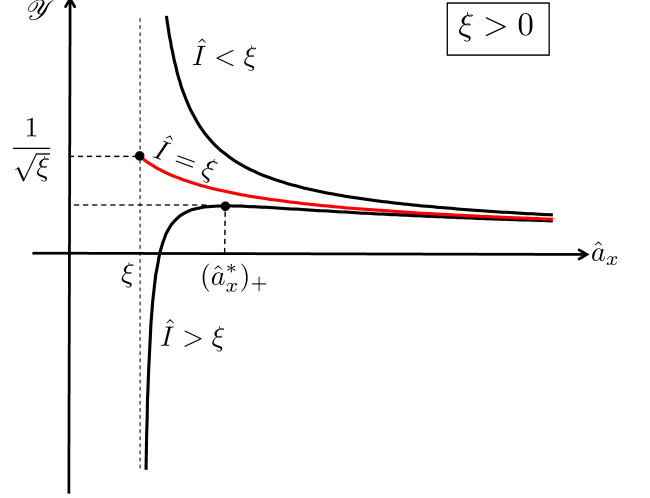


FIG. 27: Summary of the general behaviour of the level curves in the case  $\xi > 0$ .

with  $\hat{I} \neq 0$ . The curves defined by  $\hat{I}$  are distinguished into two classes of behaviour for the limit  $\hat{a}_x \rightarrow 0^+$  according to the value of  $\hat{I}$ :

$$\hat{a}_x \rightarrow 0^+ \implies \begin{cases} \mathcal{Y} \rightarrow -\infty & \text{for } \hat{I} > 0 \\ \mathcal{Y} \rightarrow +\infty & \text{for } \hat{I} < 0 \end{cases}. \quad (202)$$

If  $\hat{I} = 0$  the behaviour of  $\mathcal{Y}$  is different, in fact  $\mathcal{Y}$  takes the form

$$\mathcal{Y}(\hat{a}_x) = \frac{1}{\sqrt{\hat{a}_x}}, \quad (203)$$

and for  $\hat{a}_x \rightarrow 0^+$  we find  $\mathcal{Y} \rightarrow \infty$ . This particular level line is shown in Fig. 28 by the red curve. The curves below the red curve diverge to  $-\infty$  for  $\hat{a}_x \rightarrow 0^+$ , while the curves above the red curve will diverge to  $+\infty$  for  $\hat{a}_x \rightarrow 0^+$ .

- 4) If  $\hat{a}_x = \hat{I}$  then  $\mathcal{Y} = 0$ . Therefore for  $\hat{I} > 0$  the level curve identified by  $\hat{I}$  will definitely cross  $\mathcal{Y} = 0$ .
- 5) The equation of  $\hat{a}_x^*$ , Eq. 196, becomes now simply  $(\hat{a}_x^*)_{\pm} = 3\hat{I}(1 \pm |\hat{I}|/\hat{I})/2$ , with solutions for  $-\infty < \hat{I} < \infty$ .
- 6) Now we check if the solutions of Eq. 196, i.e. of the point 5) satisfy the acceptance criteria expressed in Eq. 83, which in 1) reads  $0 < \hat{a}_x$ . According to the value of  $\hat{I}$  we find the following cases

$$\hat{I} < 0 \implies \begin{cases} (\hat{a}_x^*)_+ = 0 & \text{not acceptable} \\ (\hat{a}_x^*)_- = 3\hat{I} & \text{not acceptable} \end{cases} \quad (204)$$

$$\hat{I} > 0 \implies \begin{cases} (\hat{a}_x^*)_+ = 3\hat{I} & \text{acceptable} \\ (\hat{a}_x^*)_- = 0 & \text{not acceptable} \end{cases} \quad (205)$$

$$\hat{I} = 0 \Rightarrow \begin{cases} (\hat{a}_x^*)_+ = 0 & \text{not acceptable} \\ (\hat{a}_x^*)_- = 0 & \text{not acceptable} \end{cases} \quad (206)$$

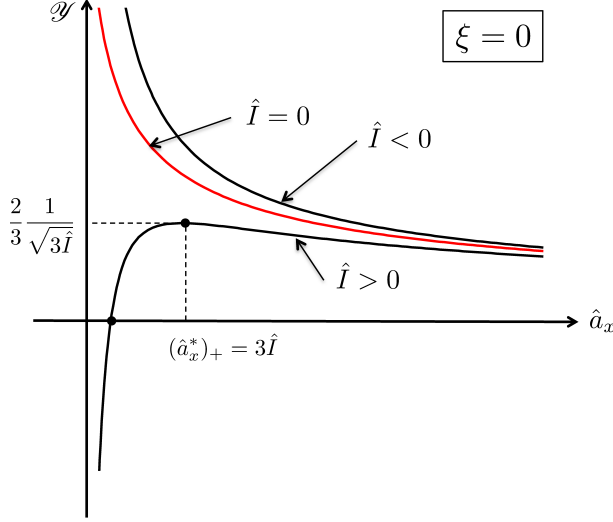


FIG. 28: Summary of the general behaviour of the level curves in the case  $\xi = 0$ .

We conclude that in the region  $\hat{I} < 0$  the level curves have no maximum; in the interval  $\hat{I} > 0$  the level curves have a maximum at  $(\hat{a}_x^*)_+ = 3\hat{I}$  which value is  $\frac{2}{3} \frac{1}{\sqrt{3\hat{I}}}$ . The description of this behaviour is shown in Fig. 28.

### C. $\xi < 0$

The level lines have the following properties:

- 1) The range of  $\hat{a}_x$  is  $0 < \hat{a}_x$ , because at  $\hat{a}_x = 0$  the function  $\mathcal{Y}$  is not defined.
- 2) For  $\hat{a}_x \rightarrow +\infty$  we find  $\mathcal{Y}(\hat{a}_x) \rightarrow 0$ .
- 3) Let's study  $\mathcal{Y}$  in proximity of  $\hat{a}_x = 0$ . We take  $\epsilon$  an arbitrarily small, positive number. For  $\hat{a}_x = \epsilon$  we find

$$\mathcal{Y}(\epsilon) = \frac{\hat{I}}{\sqrt{\epsilon\xi}}. \quad (207)$$

Therefore the curves defined by  $\hat{I}$  are distinguished into two classes of behaviour for the limit  $\hat{a}_x \rightarrow 0^+$  according to the value of  $\hat{I}$ :

$$\hat{a}_x \rightarrow 0^+ \Rightarrow \begin{cases} \mathcal{Y} \rightarrow -\infty & \text{for } \hat{I} > 0 \\ \mathcal{Y} \rightarrow +\infty & \text{for } \hat{I} < 0 \end{cases}. \quad (208)$$

If  $\hat{I} = 0$  the behaviour of  $\mathcal{Y}$  is different, in fact  $\mathcal{Y}$  takes the form

$$\mathcal{Y}(\hat{a}_x) = \frac{\sqrt{\hat{a}_x}}{\hat{a}_x - \xi} \quad (209)$$

and for  $\hat{a}_x \rightarrow 0^+$  we find  $\mathcal{Y} \rightarrow 0$ . This particular level line is shown in Fig. 29 by the blue curve. The curves below the blue curve diverges to  $-\infty$  for  $\hat{a}_x \rightarrow 0^+$ , while the curves above the blue curve will diverge to  $+\infty$  for  $\hat{a}_x \rightarrow 0^+$ .

- 4) If  $\hat{a}_x = \hat{I}$  then  $\mathcal{Y} = 0$ . Therefore for  $\hat{I} > 0$  the level curve identified by  $\hat{I}$  will cross  $\mathcal{Y} = 0$ .
- 5) The equation of  $\hat{a}_x^*$ , Eq. 196 allows solutions for  $\hat{I}$  in the range

$$\hat{I} \leq \xi \quad \text{or} \quad \frac{\xi}{9} \leq \hat{I}. \quad (210)$$

- 6) Now we check if the solutions of Eq. 196 satisfy the acceptance criteria expressed in Eq. 83, which in 1) reads  $\hat{a}_x > 0$ . According to the value of  $\hat{I}$ , and  $\xi$  we find the following cases

$$\hat{I} \leq \xi \Rightarrow \begin{cases} (\hat{a}_x^*)_+ < 0 & \text{not acceptable} \\ (\hat{a}_x^*)_- \leq \xi & \text{not acceptable} \end{cases} \quad (211)$$

$$\frac{\xi}{9} \leq \hat{I} < 0 \Rightarrow \begin{cases} (\hat{a}_x^*)_+ > 0 & \text{acceptable} \\ (\hat{a}_x^*)_+ = 0 & \text{not acceptable} \\ (\hat{a}_x^*)_- > 0 & \text{acceptable} \end{cases} \quad (212)$$

$$0 \leq \hat{I} \Rightarrow \begin{cases} (\hat{a}_x^*)_+ > 0 & \text{acceptable} \\ (\hat{a}_x^*)_- \leq 0 & \text{not acceptable} \end{cases} \quad (213)$$

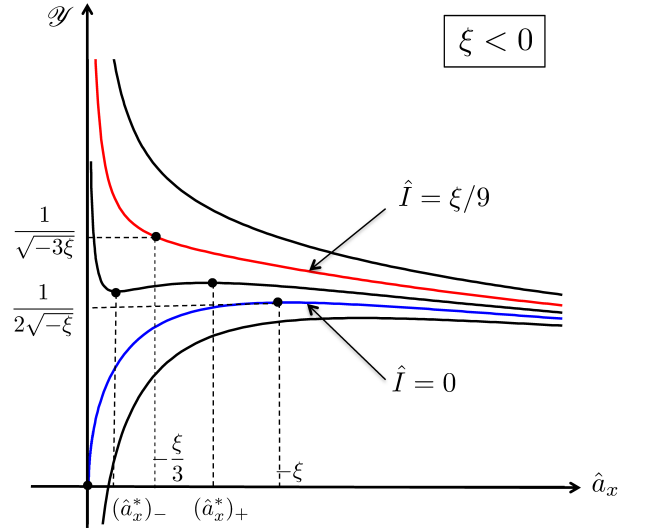


FIG. 29: Summary of the general behaviour of the level curves in the case  $\xi < 0$ .

We conclude that in the region  $\hat{I} > 0$  the level curves have only a maximum  $(\hat{a}_x^*)_+$ ; in the interval  $\xi/9 < \hat{I} < 0$  the level curves have a minimum  $(\hat{a}_x^*)_-$  and a maximum  $(\hat{a}_x^*)_+$ ; for  $\hat{I} < \xi/9$  the level curves have no maximum, but a minimum at  $\hat{a}_x \rightarrow \infty$ . The description of this

behaviour is shown in Fig. 29, the red curve is the curve for  $\hat{I} = \xi/9$ . In this curve the maximum and minimum overlap at  $\hat{a}_x = -\xi/3$ , which is an inflection point with  $\mathcal{V} = 1/\sqrt{-3\xi}$ .

- 
- [1] B.V. Chirikov, “A universal instability of many-dimensional oscillator systems”, *Phys. Rep.* **52**, 263 (1979).
  - [2] A.J. Lichtenberg and M.A. Lieberman, *Regular and Chaotic Dynamics*, 2nd ed. (Springer-Verlag, New York, 1992).
  - [3] R. Hagedorn, “Stability and amplitude ranges of two dimensional non-linear oscillations with periodical Hamiltonian applied to betatron oscillations in circular particle accelerators – Part I and Part II”, CERN Report No. CERN 57-1, 1957.
  - [4] R. Hagedorn and A. Schoch, “Stability and amplitude ranges of two dimensional non-linear oscillations with periodical Hamiltonian applied to betatron oscillations in circular particle accelerators – Part III”, CERN Report No. CERN 57-14, 1957.
  - [5] A. Schoch, “Theory of linear and non-linear perturbations of betatron oscillations in alternating gradient synchrotrons”, CERN Report No. CERN 57-23, 1958.
  - [6] G. Guignard, “The general theory of all sum and difference resonances in a three-dimensional magnetic field in a synchrotron”, CERN Report No. CERN 76-06, 1976.
  - [7] G. Guignard, “A general treatment of resonances in accelerators”, CERN Report No. CERN 78-11, 1978.
  - [8] F. Schmidt, “Untersuchungen zur dynamischen Akzeptanz von Protonenbeschleunigern und ihre Begrenzung durch chaotische Bewegung”, PhD thesis, DESY HERA 88-02 (1988).
  - [9] E. Todesco, “Analysis of resonant structures of 4D symplectic mappings, using normal forms”, *Phys. Rev. E* **50**, R4298 (1994).
  - [10] M.N. Vrahatis, H. Isliker and T.C. Bountis, “Structure and breakdown of invariant tori in a 4-d mapping model of accelerator dynamics”, *Int. J. Bif. Chaos*, **7**(12) 2707-2722 (1997).
  - [11] P. Spiller, G. Franchetti, *Nucl. Instr. and Meth. A* **561**, 305-309 (2006).
  - [12] J. Coupard *et al.*, LIU Technical Design Report (TDR), CERN-ACC-2014-0337.
  - [13] G. Franchetti *et al.*, “Experiment on space charge driven nonlinear resonance crossing in an ion synchrotron,” *Phys. Rev. ST Accel. Beams* **13**, 114203 (2010).
  - [14] G. Franchetti, I. Hofmann, M. Giovannozzi, M. Martini, and E. Metral, *Phys. Rev. ST Accel. Beams* **6**, 124201 (2003); E. Metral *et al.*, *Nucl. Instr. and Meth. A* **561**, (2006), 257-265.